REPUBLIQUE ALGERIENNE DEMOCRATIQUE ET POPULAIRE
الجمهورية الجزائرية الديمقراطية الشعبية

MINISTRY OF HIGHER EDUCATION
AND SCIENTIFIC RESEARCH

HIGHER SCHOOL IN APPLIED SCIENCES
–T L E M C E N–



المدرسة العليا في العلوم التطبيقية
École Supérieure en
Sciences Appliquées

وزارة التعليم العالي والبحث العلمي
المدرسة العليا في العلوم التطبيقية
ـ تلمسان ـ

Engineering's Thesis

For the award of the Engineering's Degree

Field of study : Electronics
Specialization : Industrial Informatics

Presented by : Amina HAMRI

Topic

Design and Development of an STM32-Based Embedded System for Power Quality Analysis

Publicly defended on 30/09/2026 , before a jury composed of:

Mr Mohhamed ABDI	MCA	ESSA-Tlemcen	President
Mr Ghouti ABDELLAOUI	MCA	ESSA-Tlemcen	Thesis Supervisor 01
Mrs Faiza MIMOUNI	MCA	ESSA-Tlemcen	Thesis Supervisor 02
Mr Ahmed Ali KANOUN	MCB	USTHB	Examiner
Mr Reda BELMERAH	Cief engineer, IT department	SONALGAZ	Socio-economic partner
Mrs Hafidha SEBBAGH	MCA	ESSA-Tlemcen	Incubator representative

Academic Year: 2025/2026


بسم الله الرحمن الرحيم

Dedication

To myself,

for the patience, strength, and courage I have shown throughout this challenging year. A year that brought unexpected difficulties and marked a turning point in my life. Despite everything I went through, I chose not to give up. I kept moving forward, even when it was difficult, and found the courage to complete this thesis. I dedicate this achievement to the person I have become through it all.

To my beloved mother, who, despite her own struggles and the burdens she carried, never stopped supporting me, especially throughout this challenging year. Her love, strength, and sacrifices have been my greatest source of courage. And to my father, you were always there for me, supporting me in my studies journy from the beginning, without your support, I wouldn't be where I am today.

You always taught me that anything is achievable, and now I can prove to you that you were right.

To my grandmother, whose prayers have blessed me throughout my entire journey, bringing me strength and peace.

To my friends, for the memories and support.

Acknowledgement

First and foremost, I thank Almighty God for granting me His blessings, guidance, and patience, and for giving me the courage to successfully complete this work on time.

I would like to extend my sincere gratitude and deep appreciation to my research supervisors, **Mr. Ghouti ABDELLAOUI** *and* **Mrs. Faiza MIMOUNI***, for giving me the opportunity and confidence to develop my research project. I am deeply grateful for their continuous support, valuable guidance, insightful advice, and enriching suggestions throughout the realization of this work. Their encouragement and expertise have been invaluable to the successful completion of this project.*

I also extend my respectful thanks to the honorable members of the jury for accepting to review and evaluate this work, and for their valuable time and insights.

I would also like to express my sincere thanks to **Mr. OUDJAMA Farid**, **Mr. BELLAROUCI Salim** *and* **Mr. MESSIRDI Mohammed** *for their valuable help and constant presence throughout the year, extended not only to me but to all the students. Their support was truly a pillar we could all count on.*

I would also like to express my sincere thanks to **Mr. Achraf SAI** *for his encouragement, valuable discussions, and helpful advice throughout this project. His support and willingness to share his experience have been greatly appreciated.*

I would like to sincerely thank my dear friends ***Ikram, Asmaa,*** *and* ***Nessrine*** *for their continuous support, encouragement, and friendship throughout all these years. Their presence and motivation have been invaluable during our academic journey and the completion of this project.*
I also thank ***Djihane*** *for her encouragement and support during this academic year. Her kindness and motivation were greatly appreciated.*

I wish to express my gratitude to the entire department, especially to **Mr. ADJIM Ramz-Eddine Abderrazak***, FabLab Engineer, and* **Mr. KAID Abdelatif***, the laboratory engineer, for their patience, availability, and continuous support throughout our work. Their assistance has been invaluable.*

Finally, we would like to pay tribute to **Mr. ROUISSAT Boucherit***, Director of ESSAT,* **Mr. MEGNAFI Hichem***, Head of the Graduate Department,* **Mr. Ghouti**

ABDELLAOUI, *again as head of the electronic option industrial computing Department, and* **Mr. KHEFIF Sidi-Mohammed** *for granting us access to the FabLab.*

Abstract

This work presents the design and development of an STM32H743-based embedded system for real-time electrical power quality analysis. The system acquires voltage and current signals, performs digital processing, and transmits the calculated parameters to a mobile application via Bluetooth. Signal acquisition is performed using the ADCs integrated into the microcontroller. The FFT implementation was validated using a controlled 50 Hz signal generated by the DAC, with the fundamental component correctly detected at the 50 Hz bin. Real-network measurements were also performed after sensor calibration. Using the three voltage inputs, a voltage unbalance of 0.52% was measured. The system enables real-time visualization of waveforms and main electrical parameters. THD and power measurements still require additional experimental validation before their final integration.

Keywords: Power Quality, STM32H743, Data Acquisition, RMS, Voltage Unbalance, FFT, Embedded System, Bluetooth.

Résumé

Ce travail présente la conception et le développement d'un système embarqué basé sur le STM32H743 pour l'analyse en temps réel de la qualité de l'énergie électrique. Le système assure l'acquisition des signaux de tension et de courant, leur traitement numérique et la transmission des paramètres calculés vers une application mobile via Bluetooth. L'acquisition est réalisée à l'aide des ADC intégrés au microcontrôleur. L'implémentation de la FFT a été validée avec un signal contrôlé de 50 Hz généré par le DAC, dont la composante fondamentale a été correctement détectée au bin de 50 Hz. Des mesures sur le réseau réel ont également été effectuées après calibration des capteurs. Lors de l'utilisation des trois entrées de tension, un déséquilibre de 0,52% a été mesuré. Le système permet la visualisation en temps réel des formes d'onde et des principaux paramètres électriques. La THD et les mesures de puissance nécessitent toutefois une validation expérimentale complémentaire avant leur intégration finale.

Mots-clés : Qualité de l'énergie, STM32H743, Acquisition de données, RMS, Déséquilibre de tension, FFT, Système embarqué, Bluetooth.

الملخص

يتناول هذا العمل تصميم وتطوير نظام مدمج يعتمد على المتحكم STM32H743 لتحليل جودة الطاقة الكهربائية في الزمن الحقيقي. يقوم النظام باقتناء إشارات الجهد والتيار ومعالجتها رقميا، ثم إرسال القيم المحسوبة إلى تطبيق هاتف محمول عبر تقنية Bluetooth . تم تنفيذ عملية الاقتناء باستعمال محولات ADC المدمجة داخل المتحكم. كما تم التحقق من تنفيذ خوارزمية FFT باستخدام إشارة مضبوطة بتردد 50
Hz مولدة بواسطة DAC ، حيث تم الكشف بشكل صحيح عن المركبة الأساسية عند حزمة 50 Hz . كذلك تم إجراء قياسات على الشبكة الكهربائية الحقيقية بعد معايرة الحساسات. وعند استخدام مداخل الجهد الثلاثة، تم قياس نسبة عدم توازن في الجهد قدرها 0.52% . يسمح النظام بعرض أشكال الموجات

وأهم القيم الكهربائية في الزمن الحقيقي. ومع ذلك، ما تزال قياسات THD والقدرة بحاجة إلى تحقق تجريبي إضافي قبل دمجها النهائي.
الكلمات المفتاحية: جودة الطاقة الكهربائية، STM32H743 ، اقتناء البيانات، RMS ، عدم توازن الجهد، FFT ، الأنظمة المدمجة، Bluetooth .

Contents

List of Figures

List of Tables

Abbreviations List

General introduction **1**

1 Context of the Study and State of the Art **4**
1.1 Introduction 4
1.2 Sources of Power Quality Disturbances 4
1.3 Power Quality Disturbances 5
1.3.1 Transients 5
1.3.2 Voltage Sag 5
1.3.3 Voltage Swell 6
1.3.4 Harmonics 6
1.3.5 Voltage and Current Unbalance 8
1.3.6 Sources of Voltage Unbalance 8
1.3.7 Effects of Voltage Unbalance 9
1.3.8 Voltage Unbalance Factor Calculation Using Symmetrical Components 10
1.4 Impact on electrical equipment 12
1.4.1 Equipment sensitivity to voltage distortion 12
1.4.2 Cumulative effects on equipment lifetime 12
1.5 Importance of Power Quality Monitoring 12
1.5.1 Continuous spectral surveillance 13
1.5.2 THD as a Standardised Compliance Metric 13
1.5.3 Data Logging and Future Predictive Maintenance 13
1.5.4 From Disturbance Detection to Compensation Claims: The Role of Norm-Certified Power Quality Monitoring in Industrial and Residential Networks 13
1.6 Signal Definition 14
1.7 Sampling Theory 14
1.7.1 Sampling Rate 14
1.7.2 Bandwidth Considerations 15

1.8 FFT (Fast Fourier Transform) . . . 15
1.8.1 Fourier Transform . . . 15
1.8.2 Discrete Fourier Transform . . . 16
1.8.3 Fast Fourier Transform . . . 16
1.8.4 Real FFT . . . 18
1.8.5 Mathematical and Computational Co-Design . . . 18
1.9 Total Harmonic Distortion (THD) . . . 19
1.9.1 IEEE 519-2022 Standard for Harmonic Control . . . 19
1.10 RMS calculations . . . 20
1.10.1 RMS Voltage Measurement . . . 20
1.10.2 RMS Current Measurement . . . 20
1.10.3 Power Measurement . . . 20
1.10.4 Power Factor . . . 22
1.10.5 Regulatory Framework: Sonelgaz Billing Policy . . . 22
1.11 Acceptable limits . . . 23
1.11.1 Voltage Unbalance Limits . . . 23
1.11.2 Acceptable THD limits . . . 23
1.11.3 Acceptable Limits for Voltage Disturbances . . . 23
1.12 Key Measurement Concepts . . . 24
1.13 Conclusion . . . 25

2 System Specifications and Engineering Design 26
2.1 Introduction . . . 26
2.1.1 IEEE 1159 Standard Definition . . . 26
2.2 IEC 61000-4-30 standard . . . 27
2.2.1 Power quality parameters defined in the standard . . . 28
2.3 Measurement Methodologies . . . 29
2.3.1 IEC 61000-4-7: Measurement Methodology for Harmonic Analysis 29
2.3.2 Rectangular Windowing . . . 29
2.3.3 Sampling Parameter Selection . . . 30
2.4 Instrument Classification According to Measurement Performance . . . 32
2.4.1 Class A . . . 32
2.4.2 Class S . . . 32
2.4.3 Key Differences Between Class A and Class S . . . 32
2.5 System architecture . . . 34
2.6 Microcontrollers selection . . . 36
2.6.1 ARM processors . . . 36
2.7 STM32 . . . 37
2.7.1 Selection Criteria . . . 37
2.7.2 STM32 Development Tools and Software Environment . . . 39
2.7.3 Direct memory access controller (DMA) . . . 40
2.8 Voltage sensor . . . 41
2.9 Current sensor . . . 45
2.9.1 Current Signal Conditioning and Calibration . . . 45
2.10 Voltage and Current measurment . . . 46
2.11 Signal processing implementation . . . 47
2.11.1 CMSIS-DSP . . . 47
2.11.2 CMSIS-DSP Implementation: `arm_rfft_fast_f32` . . . 48

2.11.3 Harmonic Extraction and THD Computation 49
2.12 Graphical user interface 49
2.12.1 Mobile Application 50
2.12.2 Wireless Communication 53
2.13 Software Design 56
2.13.1 UML Class Diagram 56
2.13.2 UML Sequence Diagram 56
2.13.3 UML Deployment Diagram 57
2.14 Implementation Challenges 58
2.15 PCB Design and Fabrication 59
2.16 Conclusion 64

3 System Implementation, Experimental Testing, and Metrological Validation 65
3.1 Introduction 65
3.2 Project Presentation 65
3.3 Data Acquisition Configuration 66
3.3.1 STM32 Timer configuration 66
3.3.2 ADC3 Acquisition and DMA Configuration 69
3.3.3 ADC Sampling Time Optimization 69
3.4 Laboratory testing 70
3.5 Debugging and Validation Methods 71
3.6 Real-Time Voltage Measurement 72
3.6.1 Voltage sensor ZMPT101B 72
3.6.2 Voltage Unbalance Measurement 73
3.7 Frequency-Domain Validation 74
3.7.1 FFT Validation Using the DAC-Generated 50 Hz Signal 74
3.7.2 FFT Analysis of the Real Network Voltage 74
3.7.3 THD Implementation and Validation Status 75
3.7.4 Power Measurement Implementation Status 75
3.8 Conclusion 76

General conclusion 77

Bibliography 79

List of Figures

1.1 Harmonic distortion. 8
1.2 Resolving phase voltages into three sets of sequence components. 10
1.3 Waveform distortion 15
1.4 Waveform aliasing 15
1.5 ITIC curve is a modified version of the CBEMA curve. 24

2.1 Analysis window according to IEC 61000-4-7. 29
2.2 Rectangular window function. 30
2.3 System block diagram 35
2.4 STM32H743VIT6 developpement board 38
2.5 CubeMX clock view 39
2.6 ZMPT101B voltage sensor 42
2.7 ZMPT101B output signal 43
2.8 Industrial Voltage Transducer (LEM LV 25-P). 45
2.9 Downloading the CMSIS-DSP library as a ZIP file 47
2.10 CMSIS-DSP file placement in the STM32CubeIDE project 48
2.11 Placement of the `arm_math.h` header file 48
2.12 Communication protocol stack used for wireless data transmission between the STM32H743 and the mobile application. 50
2.13 Oscilloscope Control Interface 51
2.14 Measurement Panel 52
2.15 Main Dashboard 52
2.16 Low-cost Bluetooth 2.0 SPP (Serial Port Protocol) module. 53
2.17 Low-cost Bluetooth 2.0 SPP (Serial Port Protocol) module. 54
2.18 UML class diagram. 56
2.19 UML sequence diagram. 57
2.20 UML deployment diagram. 57
2.21 Schematic of the proposed PCB. 60
2.22 PCB for the proposed board. 61
2.23 3D visualization of the proposed PCB. 61
2.24 Error between the drilling stage and the subsequent milling of the copper traces 62
2.25 PCB fabrication using the LPKF CNC prototyping system. 63
2.26 Chemical metallization process. 63
2.27 Final Breakout PCB for the Prototype 64

3.1 Overall architecture of the proposed three-channel power quality monitoring system. 66
3.2 Advanced Peripheral Bus 2 67
3.3 PWM Signal Generated by the STM32 Timer (Oscilloscope Visualization) . 68
3.4 Signal before increasing the ADC sampling time 69
3.5 Signal before ADC sampling time optimization 70
3.6 Validation test bench architecture for signal acquisition and processing. . . 71
3.7 Calibration of the ZMPT101B output using the onboard potentiometer and oscilloscope 72
3.8 Real-time voltage waveform and calculated electrical parameters 73
3.9 FFT analysis of the DAC-generated 50 Hz signal 74
3.10 FFT analysis of the real network voltage 75

List of Tables

1.1 Comparison of computational complexity for direct computation of the DFT versus the radix-2 FFT algorithm. [10] 17
1.2 IEEE 519-2022 Recommended Voltage Distortion Limits at the PCC 23

2.1 Classification of voltage disturbances according to IEEE 1159 (220 V_{rms} / 50 Hz network) 27
2.2 IEC 61000-4-30 Class A and Class S Key Differences 33
2.3 Instruments used for experimental validation of the developed PQA 34
2.4 Available DMA transfer directions 41
2.5 Comparison between a 220V/9V transformer and the ZMPT101B voltage sensor 43
2.6 Comparison of common Bluetooth data encoding formats. 54
2.7 Structure of the real-time measurement data frame. 55

Abbreviations List

Acronyme	Signification
AC	Alternating Current
ADC	Analog-to-Digital Converter
APE	Absolute Percentage Error
APB	Advanced Peripheral Bus
ARM	Advanced RISC Machine
BDMA	Basic Direct Memory Access
BLE	Bluetooth Low Energy
CAN	Controller Area Network
CBEMA	Computer and Business Equipment Manufacturers Association
CCR	Capture Compare Register
CDC	Communications Device Class
CMSIS	Cortex Microcontroller Software Interface Standard
COM	Communication Port
CPU	Central Processing Unit
CRC	Cyclic Redundancy Check
DC	Direct Current
DFT	Discrete Fourier Transform
DMA	Direct Memory Access
DSP	Digital Signal Processing
EMC	Electromagnetic Compatibility
FFT	Fast Fourier Transform
FMC	Flexible Memory Controller
FPU	Floating-Point Unit
GPS	Global Positioning System
HAL	Hardware Abstraction Layer
IC	Integrated Circuit
IEC	International Electrotechnical Commission
IEEE	Institute of Electrical and Electronics Engineers
IH	Individual Harmonic
IT	Information Technology
ITIC	Information Technology Industry Council
LCD	Liquid Crystal Display
MAC	Multiply-Accumulate

Acronyme	Signification
MCU	Microcontroller Unit
PCB	Printed Circuit Board
PCC	Point of Common Coupling
PQA	Power Quality Analyzer
PSC	Prescaler
Pu	Per Unit
PWM	Pulse-Width Modulation
RAM	Random Access Memory
RFFT	Real Fast Fourier Transform
RISC	Reduced Instruction Set Computer
RMS	Root Mean Square
ROM	Read-Only Memory
RSS	Root Sum Square
RVC	Rapid Voltage Change
SD	Secure Digital
SDMMC	Secure Digital / MultiMediaCard
SPI	Serial Peripheral Interface
SPP	Serial Port Profile
TFT	Thin-Film Transistor
THD	Total Harmonic Distortion
UART	Universal Asynchronous Receiver-Transmitter
UML	Unified Modeling Language
USB	Universal Serial Bus
USART	Universal Synchronous/Asynchronous Receiver-Transmitter
UTC	Coordinated Universal Time
VFD	Variable Frequency Drive
VUF	Voltage Unbalance Factor

General Introduction

Electric power quality is an important issue concerning the generation, distribution, and utilization of electrical energy. It reflects the ability of the electrical supply to provide voltage and current conditions that allow connected equipment to operate correctly and reliably. Disturbances such as voltage sags, voltage swells, harmonics, transients, and voltage unbalance can affect power quality and consequently influence the performance of electrical installations and sensitive equipment.

These variations can create problems for consumers depending on their severity, duration, and the sensitivity of the connected loads. Such phenomena, commonly referred to as power quality disturbances, may result from several events, including motor starting, equipment switching and nonlinear loads. Therefore, the accurate measurement and continuous monitoring of electrical quantities are essential for evaluating power quality and identifying abnormal operating conditions.

An oscilloscope is an electronic measuring instrument that allows the visualization and time-domain analysis of one or more variable electrical signals. In modern industrial systems, traditional processing of these signals becomes limited when advanced measurements and continuous monitoring are required. The transition toward moderne and digital architectures, based on analog-to-digital converters (ADCs), microcontrollers, and digital signal processing techniques, has enabled the implementation of more advanced measurement and analysis functions.

In this context, combining electrical measurement, embedded processing, communication, and software visualization provides the basis for the development of intelligent monitoring instruments. Such systems can acquire electrical signals, calculate relevant power quality parameters, analyze their frequency content, detect abnormal conditions, and transmit the resulting information to an external interface. This approach contributes to the development of compact monitoring solutions suitable for industrial diagnostics and power quality assessment.

Problem Statement

Conventional oscilloscopes are mainly designed for signal visualization and general-purpose electrical measurements. However, power quality monitoring requires not only waveform acquisition but also the real-time processing and interpretation of electrical signals to identify disturbances and evaluate relevant power quality parameters.

The main challenge of this work is therefore to develop a compact embedded system capable of safely acquiring electrical signals, processing them in real time, detecting power quality disturbances, and transmitting the results to a user interface, while ensuring reliable measurement performance.

Objectives

The primary objective of this engineering thesis is to design and develop an embedded power quality monitoring system based on an industrial oscilloscope architecture for the acquisition, processing, and analysis of electrical signals.

More specifically, this work aims to:

- study the main power quality disturbances and the electrical quantities required for their characterization;
- study the theoretical principles required for digital signal acquisition and processing, including sampling, analog-to-digital conversion, FFT, RMS calculation, and THD evaluation;
- define the system specifications according to the targeted measurement functions and relevant power quality standards;
- design and implement the hardware architecture required for voltage and current signal acquisition and conditioning;
- configure and program the STM32 microcontroller and the associated ADC acquisition system for real-time data acquisition;
- implement digital signal processing algorithms for the calculation of RMS values, harmonic components, THD, active power, power factor, and voltage unbalance;
- implement the detection of selected power quality disturbances, particularly voltage sags and swells;
- develop a communication interface for transferring the acquired and processed data to an external visualization system;
- develop a mobile application for displaying measurements, signal waveforms, frequency-domain information, and detected events;
- experimentally validate the developed system using generated and real electrical signals and evaluate its measurement performance.

Research Hypotheses

- H1: An STM32-based embedded system can perform real-time acquisition and processing of electrical signals to accurately estimate the main power quality parameters, including RMS voltage, frequency components using FFT, THD, and voltage unbalance.

Thesis Organization

This thesis is organized into three chapters, each addressing a specific stage in the development of the proposed power quality monitoring system:

- **Chapter 1: Context of the Study and State of the Art** presents the theoretical background required for the development of the proposed system. It introduces the main sources and types of power quality disturbances, including transients, voltage sags, voltage swells, harmonics, and voltage unbalance. The chapter also discusses their impact on electrical equipment and the importance of power quality monitoring. The fundamental concepts of signal sampling, analog-to-digital conversion, Fourier analysis, FFT, RMS calculation, THD, and power measurement are subsequently presented. Finally, the chapter introduces the regulatory framework and acceptable limits associated with the considered power quality parameters.

- **Chapter 2: System Specifications and Engineering Design** presents the specifications, architecture, and engineering choices of the proposed system. It describes the applicable standards, measurement methodologies, instrument classification, and system architecture. The selection and configuration of the microcontroller and ADC are presented, followed by the design of the voltage and current sensors and their signal conditioning and calibration. The chapter then describes the digital signal processing implementation using CMSIS-DSP, including RMS, harmonic extraction, and THD calculation. Finally, the Bluetooth communication protocol, mobile application architecture, and hardware and software design are presented.

- **Chapter 3: System Implementation, Experimental Testing, and Metrological Validation** presents the practical implementation and experimental evaluation of the developed system. It describes the prototype realization, the STM32 configuration, the signal acquisition and data transmission mechanisms, the laboratory testing procedure and real network measurments.

Chapter 1
Context of the Study and State of the Art

1.1 Introduction

Power quality has become a major concern in modern electrical networks due to the increasing use of power electronic converters, nonlinear loads, renewable energy systems, and sensitive electronic equipment. These technologies improve efficiency but also introduce disturbances such as voltage sags, swells, harmonics, transients, and voltage unbalance, which may affect the reliability and performance of electrical installations.

The development of an industrial oscilloscope capable of monitoring electrical signals and analyzing power quality requires a solid understanding of these disturbances, together with the principles of signal acquisition and digital signal processing. This chapter therefore presents the theoretical background necessary for this work. It reviews the main power quality phenomena, their causes and effects, as well as the fundamental concepts of sampling, analog-to-digital conversion, FFT-based spectral analysis, RMS and power measurements, and the relevant measurement standards that support the design presented in the following chapter.

1.2 Sources of Power Quality Disturbances

The primary source of power quality issues are:

- **Nonlinear Load:** In a nonlinear load, the current is not proportional to the applied voltage, resulting in waveform distortion and the generation of harmonic currents. This results in harmonic distortion which causes overheating of electrical equipment and are admitted to voltage dips if they are not properly protected

- **IT and Office Equipment (sensitive loads):** Modern IT and office equipment relies on integrated circuits (ICs), which are highly sensitive to power quality disturbances. Voltage disturbances may lead to data corruption, unexpected resets, or malfunction of sensitive electronic equipment.

- **Large Motor Starting:** During starting, the current in the induction machines is about six to eight times the rated current. It increases the network loading and hence causing a voltage sag.
  . Modern motors often use power electronic converters known as variable frequency drives (VFDs). These drives limit the starting current, thereby reducing voltage sags.

– **Arc Producing Devices:** These are non-linear devices and are a major source of harmonic distortion, e.g., electric discharge lamps, electric arc furnaces and arc welders.

–

Load Switching: The switching of large electrical loads may generate transient disturbances due to sudden changes in current and voltage. Surge protection devices and appropriate switching techniques are commonly used to mitigate these disturbances.

– **Interconnection of Power Systems:** In recent years the extent of interconnection in the power system has increased. Consequently, power quality disturbances generated in one interconnected network can propagate to neighbouring networks, making their mitigation more challenging.

– **Lightning Strikes and Environmental issues:** Lightning Strikes and Environmental issues The Lightning strike produces transient over voltage issues and also it frequently leads to fault in power system. When the lightning strike hits the overhead transmission lines it causes 'flash-over' to the neighbouring conductors. It consists of transient overvoltage, voltage dips and also fault-clearing interruptions.

1.3 Power Quality Disturbances

They are caused by electrical disturbances such as transients, surges, sags and harmonics. The power quality signature, or characteristic, of the disturbance identifies the type of power quality problem. The nature of the variation in the basic components of the sine wave, i.e., voltage, current, and frequency, identifies the type of power quality problem. [1]

1.3.1 Transients

These are the unexpected and small duration interruption which is occur due to intense variation in balanced situation of current ,voltage or both. [1]
Transients can be classified into two categories, impulsive and oscillatory. These terms reflect the wave shape of a current or voltage transient. [1]

1.3.2 Voltage Sag

Voltage sag as defined by IEEE Standard 1159- 1995, is a decrease in root mean square (RMS) voltage at the power frequency for durations from 0.5 cycles to 1 minute. Typical magnitudes are between 0.1 and 0.9 pu. Voltage sags are usually caused by: [1]

– Operation of Circuit breakers.

– Inrush currents

– Switching on of large loads.

– Switching off of capacitor bank.

The effect of voltage sag mainly affects sensitive electronic equipment than the conventional electrical equipment, such as computers, microprocessor and the micro-controller etc. [1]
The three important characteristics of voltage sags are: [1]

- Magnitude (depth).
- Duration.
- Phase Angle Jump.

1.3.3 Voltage Swell

Voltage swell as defined by IEEE Standard 1159-1995, is an increase in root mean square (RMS) voltage at the power frequency for durations from 0.5 cycles to 1 minute. Magnitudes are between 1.1 and 1.8 pu. [1]
Voltage swells may also be caused by: [1]

- Switching off a large load
- Switching on a large capacitor bank

1.3.4 Harmonics

Power systems are designed to operate at frequencies of 50 or 60Hz. However, certain types of loads produce currents and voltages with frequencies that are integer multiples of the 50 or 60 Hz fundamental frequency. These higher frequencies are a form of electrical pollution known as power system harmonics. [2]
Unlike transient events such as lightning that last for a few microseconds, or voltage sags that last from a few milliseconds to several cycles, harmonics are steady-state periodic phenomena that produce continuous distortion of voltage and current waveforms. These periodic nonsinusoidal waveforms are described in terms of their harmonics, whose magnitudes and phase angles are computed using Fourier analysis. [2]
The analysis permits a periodic distorted waveform to be decomposed into an infinite series containing dc, fundamental frequency (e.g. 60Hz), second harmonic (e.g. 120Hz), third harmonic (e.g. 180Hz), and so on. [2]
The most common measure of distortion is total harmonic distortion, THD. THD applies to both current and voltage and is defined as the rms value of harmonics divided by the rms value of the fundamental, and then multiplied by 100%. THD of current varies from a few percent to more than 100%. THD of voltage is usually less than 5%. Voltage THDs below 5% are widely considered to be acceptable, but values above 10% are definitely unacceptable and will cause problems for sensitive equipment and loads. [2]
There are two general categories of harmonic sources:

- **Saturable devices:** produce harmonics due mainly to iron saturation, as is the case for transformers, machines, and fluorescent lamps (with magnetic ballasts). For economic reasons, most transformers and motors are designed to operate slightly past the knee of the iron core saturation curve. The resulting magnetizing currents are peaked and rich in the third harmonic. Unless blocked by a delta transformation, a synchronous machine will produce a third harmonic current of approximately 30% of the fundamental. [2]

– **Power electronic devices:** Power electronic loads draw power only during portions of the applied voltage waveform. These loads include switch-mode power supplies, voltage source converters, pulse-width modulated converters. [2]

Harmonic distortion levels are described by the complete harmonic spectrum with magnitudes and phase angles of each individual harmonic component. It is also common to use a single quantity THD, as a measure of the effective value of harmonic distortion.

Harmonic Impacts

Harmonics have a number of undesirable effects on power system components and loads. These fall into two basic categories: short-term and long-term.
Short-term effects are usually the most noticeable and are related to excessive voltage distortion. [2]

Short-term effects can cause nuisance tripping of sensitive loads. Some computer-controlled loads are sensitive to voltage distortion. For example, one documented case showed that a voltage distortion of 5.5% regularly shut down computerized lathes at a large pipe company heat treatment operation. While voltage distortions of 5% are not usually a problem, voltage distortions above 10% will almost always cause significant nuisance tripping or transformer overheating. [2]

Harmonics as shown in **Figure 1.1** can also cause transformer overheating. This usually occurs when a dedicated transformer serves only one large nonlinear load. [2]

On the other hand, long-term effects often go undetected and are usually related to increased resistive losses or voltage stresses. [2]

Therefore, it is important to characterize and measure harmonics in power grid signals in a well-defined and standard manner, allowing to define limits on the maximum amount of harmonics energy in the grid signals.

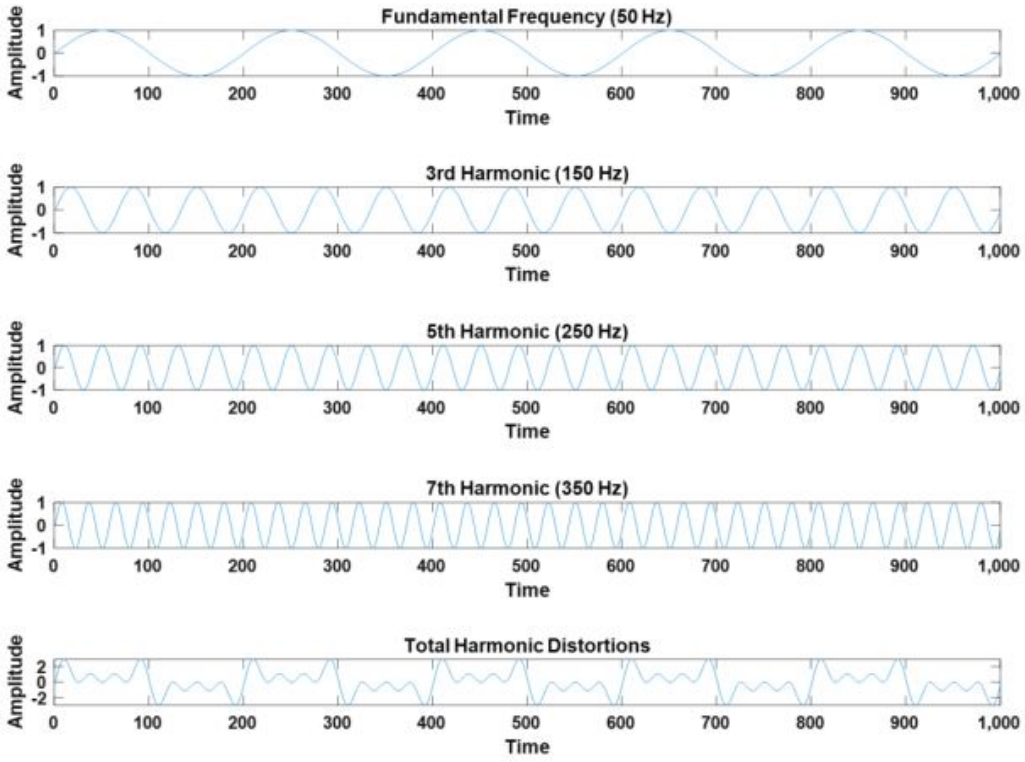


Figure 1.1: Harmonic distortion.

1.3.5 Voltage and Current Unbalance

Synchronous generators are the sources of a three-phase voltage in a power system. The voltages at generator phase terminals are equal in magnitude and displaced to each other by 120°. [3]

If the components of the power system are linear and symmetrical, and individual phases of the system are equally loaded, the voltages measured at load buses remain symmetrical. The main sources of the long-term unbalance are unbalanced loads, primarily single-phase loads existing mainly in low-voltage and medium-voltage networks. [3]

These loads cause non-equal phase currents to flow in the power system and unsymmetrical voltage drop on the system components. As a consequence, voltage balance at the nodes is lost. [3]

In three-phase systems voltage unbalance is defined as a condition in which the three phase voltages are not equal in magnitude and/or the displacement angles between them are different from 120°, an analogous definition is applied to currents. [3]

1.3.6 Sources of Voltage Unbalance

The main sources of voltage unbalance in electric power systems are the following:

- **Unbalanced single-phase loads:** Most low-voltage loads and certain medium-voltage ones – such as electric traction motors – are single-phase appliances. Their operation

in a three-phase system results in unbalanced load currents, which produce unsymmetrical voltage drops across individual phases, causing voltage unbalance at network nodes. [3]

- **Asymmetrical transmission line geometry:** Overhead lines with non-transposed or asymmetric tower geometries present different electrical parameters per phase, since the conductors are not simultaneously at the same position relative to each other and to earth. This asymmetry leads to unequal voltage drops across the individual phases. [3]

1.3.7 Effects of Voltage Unbalance

Voltage unbalance in a power system produces the following adverse effects:

- additional losses of power and energy;
- additional heating, which limits the transmission capability of lines;
- further voltage unbalance at network nodes.

Voltage unbalance adversely affects the operation of several types of loads, the most sensitive being asynchronous motors, synchronous generators, and converters. [3]

Asynchronous motors:

Voltage unbalance causes:

- Additional heating of the stator windings.
- Increased power losses.
- Reduced useful torque.
- Additional mechanical vibrations

Motor current under unbalanced conditions can be several times higher than the rated current, accelerating insulation deterioration and shortening the motor service life.
Most asynchronous motors are not affected by a supply voltage unbalance below 2%. [3]

Synchronous generators:

Unbalanced loads cause additional heating, increased power losses, and additional mechanical forces acting on the rotor and stator, which are hazardous to structural components. In general, unbalance is not a critical issue under normal operating conditions, but may cause severe hazards during disturbances such as unsymmetrical short-circuits.[3]

Converters:

Voltage unbalance generates an additional variable component in the rectified output and produces non-characteristic harmonics and interharmonics. [3]

Other loads:

Voltage unbalance can alter the operating characteristics and reduce the service life of other three-phase loads, and may also disturb the functioning of control systems, potentially interrupting the operation of equipment. [3]

1.3.8 Voltage Unbalance Factor Calculation Using Symmetrical Components

Among the different voltage unbalance definitions proposed in the literature (according to: IEC 61000-2-12, IEC 61000-4-30, IEEE P1159.1, Gost 13109-97, IEC 61000-2-1, IEC 61000-4-27, etc) [3], the Voltage Unbalance Factor (VUF), defined as the ratio of the negative-sequence voltage component to the positive-sequence voltage component, is the preferred method according to IEC-based standards because it directly represents the physical phenomenon of voltage asymmetry. This definition is also adopted by modern power quality analyzers compliant with IEC 61000-4-30. [4]

Definition of symmetrical components

The analysis of voltage unbalance relies on the theory of symmetrical components, introduced by Fortescue, which states that any set of unbalanced three-phase phasors can be decomposed into three balanced sets [5]:

- **Zero-sequence components:** three phasors of equal magnitude with zero phase displacement, as shown in Figure 1.2. [5]
- **Positive-sequence components:** three phasors of equal magnitude with $\pm 120^\circ$ phase displacement in the positive rotation direction, as shown in Figure 1.2. [5]
- **Negative-sequence components:** three phasors of equal magnitude with $\pm 120^\circ$ phase displacement in the negative rotation direction, as shown in Figure 1.2. [5]

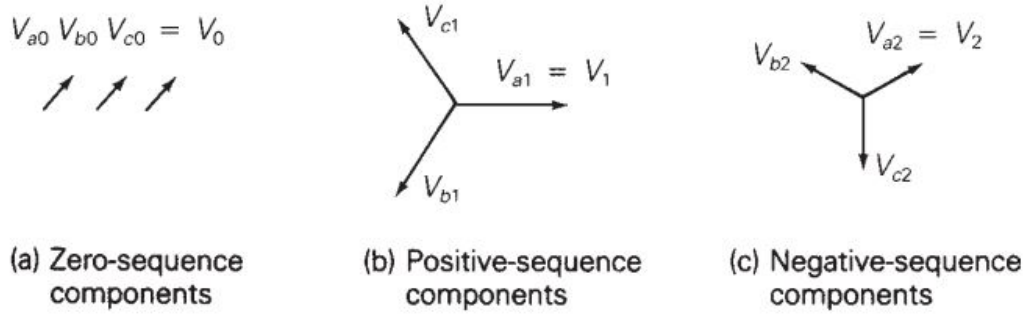


Figure 1.2: Resolving phase voltages into three sets of sequence components.

Where **phasors** are complex numbers of the form $|V|e^{j\varphi}$ that represent sinusoidal signals by their magnitude $|V|$ and phase angle φ simultaneously.

Extraction of the fundamental phasors

In this work, the voltage signals of the three phases are sampled simultaneously at $f_s = 10.24$ kHz and processed using a 2048-point FFT, giving a frequency resolution of:

$$\Delta f = \frac{f_s}{N} = \frac{10240}{2048} = 5 \text{ Hz} \tag{1.1}$$

The 50 Hz fundamental therefore falls exactly on the 10^{th} FFT bin. Unlike the RMS value, each bin is a complex number that carries both magnitude and phase information:

$$V = \text{Re} + j\,\text{Im} \tag{1.2}$$

The three phase voltages at the fundamental frequency are thus represented by the complex phasors V_a, V_b, and V_c.

Fortescue's transformation

These phasors are transformed into zero-, positive-, and negative-sequence components, denoted V_0, V_1, and V_2, through the matrix relation [5]:

$$\begin{bmatrix} V_0 \\ V_1 \\ V_2 \end{bmatrix} = \frac{1}{3} \begin{bmatrix} 1 & 1 & 1 \\ 1 & a & a^2 \\ 1 & a^2 & a \end{bmatrix} \begin{bmatrix} V_a \\ V_b \\ V_c \end{bmatrix} \tag{1.3}$$

where $a = e^{j120^\circ} = -\frac{1}{2} + j\frac{\sqrt{3}}{2}$ is the complex rotation operator [5]. Equation (1.3) expands to:

$$\begin{aligned} V_0 &= \tfrac{1}{3}\left(V_a + V_b + V_c\right), \\ V_1 &= \tfrac{1}{3}\left(V_a + aV_b + a^2V_c\right), \\ V_2 &= \tfrac{1}{3}\left(V_a + a^2V_b + aV_c\right). \end{aligned} \tag{1.4}$$

Voltage Unbalance Factor

The Voltage Unbalance Factor (VUF) is defined, in accordance with IEC 61000-4-30 [4] and the method of symmetrical components [3], as the ratio of the negative-sequence component magnitude to the positive-sequence component magnitude: [3]

$$\text{VUF} = \frac{|V_2|}{|V_1|} \times 100\% \tag{1.5}$$

In a perfectly balanced system $V_2 = 0$ and $\text{VUF} = 0\%$. As asymmetry increases, $|V_2|$ grows while $|V_1|$ remains close to the nominal voltage, yielding a higher unbalance factor. [3]

This method captures both magnitude and phase angle deviations simultaneously, since each phasor carries both quantities, making it sensitive to any form of three-phase unbalance.[3]

Evaluation methods

The method of evaluation depends on the purpose of measurements.

- Determination of a number or a percentage of values which in the observation period exceed contractual values;
- Comparison of maximum measured values to contractual ones (a longer observation period can be taken in this case, e.g. one year);
- Comparison of statistical parameters of measured quantities to contractual values.

1.4 Impact on electrical equipment

The power quality disturbances described in the preceding sections do not merely represent abstract deviations from ideal sinusoidal waveforms; they translate into quantifiable, often irreversible, degradation of electrical and electronic equipment. The severity of this impact depends on the nature of the disturbance, its magnitude, its duration, and the susceptibility of the affected load.

1.4.1 Equipment sensitivity to voltage distortion

Electronic equipment connected to the supply network does not respond to the RMS voltage alone; it responds to the instantaneous waveform. Switch-mode power supplies with capacitor-input rectifiers, for instance, draw current in narrow pulses centred near the voltage peaks, flowing only when the instantaneous AC voltage exceeds the DC bus voltage. When harmonic components distort the waveform, these peak values shift and broaden unevenly, causing the internal DC bus voltage to fluctuate and potentially driving the supply outside its regulation range. IEEE 519-2022 limits voltage THD at the point of common coupling to 5 % for systems at or below 1 kV; distortion levels approaching or exceeding this threshold are generally considered sufficient to induce measurable performance degradation in sensitive loads. [6]

1.4.2 Cumulative effects on equipment lifetime

Even when individual harmonic levels remain below alarm thresholds, sustained exposure to a distorted voltage waveform accelerates the ageing of dielectric materials in capacitors and insulation systems. The repetitive overvoltage stress associated with each harmonic cycle accumulates over time, gradually degrading insulation integrity in a manner that THD alone does not fully capture. By resolving the amplitude of each harmonic order individually, the FFT provides the spectral detail necessary to assess which frequency components contribute most to this cumulative stress, supporting a more informed evaluation of equipment condition than a single aggregated index would allow.

1.5 Importance of Power Quality Monitoring

The consequences described above can only be anticipated, quantified, and mitigated if the voltage waveform is continuously observed and analysed. Monitoring through FFT-based instruments provides both the time-domain record of discrete events and the frequency-domain

characterisation of steady-state distortion, making it the cornerstone of any serious power quality management strategy.

1.5.1 Continuous spectral surveillance

Unlike averaging instruments that report RMS values over a fixed window, an oscilloscope computes the FFT on successive waveform records, producing a dynamic spectrum that reveals how harmonic content evolves with load switching, network reconfiguration, or equipment start-up. This temporal resolution is critical for distinguishing between persistent harmonic sources and transient spectral events, a distinction that a single THD snapshot cannot provide.

1.5.2 THD as a Standardised Compliance Metric

Standards such as IEC 61000-2-2 and IEEE 519 define limits on individual harmonic voltages as well as on the global THD index. Continuous monitoring of THD against these thresholds provides an auditable compliance record for utilities and industrial operators alike. Whenever THD exceeds a predefined limit, the monitoring system can trigger an alarm and store the corresponding FFT spectrum, thereby preserving the evidence necessary to identify the offending source. [6]

1.5.3 Data Logging and Future Predictive Maintenance

The proposed oscilloscope system is capable of storing electrical parameters such as FFT spectra, THD values for future analysis. These measurements can be archived on external storage devices such as an SD card or a local database.

The collected historical data may later be exploited to analyze the long-term evolution of harmonic distortion and signal quality. Such an approach could enable the implementation of predictive maintenance algorithms capable of detecting abnormal operating conditions before critical failures occur.

Although advanced fault prediction is outside the scope of the current engineering project, the proposed architecture was designed to support future integration of intelligent diagnostic and maintenance functions.

1.5.4 From Disturbance Detection to Compensation Claims: The Role of Norm-Certified Power Quality Monitoring in Industrial and Residential Networks

quality disturbances can cause significant financial and operational damage in both industrial facilities and residential environments. When such anomalies are detected and measured in strict accordance with international standards, the resulting data acquires a normative validity that transcends mere technical observation. A measurement system certified against these frameworks produces evidence that is not only scientifically rigorous but also legally admissible, enabling affected parties to substantiate compensation claims against electricity suppliers or responsible industrial operators. This dual role of power quality monitoring — as both a diagnostic tool and a juridical instrument, underscores the critical importance of deploying reliable, standards-compliant analyzers in real-world electrical networks.

1.6 Signal Definition

A signal is the physical representation of information that carries it from its source to its recipient. It can be defined as any physical quantity such as voltage, current, pressure, etc. That varies with time, space, or another independent variable, and serves to convey information.

1.7 Sampling Theory

Many researchers and scientists have worked on these, giving rise to the discipline of signal processing. [7]

Indeed, it was while working on solving the equation of heat propagation that Joseph FOURIER (1768-1830) implemented a method known as "Fourier analysis," which consists of decomposing a mathematical function, difficult to describe, into an infinite sum of cosine and sine functions. Later, other scientists, such as Harry NYQUIST and Claude SHANNON, built upon Fourier analysis and were able to develop the science of signal processing, thanks to the sampling theorem. [7]

By sampling a signal $f(t_i)$ at a discrete set of points, we are actually applying a linear transformation to it to convert it into a digital signal: [7]

$$\{f(t_i)\}_{i=1}^{\infty}$$

The Nyquist–Shannon sampling theorem states that a band-limited signal with a maximum frequency f_{max} can be perfectly reconstructed if the sampling frequency f_s is greater than or equal to twice f_{max}. This condition prevents aliasing and ensures accurate signal reconstruction.[7]

$$fs \geq 2.fmax$$

The other requirement of this theorem is that the samples be taken at equal intervals.
To understand sampling modes and oscilloscope acquisition, it is a necessary to understand sampling theory, the sampling rate, waveform distortion, wave aliasing. [7]

1.7.1 Sampling Rate

The sampling rate (or sampling frequency) is the number of measurements taken per second to convert an analog signal to digital, expressed in Hertz (Hz). The units for sample rate are samples per second **(sps)** or **Hertz (Hz)**.A higher sampling rate gives a more accurate version of the original signal. [8]

– **Waveform distortion:** When the sampling rate is too low, waveform as illustrated in **Figure 1.3** details are lost and the reconstructed signal differs from the original signal.

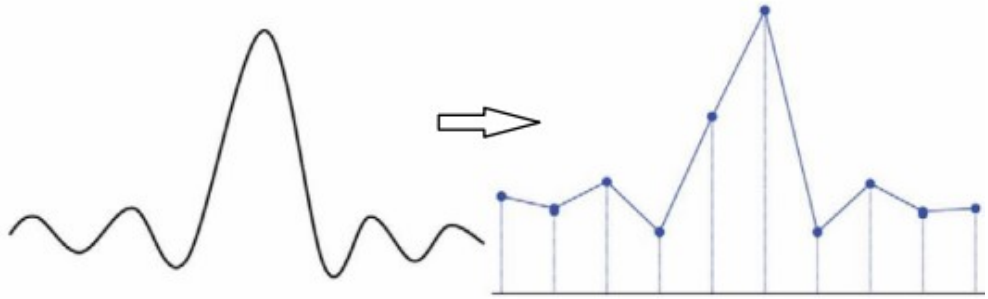


Figure 1.3: Waveform distortion

– **Waveform aliasing:** When the sampling rate is lower than twice the Nyquist frequency, the frequency of the reconstructed signal from the sample data is lower than the frequency of the original signal as illustrated in **Figure 1.4**

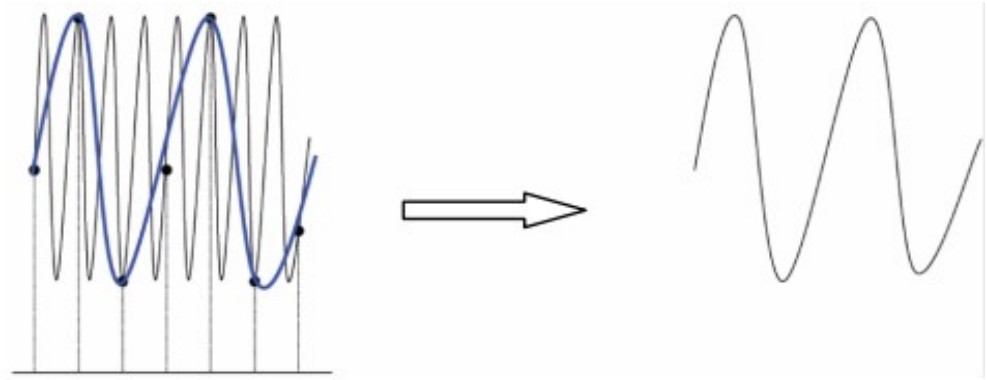


Figure 1.4: Waveform aliasing

1.7.2 Bandwidth Considerations

Building on the Nyquist–Shannon theorem established in the preceding section, the bandwidth of the acquisition chain must be carefully bounded to prevent aliasing. The Nyquist frequency of the system is $f_N = f_s/2 = 5.12\,\text{kHz}$; any spectral component above this limit is folded back into the baseband, corrupting the acquired spectrum irreversibly. In the specific case of a 50 Hz mains voltage signal, this condition is naturally satisfied: the spectral energy is concentrated in the harmonic orders up to the 40^{th} ($f_{\max} = 2\,\text{kHz}$), leaving the frequency band between 2 kHz and 5.12 kHz essentially unoccupied. It should be noted the sampling frequency of $10.24kHz$ adopted in this work results from the implementation choices made to satisfy the IEC 61000-4-7 measurement requirements while remaining compatible with the embedded FFT implementation. The complete design rationale is presented in chapter 2.

1.8 FFT (Fast Fourier Transform)

1.8.1 Fourier Transform

Any periodic signal, however complex its shape, can be decomposed into a sum of pure sinusoidal components, each characterised by a frequency, an amplitude, and a phase. This

fundamental result, established by Joseph Fourier in the early nineteenth century, states that the frequency content of a continuous signal $x(t)$ is described by its Fourier transform:

$$X(f) = \int_{-\infty}^{+\infty} x(t)\, e^{-j2\pi ft}\, dt \tag{1.6}$$

The Fourier transform thus converts a signal from the time domain, where it is described as a function of time, into the frequency domain, where it is described as a function of frequency. In the context of power quality analysis, this operation reveals which harmonic components are present in the mains voltage waveform and at what amplitudes, information that is not directly visible in the time-domain oscilloscope trace. However, the Fourier transform as defined above requires a continuous, infinite signal — conditions that cannot be met by any real measurement system.

1.8.2 Discrete Fourier Transform

In a digital acquisition system, the signal is not available as a continuous function of time but as a finite sequence of N samples $x[0], x[1], \ldots, x[N-1]$, acquired at a uniform sampling interval $T_s = 1/f_s$. The Discrete Fourier Transform (DFT) is the exact counterpart of the Fourier transform adapted to this discrete, finite representation. It computes N complex coefficients $X[k]$, each corresponding to a frequency $f_k = k \cdot \Delta f = k/NT_s$: [9]

$$X[k] = \sum_{n=0}^{N-1} x[n]\, e^{-j2\pi kn/N}, \quad k = 0, 1, \ldots, N-1 \tag{1.7}$$

Each coefficient $X[k]$ encodes the amplitude and phase of the sinusoidal component at frequency f_k present in the signal. The magnitude $|X[k]|$ directly gives the amplitude of that frequency component, which is the quantity of interest for harmonic analysis. [9]

The DFT is mathematically exact; its sole limitation is computational cost. Computing all N coefficients by direct application of the formula requires N^2 complex multiplications, a workload that becomes prohibitive for large N on embedded processors.

1.8.3 Fast Fourier Transform

The definition of FFT is the same as DFT, but the method of computation differs. The basics of FFT algorithms involve a divide-and-conquer approach in which an N-point DFT is divided into successively smaller DFTs. Many FFT algorithms have been developed, such as radix-2, radix-4, and mixed radix. [9]
In most FFT algorithms, restrictions may apply. For example, a radix-2 FFT restricts the number of samples in the sequence to a power of two. [10], [9].
In addition, some FFT algorithms require the input or output to be re-ordered. For example, the radix-2 algorithm requires the output to be bit-reversed.[10], [9].
It is up to implementers to choose the FFT algorithm that best fits their application. [10]

When using the CMSIS-DSP library on STM32, the bit-reversal operation is handled automatically by the FFT functions. Therefore, the output spectrum is returned in the correct frequency order, and no additional data reordering is required in the application code.

The computational advantage of the FFT over the direct DFT is quantified by two separate operation counts, since complex multiplications and complex additions have different costs on a processor: [10]

Number of points N	Direct computation of the DFT		Radix-2 FFT	
	Complex multiplies	Complex additions	Complex multiplies	Complex additions
N	N^2	N^2-N	$\frac{N}{2}\log_2 N$	$N\log_2 N$
4	16	12	4	8
16	256	240	32	64
64	4 096	4 032	192	384
256	65 536	65 280	1 024	2 048
1024	1 048 576	1 047 552	5 120	10 240

Table 1.1: Comparison of computational complexity for direct computation of the DFT versus the radix-2 FFT algorithm. [10]

$$\underbrace{N^2}_{\text{DFT}} \longrightarrow \underbrace{\frac{N}{2}\log_2 N}_{\text{FFT}} \tag{1.8}$$

$\log_2$: The binary logarithm can also be expressed using the natural logarithm as:

$$\log_2(x) = \frac{\ln(x)}{\ln(2)}$$

For $N = 1024$, the number of complex multiplications required by the direct DFT is:

$$N^2 = 1024^2 = 1\,048\,576$$

Such a workload is prohibitive for real-time embedded systems. The Cooley–Tukey FFT reduces this to:

$$\frac{N}{2}\log_2 N = \frac{1024}{2} \times \log_2(1024) = 512 \times 10 = 5\,120$$

It is this reduction — from $O(N^2)$ to $O\left(\frac{N}{2}\log_2 N\right)$ for multiplications and from $O(N^2)$ to $O(N\log_2 N)$ for additions — that makes real-time spectral analysis feasible on the STM32H7 within the 200 ms acquisition window imposed by IEC 61000-4-7.

The constraint that N must be a power of two ($N = 2^k$) is therefore not an arbitrary convention but a mathematical requirement of the radix-2 decomposition: the algorithm relies on the ability to split the transform length exactly in half at every recursion level. [11]

Data Types in FFT Computation

FFT algorithms are classified according to the nature of their input signal, as this directly determines the symmetry properties of the resulting spectrum and the computational savings that can be exploited: [11]

- **Complex data:** both real and imaginary parts are non-zero. No symmetry can be assumed; the full N-point FFT is required. [11]
- **Real data:** the input consists of real values only, with no imaginary part. The resulting spectrum satisfies Hermitian symmetry ($X[N-k] = X^*[k]$), allowing only $N/2$ bins to be computed. [11]

- **Real symmetric data:** the input is both real and symmetric in time ($x[n] = x[N-n]$), yielding a purely real spectrum. Only $N/4$ operations are required, as implemented by the DCT algorithm. [11]

The mains voltage signal acquired in this project falls into the second category: it is real-valued but not symmetric in time, since harmonic distortion, noise, transients, and DC offset all break time-domain symmetry. The RFFT is therefore the appropriate algorithmic choice, as detailed in the following section.

1.8.4 Real FFT

The FFT as described above accepts complex-valued input sequences (e.g., radar IQ signals). In practice, the acquired voltage signal is a purely real-valued discrete sequence: every sample $x[n]$ is a real number with no imaginary part. Applying the standard complex FFT to such a signal treats the imaginary part as identically zero, performing twice the necessary arithmetic.
A fundamental theorem of signal processing — the Hermitian symmetry property — states that the DFT of any real-valued sequence satisfies:

$$X[N-k] = X^*[k] \tag{1.9}$$

where $X^*[k]$ denotes the complex conjugate of $X[k]$. This means that the second half of the spectrum ($k = N/2+1$ to $N-1$) is entirely redundant: it carries no additional information beyond what is already contained in the first half ($k = 0$ to $N/2$). The Real FFT (RFFT) exploits this symmetry by computing only the $N/2+1$ independent complex coefficients, discarding the redundant conjugate half. [12]
For $N = 2048$, this reduces the number of useful output coefficients from 2048 to 1025, yielding a factor-of-two reduction in both computation time and output buffer memory — a significant advantage on a resource-constrained embedded target such as the STM32 microcontroller used in the present work.

1.8.5 Mathematical and Computational Co-Design

The selection of the analytical tools deployed in this work is not merely a software implementation detail; it reflects a deliberate co-design methodology in which the mathematical formulation and the hardware constraints of the target platform are treated as a unified optimisation problem. This methodology follows a top-down approach: starting from the normative requirements of IEC 61000-4-7, each design decision — the transform length, the algorithmic variant, and the memory layout — is derived systematically rather than chosen empirically, ensuring full traceability from specification to implementation.

Concretely, a naive application of the full complex DFT to a real-valued voltage signal would allocate half the available computation to redundant conjugate-symmetric bins, a waste that is theoretically unjustified and practically unacceptable on a resource-constrained microcontroller. By substituting the Real FFT in place of its general-purpose counterpart, the transform length presented to the Cooley–Tukey butterfly engine is effectively halved, reducing both the arithmetic workload from $O(N \log N)$ complex multiplications to $O(\frac{N}{2} \log \frac{N}{2})$ and the memory footprint of the output buffer by a factor of two. [11]
This gain directly translates into a shorter processing latency per 200 ms frame and frees the Cortex-M7 FPU pipeline for the subsequent magnitude extraction and THD accumulation

loops. The method is further validated by the application constraint $N = 2048$, whose origin is detailed in Chapter 2: at this transform length, the cycle budget saved by the RFFT is sufficient to complete the entire spectral analysis — FFT, harmonic extraction, and THD computation — well within the 200 ms acquisition window, ensuring that no frame is ever dropped and that the instrument operates as a true real-time analyser.

The convergence of mathematical rigour, algorithmic efficiency, and hardware awareness at every stage of this methodology is what distinguishes a principled embedded measurement system from an implementation driven solely by convenience.

1.9 Total Harmonic Distortion (THD)

The Total Harmonic Distortion (THD) is a key indicator used in power quality analysis to quantify the distortion of a periodic waveform relative to its fundamental component:

$$\text{THD} = \frac{\sqrt{\sum_{h=2}^{H} V_h^2}}{V_1} \times 100\%, \tag{1.10}$$

where V1 is the RMS amplitude of the fundamental frequency, Vh is the RMS amplitude of the h-th harmonic, and H is the highest harmonic order considered.
The Individual Harmonic (IH) of order h is defined as the ratio of the h-th harmonic voltage component to the fundamental voltage:

$$IH_h = \frac{V_h}{V_1} \times 100\% \tag{1.11}$$

1.9.1 IEEE 519-2022 Standard for Harmonic Control

The IEEE 519-2022 standard, entitled *"IEEE Standard for Harmonic Control in Electric Power Systems"*, represents the most recent revision of the IEEE guidelines concerning harmonic management in electrical power networks. Published in 2022, it supersedes the IEEE 519-2014 edition and establishes recommended practices and requirements for controlling harmonic distortion in order to ensure the reliable and efficient operation of modern power systems. For example in an industrial context, the PCC generally corresponds to the Point of delivery of the facility, namely the secondary terminals of the main step-down transformer supplying the plant. [13], [6]
The principal objective of this standard is to limit the propagation of harmonic currents and voltages within the electrical grid, thereby preserving power quality and maintaining electromagnetic compatibility between utility providers and end-users. To achieve this objective, IEEE 519-2022 defines maximum permissible levels for voltage and current harmonic distortions, measured at the *Point of Common Coupling (PCC)*, which corresponds to the interface between the utility network and the customer's installation. [13]
The standard introduces several key indicators used for harmonic assessment: [13]

- **Voltage Harmonics:** Harmonic components superimposed on the fundamental voltage waveform.
- **Current Harmonics:** Harmonic currents injected into the electrical network by nonlinear loads.

- **Total Harmonic Distortion (THD):** The ratio between the root-mean-square (RMS) value of all harmonic components and the RMS value of the fundamental component.

1.10 RMS calculations

1.10.1 RMS Voltage Measurement

The RMS value of the sampled waveform is calculated by the following equation:

$$V_{rms} = \sqrt{\frac{1}{N}\sum_{n=0}^{N-1}|v(n)|^2} \tag{1.12}$$

where:

- V_{rms} : Root Mean Square value of the voltage signal *[V]*
- N : Total number of samples per period (window length)
- $v(n)$: Discrete voltage sample at index *n [V]*
- n : Sample index, $n = 0, 1, 2, \ldots, N-1$

1.10.2 RMS Current Measurement

The current transducer is connected to the input DAQ Card. The device will sample the signal and the current RMS is computed using the equation as:

$$I_{rms} = \sqrt{\frac{1}{N}\sum_{n=0}^{N-1}|i(n)|^2} \tag{1.13}$$

where:

- I_{rms} : Root Mean Square value of the current signal *[A]*
- N : Total number of samples per period
- $i(n)$: Discrete current sample at index *n [A]*
- n : Sample index, $n = 0, 1, 2, \ldots, N-1$

1.10.3 Power Measurement

Active energy

Active energy, expressed in kilowatt-hours (kWh), represents the portion of electrical energy that is effectively converted into useful work by the load, whether in the form of heat, mechanical work, or light. It directly characterizes the active power consumed by the installation over a given period of operation, according to the following relation:

$$P = \frac{W}{1\,\mathrm{h}} \quad [\mathrm{kW}] \tag{1.14}$$

$$P = \frac{1}{N} \sum_{n=0}^{N-1} v(n)\, i(n) \tag{1.15}$$

Reactive energy

Reactive energy, expressed in kilovolt-ampere reactive hours (kVArh), is derived from reactive power and plays no direct role in the conversion of electrical energy into useful work. Its primary function lies in the establishment and sustenance of rotating magnetic fields within inductive devices, which is an essential requirement for the operation of numerous industrial equipment. [14]
The principal consumers of reactive energy in industrial installations include: Power measurements consist of real power, reactive power, apparent power and power factor. These can be calculated as follows: [14]

- **Asynchronous (induction) motors**, which require reactive power to generate and maintain their rotating magnetic field;
- **Power transformers**, whose magnetizing inductance draws reactive current even under no-load conditions;
- **Static power converters**, including rectifiers and AC/DC converters, which generate reactive current due to their nonlinear switching characteristics.

Unlike active energy, reactive energy does not appear as useful output at the load terminals; however, it circulates between the source and the load, increasing the apparent current in the distribution network and thereby causing additional Joule losses, voltage drops, and overloading of network equipment.
where: [14]

- P : Active (real) power *[W]*
- $v(n)$: Instantaneous voltage sample at index n *[V]*
- $i(n)$: Instantaneous current sample at index n *[A]*
- N : Total number of samples per period

$$Q = \sqrt{S^2 - P^2} \tag{1.16}$$

And:

$$S = |V_{rms}| \cdot |I_{rms}| \tag{1.17}$$

where:

- Q : Reactive power *[VAR]*
- S : Apparent power *[VA]*

1.10.4 Power Factor

The power factor (pf) is a dimensionless quantity defined as the ratio of the active power P consumed by a load to the apparent power S supplied by the source. It constitutes a fundamental indicator of the efficiency with which electrical energy is converted into useful work within an electrical installation. Mathematically, it is expressed as: [14]

$$pf = \frac{P}{S} = \frac{P}{\sqrt{P^2 + Q^2}} \tag{1.18}$$

The power factor takes values in the range $[0,\ 1]$, where a unity value ($pf = 1$) indicates a purely resistive load in which all supplied power is entirely converted into active power, and a value approaching zero characterizes a highly reactive load where a significant portion of the current circulates without performing useful work, thereby increasing reactive power Q and causing unnecessary losses in the distribution network.

Physical Interpretation

From a physical standpoint, a low power factor implies that the electrical network must carry a current substantially higher than strictly necessary to supply the required active power. This excess current induces additional Joule losses in conductors and transformers, voltage drops along feeders, and premature aging of network equipment, ultimately degrading the overall power quality of the distribution system.

1.10.5 Regulatory Framework: Sonelgaz Billing Policy

In the context of the Algerian electrical distribution network, the national utility *Sonelgaz* (Société Nationale de l'Électricité et du Gaz) enforces a regulatory threshold on the power factor for industrial consumers, in accordance with the national energy regulation framework. [14]. The applicable rule is as follows:

- If the power factor of the industrial installation satisfies the condition: [14]

  $$pf \geq 0.894 \tag{1.19}$$

  the industrial consumer is considered to be operating within acceptable reactive power limits. In this case, *Sonelgaz* applies no reactive energy surcharge, and the consumer benefits from standard billing conditions. [14]

- Conversely, if:

  $$pf < 0.894 \tag{1.20}$$

  the industrial installation is deemed to absorb an excessive amount of reactive power from the distribution network. Under this condition, *Sonelgaz* applies a **reactive energy penalty** to the consumer's electricity bill, proportional to the quantity of reactive energy consumed beyond the authorized limit. [14]

This regulatory mechanism incentivizes industrial consumers to install reactive power compensation devices, such as capacitor banks, in order to maintain their power factor above the prescribed threshold, thereby reducing both their energy costs and their impact on the quality of the public distribution network.

1.11 Acceptable limits

1.11.1 Voltage Unbalance Limits

Most international standards and documents are in agreement on the definition of the unbalance phenomenon and its parameters. Compatibility levels for LV and MV systems are 2% and under special conditions 3%. No separate specifications for HV networks are given in most analyzed documents, except for the document [15], in which a method of assessment of voltage unbalance is included for a network node to which an unbalanced load is connected, depending on the power of this load and the short-circuit power of the network.

1.11.2 Acceptable THD limits

According to IEEE 519-2022, the permissible voltage distortion limits depend on the nominal voltage level, as summarized in Table 1.2. [6]

Table 1.2: IEEE 519-2022 Recommended Voltage Distortion Limits at the PCC

Bus Voltage at PCC	Individual Harmonic	Maximum THD
$V \leq 1\,\text{kV}$	5%	8%
$1\,\text{kV} < V \leq 69\,\text{kV}$	3%	5%
$69\,\text{kV} < V \leq 161\,\text{kV}$	1.5%	2.5%
$V > 161\,\text{kV}$	1%	1.5%

Unlike voltage distortion limits, current harmonic limits are determined according to the short-circuit ratio of the electrical system.
The short-circuit ratio R_{sc} is defined as:

$$R_{sc} = \frac{I_{SC}}{I_L} \tag{1.21}$$

where I_{SC} is the maximum available short-circuit current at the PCC, and I_L is the maximum demand load current.

It should be noted that a power system with a higher short-circuit capacity can generally withstand larger harmonic current injections without significantly affecting the overall voltage quality.

1.11.3 Acceptable Limits for Voltage Disturbances

There is no single international standard that specifies universally acceptable limits for voltage sags and swells. IEEE 1159 presented in chapter 02, defines the characteristics of these disturbances, such as their magnitude and duration, but does not establish thresholds indicating whether a disturbance is acceptable or unacceptable for all applications. The acceptable limits depend on the sensitivity of the connected equipment and the specific industrial application.

To evaluate the tolerance of electrical and electronic equipment, the **ITIC (Information Technology Industry Council) curve**, formerly known as the **CBEMA** curve as illustrated

in **Figure 1.5**, is widely used. Rather than defining power system quality requirements, this curve represents the operating tolerance envelope of information technology equipment (ITE) subjected to voltage variations.

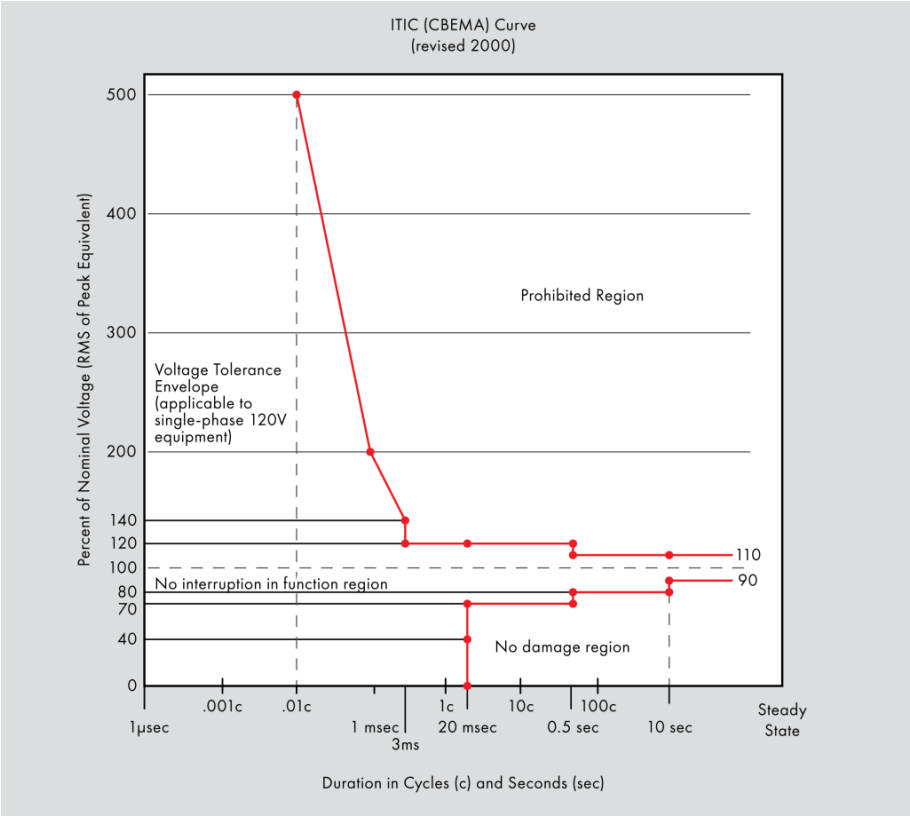


Figure 1.5: ITIC curve is a modified version of the CBEMA curve.

Commercial power quality analyzers generally separate the classification of disturbances from the decision thresholds used to detect and record them. Their operating principle can be summarized as follows:

- IEEE Std 1159 is used to identify and classify voltage disturbances according to their magnitude and duration.
- The voltage thresholds used for event detection (e.g., 90%, 80%, 70%, 110%, or 120% of the nominal voltage) are typically user-configurable, allowing the analyzer to be adapted to different network conditions and equipment sensitivities.
- Any disturbance exceeding the configured thresholds is detected, recorded, and stored for subsequent analysis.

This approach provides flexibility for different industrial environments while maintaining compliance with internationally recognized disturbance classification standards.

1.12 Key Measurement Concepts

A result will be judged or compared with others and will lead to a decision, e.g. pass versus fail, accept versus reject, successful measurement depends on a sound understanding of basic metrology concepts.

- **Accuracy:** Accuracy is a measure of how close a measured value of a variable is to its true value.
- **Precision:** Precision is a measure of the extent to which independent measurements of the same variable agree when using the same measuring device and procedure
- **Measurement uncertainty:** Measurement uncertainty is a statistical parameter which describes the possible fluctuations of the result of a measurement.

1.13 Conclusion

This chapter has established the theoretical foundations required for the design and Implementation of an Industrial Oscilloscope for Electrical Signal Monitoring. The principal power quality disturbances, their origins, consequences, and standardized evaluation methods were reviewed, highlighting the importance of continuous monitoring in modern electrical networks. The chapter also introduced the fundamental concepts of signal acquisition, sampling theory, analog-to-digital conversion, digital signal processing, FFT-based harmonic analysis, THD evaluation, RMS computation, power measurement, and electrical safety.

Together, these concepts provide the scientific basis for selecting appropriate hardware and implementing reliable measurement algorithms that comply with international standards. Building upon this theoretical background, the next chapter focuses on the engineering design of the proposed system, including the adopted standards, hardware architecture, component selection, signal-conditioning circuits, protection mechanisms, and implementation strategy.

Chapter 2

System Specifications and Engineering Design

2.1 Introduction

The first chapter established the theoretical foundations of power quality by introducing the main electrical disturbances, the relevant international standards, and the signal processing techniques commonly employed for power quality monitoring and analysis.
Building upon this background, the present chapter translates these theoretical concepts into engineering specifications and design decisions. It begins by defining the applicable measurement standards and methodologies that govern the proposed instrument, followed by the selection and justification of the hardware and software components, including the microcontroller, sensing circuits, communication interface, signal processing algorithms, and mobile application architecture.

Finally, the chapter presents the PCB design and discusses the practical constraints encountered during the engineering process. The resulting system architecture establishes the foundation for the implementation, experimental evaluation, and metrological validation presented in the following chapter.

2.1.1 IEEE 1159 Standard Definition

The **IEEE 1159** standard (*IEEE Recommended Practice for Monitoring Electric Power Quality*), in its most recent revision (2019) [16], constitutes the primary international normative reference for the characterisation and classification of electromagnetic phenomena affecting alternating current power supply systems. It defines power quality disturbances in terms of *magnitude* — expressed in per-unit (pu) relative to the nominal voltage — and *duration* — expressed in cycles of the fundamental frequency or in time units.

According to this standard, short-duration RMS variations encompass voltage sags, voltage swells, and interruptions, each subdivided into three temporal sub-categories: [17]

- **Instantaneous**: 0.5 to 30 cycles
- **Momentary**: 30 cycles to 3 s
- **Temporary**: 3 s to 1 min
- **Long-duration variations**: sustained undervoltage and overvoltage, refer to deviations of the RMS voltage persisting beyond **1 minute**.

Table 2.1 summarizes the classification of voltage disturbances defined in IEEE 1159 for a 220 V_{RMS}, 50 Hz power system. [17]

Table 2.1: Classification of voltage disturbances according to IEEE 1159 (220 V_{rms} / 50 Hz network)

Event	**Magnitude (pu)** **[Volts rms, $V_n = 220$ V]**	**Duration**
Short-Duration Variations Voltage Sags		
Instantaneous	0.10 – 0.90 (22 – 198 V)	0.5 – 30 cycles (10 – 600 ms)
Momentary	0.10 – 0.90 (22 – 198 V)	30 cycles – 3 s (600 ms – 3 s)
Temporary	0.10 – 0.90 (22 – 198 V)	3 s – 1 min
Short-Duration Variations Voltage Swells		
Instantaneous	1.10 – 1.80 (242 – 396 V)	0.5 – 30 cycles (10 – 600 ms)
Momentary	1.10 – 1.40 (242 – 308 V)	30 cycles – 3 s (600 ms – 3 s)
Temporary	1.10 – 1.20 (242 – 264 V)	3 s – 1 min
Long-Duration Variations		
Undervoltage	0.80 – 0.90 (176 – 198 V)	$>$ 1 min
Overvoltage	1.10 – 1.20 (242 – 264 V)	$>$ 1 min

Note: Cycle-based durations are computed for a 50 Hz fundamental frequency (1 cycle = 20 ms). Voltage values in volts are derived from $V = \text{pu} \times V_n$, with $V_n = 220\,V_{rms}$.

2.2 IEC 61000-4-30 standard

Power quality refers to a set of electrical boundaries defined by various documented rules designed to allow electrical equipment to function in its intended manner without significant loss of performance or life expectancy. This includes the steady and stable supply of electricity delivered by the grid. In order to achieve this goal it is necessary to constantly and vigilantly monitor the power conditions within an electrical network. There is a large number of parameters involved in this, but surprisingly, many power quality parameters have not been well defined which forced leading power monitoring device manufactures to develop their own methodologies resulting in incomparable values and rules between different instruments. This where the IEC 61000-4-30 comes in; it standardizes the measurement methodologies and creates the ability to directly compare results from different analyzers.

[18]

The IEC 61000-4-30 standard defines the measurement method, accuracy and time aggregation to variety of power quality parameters in 3 performance classes to obtain repeatable and comparable results.

2.2.1 Power quality parameters defined in the standard

Following are the parameters defined in the IEC 61000-4-30 standard: [18]

- Power frequency
- Magnitude of supply voltage
- Flicker (by reference to IEC 61000-4-15)
- Supply dips/swells
- Voltage Interruptions
- Voltage unbalance
- Voltage harmonics (by reference to IEC 61000-4-7)
- Voltage Inter-harmonics (by reference to IEC 61000-4-7)
- Mains signaling
- Under- and over-deviation

In the 3rd addition the following parameter was introduced: [18]

- Rapid voltage changes
- Flicker class F1
- Magnitude of the current
- Current unbalance
- Current harmonics (by reference to IEC 61000-4-7)
- Current interharmonics (by reference to IEC 61000-4-7)
- Recording of current along with voltage during events

The scope of this thesis is limited to the implementation of a selected subset of the power quality parameters defined in IEC 61000-4-30. The implemented parameters include the magnitude of the supply voltage (RMS voltage), supply voltage dips and swells, rapid voltage changes (RVC), voltage harmonics, voltage unbalance, and the magnitude of the current (RMS current).

This selection was primarily motivated by the time constraints of the project and by the fact that these parameters are among the most widely used indicators for detecting the most

common power quality disturbances in industrial power systems.

Furthermore, each parameter requires a comprehensive study of the relevant IEC and IEEE standards, as well as the associated scientific literature, to ensure that the adopted measurement methods, signal processing techniques, and event detection algorithms are fully compliant with internationally recognized standards. Since power quality assessment is a highly standardized and metrologically sensitive field, particular attention was given to implementing a limited number of parameters with rigorous conformity rather than attempting to cover all parameters defined by the standard.

2.3 Measurement Methodologies

2.3.1 IEC 61000-4-7: Measurement Methodology for Harmonic Analysis

While IEC 61000-2-2 and IEEE 519 specify the acceptable harmonic distortion levels, IEC 61000-4-7 defines the standardized measurement procedure for harmonics and interharmonics in 50 Hz and 60 Hz power systems. [18]

The standard entitled **Electromagnetic Compatibility (EMC) – Part 4-7: Testing and Measurement Techniques – General Guide on Harmonics and Interharmonics Measurements and Instrumentation** specifies the measurement methodology without imposing harmonic distortion limits, which are addressed by other standards. [18]

For a nominal power-system frequency of 50 Hz, the observation interval is defined as ten consecutive fundamental cycles, while twelve cycles are used for a 60 Hz system, resulting in an observation window of approximately 200 ms in both cases, as illustrated in Figure 2.1. [18]

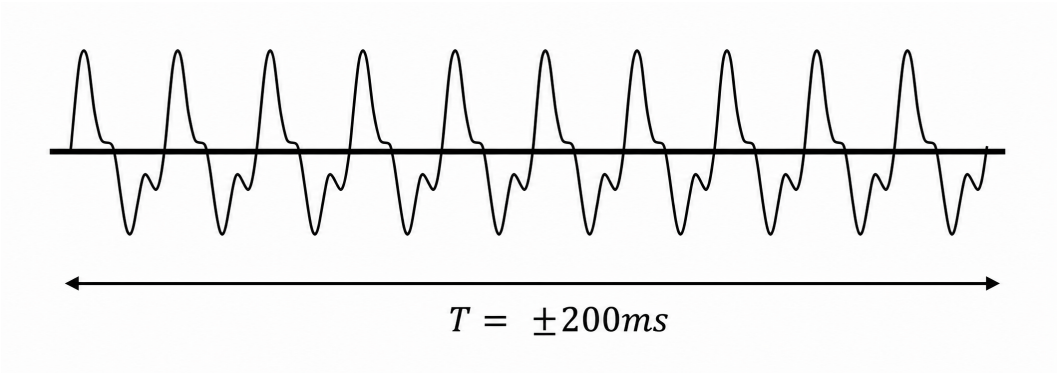


Figure 2.1: Analysis window according to IEC 61000-4-7.

Furthermore, consecutive observation windows must be contiguous without any temporal gaps to ensure continuous harmonic monitoring. [18]

2.3.2 Rectangular Windowing

According to IEC 61000-4-7, harmonic analysis shall be performed using a rectangular window over the complete observation interval. This standardized windowing method ensures consistent harmonic measurements and allows direct comparison between different measuring instruments. [18, 19]

$$w[n] = 1, \qquad n = 0, 1, \ldots, N-1 \tag{2.1}$$

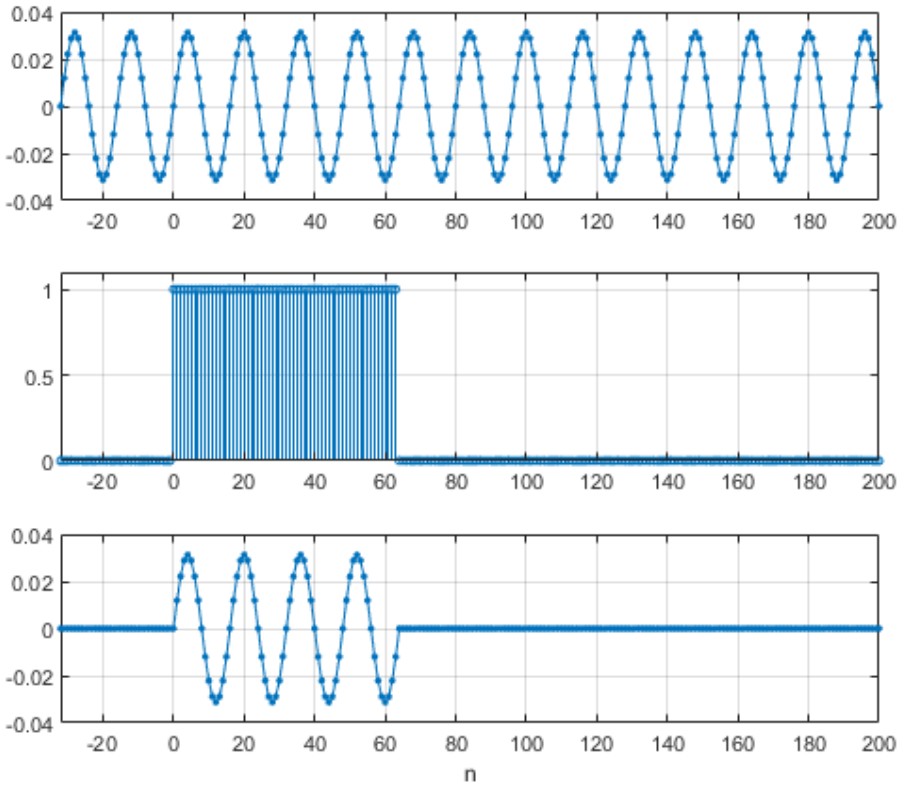


Figure 2.2: Rectangular window function.

In the STM32 implementation, no explicit window multiplication is required since the rectangular window as illustrated in **Figure 2.2** is equivalent to multiplying every sample by one. Consequently, the acquired samples are directly processed by the CMSIS-DSP `arm_rfft_fast_f32()` routine, minimizing the computational overhead.

2.3.3 Sampling Parameter Selection

IEC 61000-4-7 specifies an observation window of

$$T = 200 \text{ ms}$$

for a 50 Hz power system, corresponding to ten complete fundamental cycles. This observation interval determines the FFT frequency resolution as

$$\Delta f = \frac{1}{T} = \frac{1}{0.2} = 5 \text{ Hz}. \tag{2.2}$$

Consequently, each FFT frequency bin represents a multiple of 5 Hz, such that

$$f_k = k\Delta f = k \times 5 \text{ Hz}.$$

For a 50 Hz system, the fundamental component and all integer harmonics therefore coincide with FFT frequency bins:

- $k = 10$ corresponds to 50 Hz,
- $k = 20$ corresponds to 100 Hz,
- $k = 30$ corresponds to 150 Hz.

The sampling frequency is not prescribed by IEC 61000-4-7. In this work, it was selected as

$$f_s = 10.24 \text{ kHz},$$

to satisfy the required observation interval while remaining compatible with the embedded radix-2 FFT implementation introduced in Chapter 1.
The corresponding transform length is therefore

$$N = f_s T = 10240 \times 0.2 = 2048 \text{ samples}. \tag{2.3}$$

Since

$$2048 = 2^{11},$$

the selected transform length is directly compatible with the radix-2 Cooley–Tukey FFT algorithm while maintaining a reasonable computational complexity for the STM32H743 microcontroller.

Because the acquired signal is real-valued, the CMSIS-DSP Real FFT (RFFT) implementation is employed instead of the complex FFT, reducing both execution time and memory requirements while producing an identical frequency spectrum.

With the selected sampling parameters,

$$\frac{f_s}{f_0} = \frac{10240}{50} = 204.8$$

samples are acquired during each fundamental cycle. Consequently,

$$\frac{N}{204.8} = \frac{2048}{204.8} = 10$$

complete cycles are contained within every acquisition window, ensuring coherent sampling over the entire 200 ms observation interval.

Harmonic Subgrouping

To improve the robustness of harmonic measurements against small variations of the fundamental frequency, which may cause harmonic energy to spread over adjacent FFT frequency bins, IEC 61000-4-7 introduces the concept of harmonic subgrouping. Instead of estimating the magnitude of a harmonic from a single frequency bin, the standard defines the harmonic subgroup as the root-sum-square (RSS) of the frequency bins surrounding the harmonic. In its general form, the harmonic subgroup RMS amplitude is defined as: [20], [21]

$$G_{sg,n} = \sqrt{\sum_{i=-1}^{1} \left| X\left(n\frac{f_0}{\Delta f} + i \right) \right|^2}, \tag{2.4}$$

where $X(\cdot)$ represents the FFT spectrum, f_0 is the fundamental frequency, and Δf is the FFT frequency resolution.

In the proposed implementation, the FFT is computed over a 200 ms window, resulting in a frequency resolution of $\Delta f = 5$ Hz. Since the nominal fundamental frequency is $f_0 = 50$ Hz, the centre bin of the n-th harmonic is located at

$$k = n\frac{f_0}{\Delta f} = n \times 10.$$

Therefore, the harmonic subgroup calculation implemented in the STM32 firmware becomes: [20], [21]

$$G_{sg,n} = \sqrt{|X[k-1]|^2 + |X[k]|^2 + |X[k+1]|^2}, \qquad k = n \times 10. \tag{2.5}$$

For example, the subgroup centred on the fundamental at 50 Hz includes the frequency coefficients at 45 Hz, 50 Hz, and 55 Hz. This grouping reduces the influence of: [20], [21]

- residual spectral leakage due to frequency drift,
- measurement noise on individual coefficients,
- inter-harmonic components falling between harmonic orders.

2.4 Instrument Classification According to Measurement Performance

The **IEC 61000-4-30** standard also establishes two classes for measurement devices: Class A and Class S.

2.4.1 Class A

Defines the highest level of accuracy and precision for the measurements of PQ parameters and is used for instruments requiring very precise measurements for contractual matters and dispute resolution. It is also applicable to the devices that need to verify compliance of the standard. [22]

2.4.2 Class S

Is used for PQ assessment, statistical analysis applications, and diagnostics of PQ problems with low uncertainty. The instrument in this class can report a limited subset of the parameters defined by the standard. The measurements made with Class S instruments can be done on several sites on a network, on complete locations or even on single pieces of equipment. [22]

2.4.3 Key Differences Between Class A and Class S

Although **Class A** defines higher levels of accuracy and precision than **Class S**, the differences are beyond just levels of accuracy. Instruments must comply with requirements such

as time synchronization, quality of probes, calibration period, temperature ranges, etc. **Table 2.2** presents a list of requirements that instruments shall meet to be certified in one or the other class. [22]

Table 2.2: IEC 61000-4-30 Class A and Class S Key Differences

	Class A	**Class S**
Voltage Measurement Accuracy	$\pm 0.1\%$	$\pm 0.5\%$
Current Measurement Accuracy	$\pm 1\%$	$\pm 2\%$
Voltage and Current rms Calculation	Half-cycle steps	One-cycle steps
Frequency Measurement Accuracy	± 10 mHz	± 50 mHz
150/180-Cycle Aggregation	No gaps permitted, synchronized with UTC 10 min tick	Gaps between aggregations allowed
Measurements of Harmonics up to Order	50^{th}	40^{th}
Time-Clock Uncertainty per 24 Hours	± 1 second	± 5 seconds
Time Synchronization	GPS receiver, radio timing signals or network timing signals	Not required
Operation Temperature Range	0°C to 45°C	Specified by manufacturer

The proposed oscilloscope is designed with the objective of achieving the measurement performance required for **Class A** power quality instruments.
However, compliance with the Class A requirements defined in IEC 61000-4-30 cannot be claimed based solely on the system design or implementation. It must be demonstrated through:
Experimental validation by comparing the measured results with those obtained from a calibrated reference instrument or a certified Class A power quality analyzer under identical operating conditions.

For this purpose, the developed PQA will first be evaluated using laboratory measurement instruments, while the final validation will be performed by comparison with a Schneider Electric PowerLogic PM8000 series power quality meter under the same operating conditions.

Table 2.3: Instruments used for experimental validation of the developed PQA

Instrument	**Reference**	**Parameters to be Verified**
Multimeter	Laboratory Multimeter	RMS voltage, RMS current, and frequency
Digital Oscilloscope	Tektronix TBS2000B	Waveform, peak voltage, frequency analysis, FFT, phase shift
Power Analyzer	Laboratory Power Analyzer	Active power, reactive power, apparent power, power factor, harmonics, and THD
Power Quality Meter	Schneider PowerLogic PM8000	Final comparison of RMS values, frequency, harmonics, THD, power quantities, power factor, and power quality disturbances

Therefore, the present work aims to establish the technical foundations for a Class A instrument, while the formal verification of compliance remains a subject for future validation and performance assessment.

2.5 System architecture

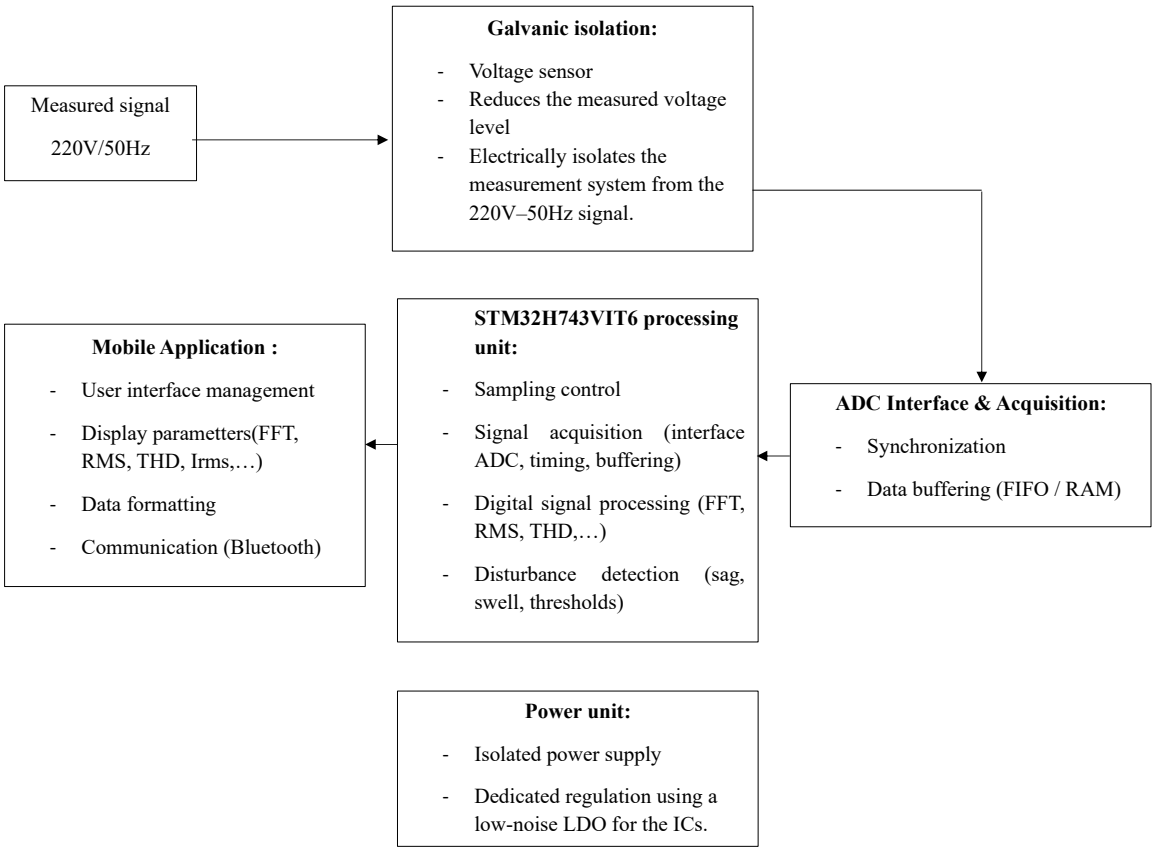


Figure 2.3: System block diagram

2.6 Microcontrollers selection

There is a vast ranges of microcontrollers models available to users. Indeed, multiple families are offered by different manufacturers, each comprising hunderds of distinct variants. Microcontrollers can be found in packages with as few six pins or more.
In order to select the appropriate microcontroller, several key features criteria should be considerd: [23]

- The number of input/output (I/O) pins
- Memory capacity: RAM and ROM
- Power consumption: operating voltage and current draw
- Suitablity of the internal architecture to the application requirements
- Developpement ecosystem: availability of hardware tools and software support.

Some of the current microcontroller families can be highlighted as follows:

- **8-bit microcontrollers:**
  - PIC: developed by the American company Microchip Technology, wich significantly contributed to the popularization of microcontrollers.
  - AVR: from Atmel, widely used in Arduino platforms.
- **16-bit microcontrollers:**
  - dsPIC: digital signal processing PIC from Microchip Technology.
  - MSP430: from Texas Instruments.
- **32-bit microcontrollers:**
  - AVR, PIC32, MIPS, PowerPC.
  - ARM: a processor architecture developed by the Britich company **Arm holdings**, which licenses its technology to numerous manufacturers to develop microcontrollers based on this architecture. These manufacturers include: NXP Semiconductors, STMicroelectronics, Texas Instruments, Samsung Electronics, Analog Devices, Infineon Technologies, and Freescale Semiconductors.

This is why ARM-based processors are currently the most widely used in the market.

2.6.1 ARM processors

The ARM stands for Advanced RISC Machine, Arm Holdings processors are 32-bit RISC architecture processors that continue to envolve. A wide range of ARM processors exists, distinguished by their architectures and cores, commonly referred to as ARM Cortex processors. These are classified into three main families: [23]

- **Cortex-A (Application):** This family is primarily designed for applications requiring complex computation and high processing capabilities, for example, the **Raspberry Pi** uses an ARM Cortex-A processor.

- **Cortex-R (Real-time):** This family target real-time systems, with processors characterized by high performance and deterministic response.

- **Cortex-M (Embadded):** Processors in this family are developed for microcontroller-based applications, offering low power consumption and reduced cost.

Within the Cortex-M Family, several models can be identified:

- **Cortex-M0/M1/M2:** Designed for general-purpuse processing and standard input/output tasks.

- **Cortex-M3:** Supports more advanced data processing and efficient bit-fiels manipulation.

- **Cortex-M4:** An extention of the Cortex-M3 with integrated DSP (digital signal processing) capabilities.

- **Cortex-M4F:** A Cortex-M4 core enhaned with an FPU (floating point unit) for efficient floating-point operations.

- **Cortex-M7:** The most advanced in this range, offering significantly higher performance.

2.7 STM32

STMicroelectronics is a company specialized in the design and development of solutions for a wide range of microelectronic applications. It provides a broad portfolio of electronic platforms, including the STM32H7 series of microcontrollers. Among these, the STM32H743VIT6 chip represents the key component of our project.

2.7.1 Selection Criteria

The microcontroller is the core processing unit of the proposed power quality analyzer, responsible for real-time data acquisition, digital signal processing (DSP), communication with peripherals, and graphical display management. Considering the computational requirements of FFT processing, high-speed sampling, and future integration of embedded artificial intelligence algorithms, the **STM32H743VIT6** from STMicroelectronics was selected. This microcontroller provides high computational performance while offering a wide range of peripherals suitable for industrial embedded systems. The developpement board used in this work is illustrated in **Figure 2.4**.



Figure 2.4: STM32H743VIT6 developpement board

The main characteristics that motivated the selection of the STM32H743VIT6 are:

- **Arm Cortex-M7:** 32-bit core operating at up to 480 MHz, providing high computational capability for real-time signal processing.
- **Double-precision Floating-Point Unit (FPU)and DSP instruction set:** Significantly accelerating FFT, filtering, RMS, THD, and other mathematical operations.
- **2 MB Flash memory and 1 MB RAM:** Allowing the implementation of complex firmware, graphical interfaces, communication stacks, and future AI models.
- **Multiple high-speed communication interfaces:** Including SPI, UART/USART, I²C, USB OTG, CAN FD, Ethernet, and SDMMC, enabling easy integration with the AD7606 ADC, TFT display, BLE module, and external storage.
- **Three 16-bit ADCs (up to 3.6 MSPS)**
- **Advanced DMA controllers:** That allow high-speed data transfers with minimal CPU intervention, which is essential for continuous real-time acquisition.
- **Numerous timers and PWM peripherals:** For precise sampling synchronization and system timing.

Although the computational requirements of the current engineering project could also be satisfied by a **lower-cost STM32F4-series microcontroller** (e.g., the STM32F407 or STM32F411), the STM32H743VIT6 was intentionally retained. The additional processing power, larger memory capacity, and enhanced DSP capabilities provide sufficient resources for the future integration of embedded machine learning and TinyML algorithms planned for the subsequent Master's thesis. Consequently, selecting the STM32H743VIT6 ensures hardware continuity between the engineering project and the future research work while avoiding a complete hardware redesign.

2.7.2 STM32 Development Tools and Software Environment

The development of embedded systems based on STM32 microcontrollers requires a software environment capable of simplifying peripheral configuration, code generation, debugging, and application development. In this project, the software environment was mainly based on STM32CubeMX and the STM32 HAL framework. These tools significantly reduce development complexity and accelerate the implementation process while ensuring **code portability** and **maintainability**.

STM32CubeMX:

CubeMX is the tool used to configure the microcontroller chosen for our project. It is used both to choose the right hardware connections and to generate the code necessary to configure the ST HAL. CubeMX is a MCU-centric application. This means that all activities performed by the tool are based on:

- The family of the STM32 MCU (F0, F1, and so on).
- The type of package chosen for our device (LQFP48, BGA144, and so on).
- The hardware peripherals we need in our project (USART, SPI, etc.).
- MCU general configurations (like clock, power management, NVIC controller, and so on)

The figure **2.5** illustrates the clock tree configuration of the STM32H743VIT6 microcontroller. This is the simplest way to deal with the STM32 clock configuration . It also reduces configuration errors while ensuring proper synchronization between the different system and peripheral clocks.

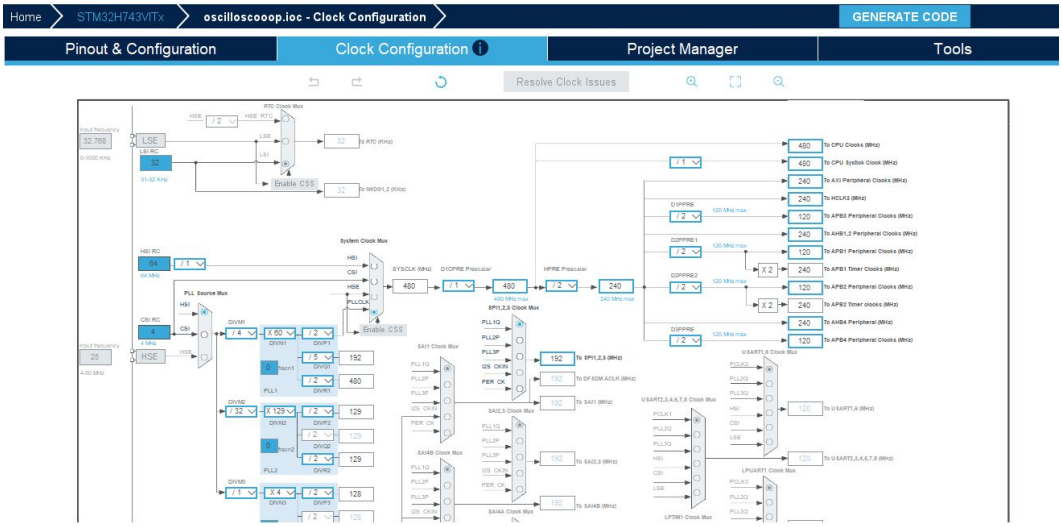


Figure 2.5: CubeMX clock view

In addition to features related to the hardware, CubeMX is also able to deal with the following software aspects:

- Management of the ST HAL for the chosen MCU family.

- Additional software library functionalities we need in our project (FatFs library, FreeRTOS, etc.).
- The development environment we will use to build the firmware

Hardware Abstraction Layer:

The HAL library provides a high-level programming interface for controlling the peripherals of the microcontroller without requiring direct manipulation of hardware registers. Instead of configuring registers manually, the developer can use standardized functions and APIs provided by the HAL drivers. This abstraction improves code readability, portability, and maintainability, especially in complex embedded applications involving multiple peripherals operating simultaneously.

Peripheral parameters configured in STM32CubeMX are automatically translated into HAL initialization routines, ensuring consistency between hardware configuration and software implementation.

2.7.3 Direct memory access controller (DMA)

DMA controller is a dedicated and programmable hardware unit that allows MCU peripherals to access to internal memories without the intervention of the Cortex-M core. The CPU is completely freed from the overhead generated by the data transfer (except for the overhead related to the DMA configuration), and it can perform other activities in parallel[1]. The DMA is designed to work in both the ways (that is, it allows data transfer from memory to peripheral and from perepheral to memory), and all STM32 microcontrollers provide at least one DMA controller, but the most of them implement two independent DMAs. [24]

DMA Features

- **Increased performance:** Frees CPU to perform other tasks, reduicing latency.
- **Real time data processing:** Essential for application requiring fast data acquisition.
- **Power efficiency:** Reduces CPU wake-up cycles, lowering power consumption.
- **Multiple channels:** Supports multiple data streams simultaneously.
- **Flexible configuration:** Configurable for various peripheral-to-memory and memory-to-memory transfers.

Applications of DMA in embedded systems

- **Data acquisition systems:** Fast data transfer from sensors to memory.
- **Audio/Video streaming:** Continuous data flow management without CPU delays.
- **Communication Protocols:** Efficient handling of UART, SPI, and I2C data transfers.

DMA transactions

A DMA transaction consists of a sequence of a given number of data transfers. The number of data items to be transferred and their width (8-bit, 16-bit or 32-bit) are software programmable. [24]
Each DMA transfer consists of three operations: [24]

- A loading from the peripheral data register or a location in memory.
- A storage of the data loaded to the peripheral data register or a location in memory.
- A post-decrement of the DMA_SxNDTR register, containing the number of transactions that still have to be performed

DMA source and destination

The DMA controller performs direct memory transfers from a single source address to a single destination address, with no built-in logic or arithmetic capability, making it unsuitable for data reconstruction that requires reading and combining multiple independent registers. [24]

Table 2.4: Available DMA transfer directions

DMA transfer direction	Description
`DMA_PERIPH_TO_MEMORY`	Peripheral to memory direction
`DMA_MEMORY_TO_PERIPH`	Memory to peripheral direction
`DMA_MEMORY_TO_MEMORY`	Memory to memory direction

Transfer modes

The DMA controller in STM32 MCUs has two working modes: DMA_NORMAL and DMA_CIRCULAR.

- **DMA_NORMAL:** In normal mode the DMA sends the specified amount of data from source to destination port and stops the activities. It must be re-armed again to do another transfer. [24]

- **DMA_CIRCULAR:** In circular mode, at the end of transmission, it automatically resets the transfer counter and starts transmitting again from the first byte of source buffer (that is, it treats the source buffer as a ring buffer). This mode is also called continuous mode, and it is the only way to achieve really high transmission speed in some peripheral (e.g. high speed SPI devices). [24]

2.8 Voltage sensor

Initially, a conventional **220 V/9 V step-down transformer**, with an approximate turns ratio of **24:1**, was selected for voltage acquisition. This solution provided a bipolar output of approximately **±9 V**, which could be directly interfaced with the bipolar **AD7606** ADC, thereby eliminating the need for an additional signal-conditioning stage to shift the AC waveform into the positive voltage range required by unipolar ADCs. However, after discussing

the design with professors, it became evident that conventional power transformers are primarily intended for power transfer rather than voltage measurement. Their large turns ratio, combined with the magnetizing and leakage inductances, results in a limited frequency response that attenuates high-frequency components and fast voltage transients. Consequently, the measured waveform may not accurately represent instantaneous voltage spikes and other power quality disturbances occurring on the mains network.

To overcome this limitation, the conventional transformer was replaced by the **ZMPT101B** voltage sensor. Unlike a standard power transformer, the ZMPT101B incorporates a miniature **1:1 turns-ratio** measurement transformer, where the voltage scaling is achieved through external current-limiting and signal-conditioning circuitry rather than by the transformer itself. This architecture preserves galvanic isolation while providing an analog signal proportional to the input voltage, allowing a more faithful acquisition of the mains waveform for subsequent digital signal processing. As a result, the proposed measurement system offers a more representative and reliable voltage acquisition method for power quality analysis.

According to the manufacturer's specifications, the ZMPT101B provides a measurement accuracy of approximately ±1% within the 45–65 Hz operating frequency range. This intrinsic sensor accuracy constitutes one of the primary contributors to the overall measurement uncertainty of the proposed system. [25]

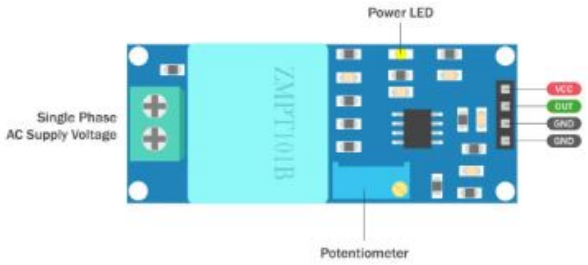


Figure 2.6: ZMPT101B voltage sensor

The ZMPT101B voltage sensor was experimentally evaluated using an oscilloscope to verify that its output waveform remained a 50 Hz sinusoidal signal and to adjust its amplitude through the onboard potentiometer.
During the experiments, it was observed that the output waveform became clipped when its amplitude approached approximately 3.3 V, indicating that the conditioning circuit was operating outside its linear region. Such clipping introduces waveform distortion, leading to errors in RMS estimation and harmonic analysis.

Consequently, the integrated potentiometer was carefully adjusted to **3.20V** to keep the sensors output within the linear operating range while maximizing the usable input range of the STM32 ADC.

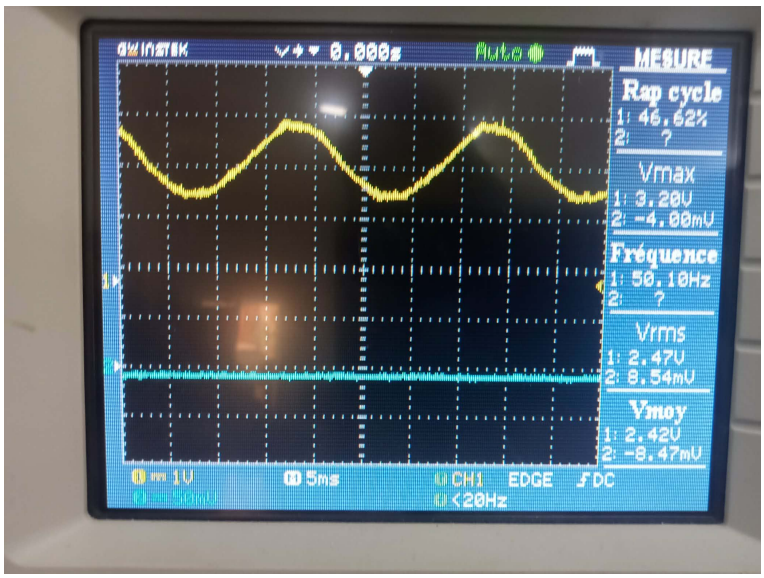


Figure 2.7: ZMPT101B output signal

A comparison between the 220V/9V transformer and the ZMPT101B voltage sensor is shown in Table **2.5**.

Table 2.5: Comparison between a 220V/9V transformer and the ZMPT101B voltage sensor

Parameter	**220V/9V Transformer**	**ZMPT101B Voltage Sensor**
Main function	Steps down the AC mains voltage from 220V to about 9V AC.	Measures AC voltage and provides a proportional low-level signal suitable for electronic circuits.
Output signal	9V AC, relatively high amplitude and may require additional conditioning before ADC acquisition.	Small analog AC signal, easier to condition and interface with a microcontroller ADC.
Measurement purpose	Mainly designed for power supply applications, not precision voltage measurement.	Specifically designed for voltage and power measurement applications.
Accuracy	Limited accuracy; affected by load, regulation, magnetic saturation, and transformer tolerance.	High accuracy; datasheet indicates class 0.2 with permissible error from -0.3% to $+0.2\%$.
Linearity	Not optimized for measurement linearity, especially under variable load conditions.	Good linearity; datasheet specifies linearity $\leq 0.2\%$ in the useful operating range.
Input voltage range	Fixed around 220V AC nominal input.	Wide operating range up to 0–1000V according to the datasheet.

Continued on next page

Parameter	220V/9V Transformer	ZMPT101B Voltage Sensor
Isolation	Provides galvanic isolation between primary and secondary windings.	Provides galvanic isolation with an isolation voltage of about 4000V according to the datasheet.
Filtering of voltage spikes	The primary winding inductance naturally attenuates fast voltage spikes and high-frequency disturbances.	Does not inherently filter voltage spikes; external filtering or protection is required.
Frequency response	Mainly suitable for 50/60Hz power frequency; high-frequency components are attenuated by the magnetic core and windings.	Suitable for AC voltage sensing, but the sensor output follows disturbances unless an external filter is added.
Size and integration	Bulky and heavier compared to sensor modules.	Compact, PCB-mountable, and easier to integrate into embedded systems.
ADC compatibility	Requires voltage divider, offset circuit, and protection before connection to an ADC or a bipolar ADC like **AD7606**.	Easier to interface with an ADC after proper calibration and signal conditioning.
Calibration	Less suitable for accurate calibration because it is not designed as a measurement sensor.	Requires calibration, but offers better repeatability and consistency for voltage measurement.
Best application	Power supply step-down and rough voltage monitoring.	Accurate AC voltage measurement in monitoring, protection, and power analysis systems.

Among the available voltage sensing solutions, the **LEM LV 25-P** as shown in Figure **2.8**, represents an industrial-grade voltage transducer that offers excellent accuracy, wide bandwidth, and fast dynamic response, making it well suited for demanding power quality monitoring applications. However, this component was not available in the laboratory inventory and could not be procured within the project's time and budget constraints.

Consequently, the ZMPT101B voltage sensor was selected as a practical alternative. Although it is primarily intended for low-cost voltage measurement applications, the ZMPT101B provides galvanic isolation, adequate accuracy after calibration, and straightforward interfacing with the data acquisition system. These characteristics make it a suitable solution for the development and experimental validation of the proposed Power Quality Analyzer prototype. Future work may consider replacing the ZMPT101B with an industrial transducer such as the **LEM LV 25-P** to further improve measurement accuracy and dynamic performance, particularly for high-frequency disturbances and fast transient events.



Figure 2.8: Industrial Voltage Transducer (LEM LV 25-P).

2.9 Current sensor

2.9.1 Current Signal Conditioning and Calibration

The ACS712-5A Hall-effect current sensor was selected for current acquisition due to its galvanic isolation, analog voltage output, simplicity of implementation, and sufficient bandwidth (80 kHz) for power quality analysis. According to the manufacturer's datasheet, the sensor exhibits a nominal sensitivity of 185 mV/A and produces an output voltage centered at half of its supply voltage. Since the sensor is powered from a 5 V supply, its output voltage at zero current is

$$V_{\text{offset}} = \frac{V_{CC}}{2} = \frac{5}{2} = 2.5 \text{ V}.$$

Consequently, the output voltage varies around this offset according to

$$V_{\text{ACS712}} = V_{\text{offset}} + I \times S,$$

where $S = 185$ mV/A represents the sensor sensitivity.

Although the STM32H743 ADC accepts input voltages only within the range of 0 V to 3.3 V, the ACS712 output may approach the supply voltage (approximately 5 V). Therefore, a voltage adaptation stage was required to guarantee safe operation of the microcontroller, a passive resistive divider was selected because of its simplicity, the resistor network consists of:

$$R_1 = 10 \text{ k}\Omega$$

connected between the ACS712 output and the ADC input, and

$$R_2 = 15 \text{ k}\Omega$$

connected between the ADC input and ground.
The divider ratio is therefore

$$K = \frac{R_2}{R_1 + R_2} = \frac{15}{10 + 15} = 0.6.$$

Consequently, the voltage applied to the STM32 ADC becomes

$$V_{\text{ADC}} = 0.6 \times V_{\text{ACS712}}.$$

The maximum possible sensor output is approximately 5 V, resulting in

$$V_{\text{ADC,max}} = 5 \times 0.6 = 3.0 \text{ V},$$

which remains safely below the STM32 ADC maximum input voltage of 3.3 V.
Likewise, the zero-current offset becomes

$$V_{\text{offset,ADC}} = 2.5 \times 0.6 = 1.5 \text{ V}.$$

The sensor sensitivity is also scaled by the divider ratio:

$$S_{\text{ADC}} = 185 \text{ mV/A} \times 0.6 = 111 \text{ mV/A}.$$

Therefore, each ampere of measured current produces a voltage variation of 111 mV. at the ADC input.
The STM32H743 employs a 16-bit ADC with a reference voltage of

$$V_{\text{REF}} = 3.3 \text{ V},$$

thus the digital conversion follows

$$V_{\text{ADC}} = \frac{\text{ADC}_{\text{raw}}}{65535} \times V_{\text{REF}}.$$

Finally, the measured current is reconstructed from the ADC value by removing the zero-current offset and dividing by the effective sensitivity:

$$I = \frac{V_{\text{ADC}} - V_{\text{offset,ADC}}}{S_{\text{ADC}}}.$$

Substituting the numerical values yields

$$I = \frac{V_{\text{ADC}} - 1.5}{0.111},$$

where the current is expressed in amperes.

2.10 Voltage and Current measurment

In the proposed three-phase Power Quality Analyzer, the three internal ADCs of the STM32 microcontroller are used to acquire the electrical signals of the three phases simultaneously. However, within each ADC, the voltage and current channels are converted sequentially rather than at exactly the same instant. Consequently, a small time delay exists between the acquisition of the voltage and current samples of the same phase. At the fundamental frequency of 50 Hz, this delay is generally very small and has a negligible effect on

RMS, harmonic, and FFT calculations. Nevertheless, it may introduce a slight error in phase angle, active power, and power factor measurements. Therefore, the magnitude of this delay should be experimentally evaluated and, if necessary, compensated by software calibration to improve the accuracy of the power measurements.

The experimental verification consists of applying the same sinusoidal signal to both channels and measuring the resulting phase shift introduced by the acquisition system.

2.11 Signal processing implementation

Based on the sampling parameters established in the previous section, the acquired voltage signals are processed using the ARM CMSIS-DSP library. This section first describes the download and integration of the CMSIS-DSP library into the STM32CubeIDE project, followed by the implementation of the FFT, harmonic extraction, and THD computation on the STM32H743 microcontroller.

2.11.1 CMSIS-DSP

For signal processing on the STM32 microcontroller, the CMSIS-DSP library is integrated into the project. CMSIS-DSP provides optimized signal-processing functions for Arm Cortex-M processors, including mathematical operations, filtering, and Fast Fourier Transform (FFT) algorithms.
The library can be obtained from the official CMSIS-DSP GitHub repository:
`https://github.com/ARM-software/CMSIS-DSP`
The repository is downloaded as a ZIP file, as illustrated in **Figure 2.9**.

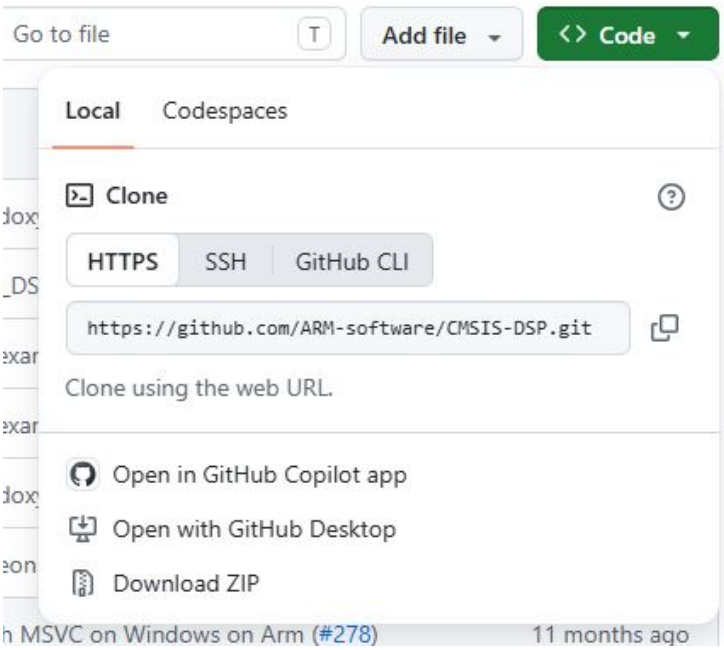
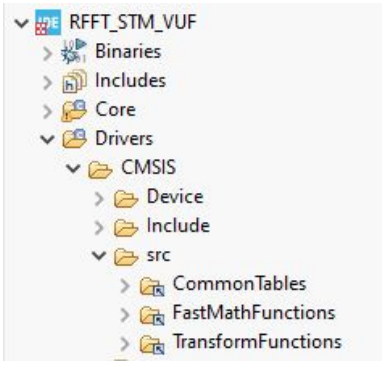
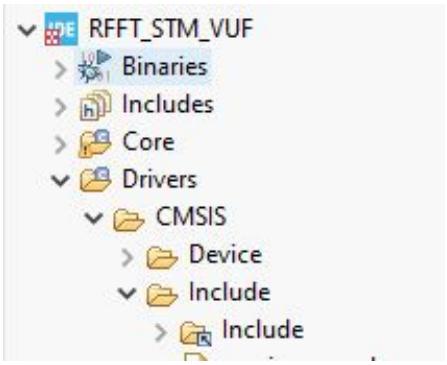


Figure 2.9: Downloading the CMSIS-DSP library as a ZIP file

After extracting the downloaded archive, the required CMSIS-DSP source and header files are added to the STM32CubeIDE project. The placement of these files within the project structure is illustrated in **Figure 2.10**.



(a) CMSIS-DSP files added to the source folder



(b) CMSIS-DSP files added to the include folder

Figure 2.10: CMSIS-DSP file placement in the STM32CubeIDE project

Finally, the `arm_math.h` header file is added to the project and included where the CMSIS-DSP functions are required. Its placement in the project is illustrated in **Figure 2.11**.

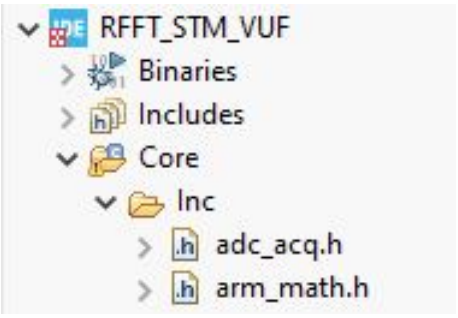


Figure 2.11: Placement of the `arm_math.h` header file

2.11.2 CMSIS-DSP Implementation: `arm_rfft_fast_f32`

The FFT is computed using the CMSIS-DSP library function `arm_rfft_fast_f32`, initialised for a 2048-point real transform via `arm_rfft_fast_init_2048_f32`.
The choice of the real FFT (RFFT) over a generic complex FFT `arm_cfft_f32()` is deliberate: since the acquired voltage waveform is a purely real-valued discrete sequence, a complex FFT would process N complex inputs, treating the imaginary part as identically zero and performing twice the necessary arithmetic.
The RFFT algorithm exploits the conjugate symmetry of the spectrum of a real signal to compute only the $N/2+1 = 1025$ independent complex frequency bins, reducing both the computation time and the memory footprint by approximately a factor of two — a critical consideration on a resource-constrained embedded target.

The `arm_rfft_fast_f32` function from the CMSIS-DSP library is used for the FFT computation. Its key characteristics are the following:

- **Architecture optimisation:** the mixed-radix decomposition is specifically optimised for ARM Cortex-M processors, making full use of the hardware multiply-accumulate (MAC) pipeline.
- **Initialisation:** `arm_rfft_fast_init_2048_f32` pre-computes the complex exponential coefficients $e^{-j2\pi kn/N}$, multiplied at each stage of the butterfly computation,

and stores them in memory once at startup. Since these coefficients depend solely on N and not on the signal content, the same table remains valid regardless of how the waveform changes, so that successive calls to `arm_rfft_fast_f32` at the acquisition rate incur no repeated computation overhead.

- **Output format:** the output buffer follows the CMSIS-DSP packed convention — bin 0 (DC) and bin $N/2$ (Nyquist) are stored as real values in the first two elements, and bins 1 through $N/2-1$ follow as interleaved real/imaginary pairs.

2.11.3 Harmonic Extraction and THD Computation

The magnitude of each FFT frequency bin is first obtained from the complex output buffer as:

$$|X[k]| = \frac{2}{N}\sqrt{\mathrm{Re}^2[k\cdot f_0/\Delta f] + \mathrm{Im}^2[k\cdot f_0/\Delta f]} \tag{2.6}$$

The factor $2/N$ converts the raw FFT coefficients into a single-sided amplitude spectrum by accounting for the symmetry of the spectrum of a real-valued signal, where the energy is distributed equally between the positive- and negative-frequency components. [26][27]

These FFT-bin magnitudes are subsequently used to compute the harmonic subgroups defined by IEC 61000-4-7, as presented in the previous section.
The THD is then computed over the first K harmonic orders as defined by IEEE 519:

$$\mathrm{THD} = \frac{\sqrt{\sum_{n=2}^{K} G_{sg,n}^2}}{G_{sg,1}} \times 100\,\% \tag{2.7}$$

2.12 Graphical user interface

Initially, the developed power quality analyzer was intended to display the acquired measurements on a dedicated graphical LCD. However, a suitable 4.3-inch TFT display, which had been selected during the design stage, was not available. Smaller LCD modules were available, but their limited resolution and display area were insufficient for simultaneously presenting waveform oscillograms, harmonic spectra, power quantities, and power quality indicators.

Another limitation concerns the communication bandwidth of embedded display interfaces. Although SPI is widely used to interface TFT displays with microcontrollers, refreshing a complete graphical screen requires the transmission of several hundred kilobytes of pixel data. Considering the relatively large acquisition frames generated by the analyzer, this solution would considerably increase the processor workload and reduce the achievable refresh rate.

To overcome these limitations, a wireless visualization approach was adopted. Instead of using an embedded LCD, a smartphone was employed as the graphical user interface, allowing real-time visualization without increasing the hardware complexity of the instrument. Communication between the STM32H743 and the smartphone is performed through a Bluetooth Classic HC-05 module operating as a wireless serial interface.

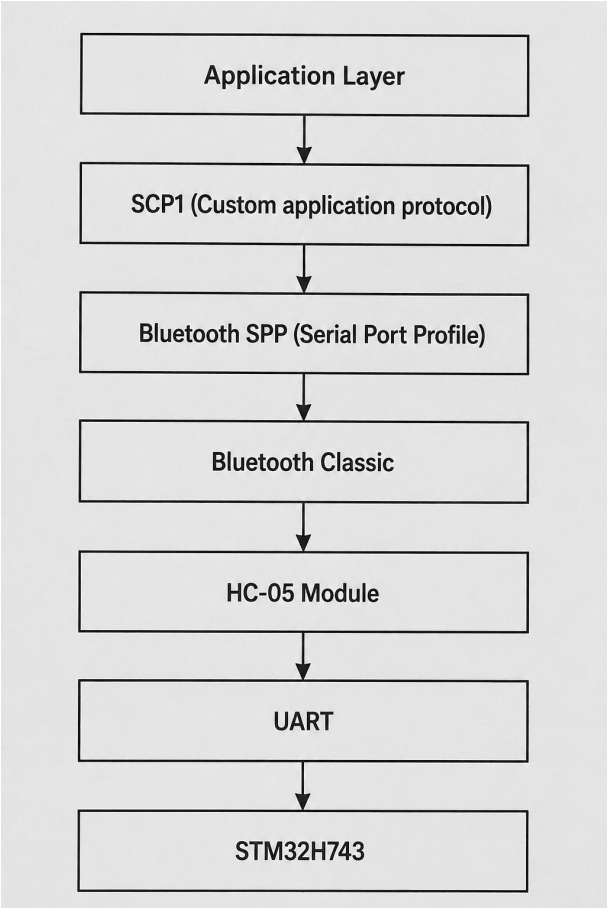


Figure 2.12: Communication protocol stack used for wireless data transmission between the STM32H743 and the mobile application.

Figure 2.12 shows the communication protocol stack used for wireless data transmission in this work.

2.12.1 Mobile Application

The initial design of the proposed oscilloscope included the integration of a dedicated LCD display for local signal visualization. However, the available displays did not fully satisfy the project requirements. Some models had limited screen dimensions, which reduced the readability of the acquired waveforms, while larger displays required high-speed graphical interfaces that were not readily available within the project constraints.

The use of an SPI-based display was also considered. Nevertheless, continuously transmitting and refreshing a large number of graphical points through SPI would introduce additional processing and communication overhead. This limitation could affect the real-time display performance, especially when visualizing acquired waveforms, FFT results, and electrical measurements simultaneously.

Another possible solution was to introduce an additional microcontroller, such as the ESP32, to provide Wi-Fi connectivity and an IoT-based monitoring interface. Although this approach would offer greater remote-access capabilities, it would require the integration and configuration of a second microcontroller, the development of an additional communication interface between the STM32 and the ESP32, and the implementation of the corresponding

network services.

Because the STM32H743 was already a new and relatively complex microcontroller platform for this project, adding another embedded platform would have increased the development time and integration complexity. The main objective of the project was to focus on signal acquisition, power-quality calculations, and digital signal processing on the STM32. Therefore, a simpler and more practical solution was selected: a Flutter mobile application communicating with the embedded system through Bluetooth.

The mobile application acts as the graphical interface of the oscilloscope. It provides real-time waveform visualization, FFT spectrum display, electrical measurement monitoring, Bluetooth connection management, and event-history consultation. In addition, the use of a smartphone provides mobility, a larger display area, and a more flexible user interface compared with a conventional embedded LCD.

Flutter Mobile Application

Flutter was selected as the development framework for the mobile application because it provides a modern environment for building responsive and cross-platform graphical interfaces. It allows the same application structure to be reused across different mobile platforms while offering suitable graphical performance for real-time signal visualization.

The application is divided into two main parts: the frontend and the backend:

- **The frontend:** represents the visible part of the application with which the user directly interacts. It includes the oscilloscope display, the FFT spectrum, measurement panels, Bluetooth controls, signal-selection buttons, scaling options, and event-history pages.

Figure 2.13 presents the interface for selecting the displayed signal (three-phase waveform or FFT), adjusting the horizontal (Time/div) and vertical (V/div) scales, and visualizing real-time data received via Bluetooth.



Figure 2.13: Oscilloscope Control Interface

Figure 2.14 presents the real-time measurement panel, where the calculated electrical quantities, including the RMS voltage (V_{RMS}), peak voltage (V_{max}), RMS current (I_{RMS}), Total Harmonic Distortion (THD), and Voltage Unbalance Factor (VUF), are continuously updated from the received data frames.

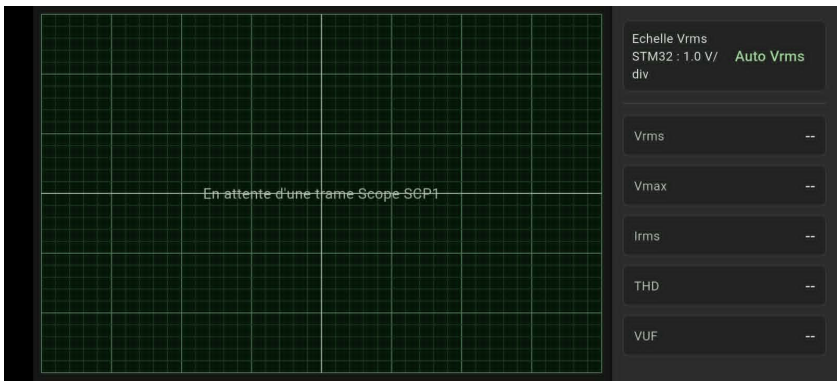


Figure 2.14: Measurement Panel

Figure 2.15 illustrates the Flutter mobile application, displaying Bluetooth connection status, voltage disturbance indicators (SAG and SWELL), SCP1 communication status, and access to the event history.

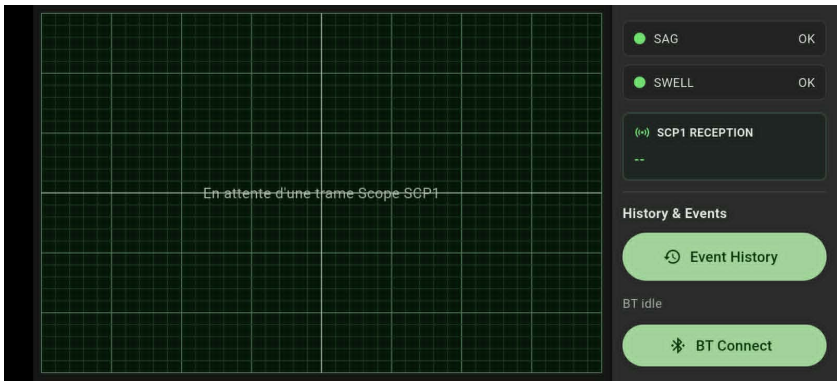


Figure 2.15: Main Dashboard

- **The backend:** manages the internal application logic. It is responsible for establishing the Bluetooth connection, receiving the transmitted data, decoding the SCP1 frames, checking data integrity, converting received samples into physical values, and providing the processed information to the graphical interface.

Application Architecture

The mobile application was organized using a modular software architecture. Each module performs a specific function and communicates with the other modules through clearly defined data exchanges.

The Bluetooth management module is responsible for detecting paired devices, establishing and terminating the connection, receiving raw bytes, and transmitting control commands to the embedded system.

The SCP1 parsing module processes the received byte stream and reconstructs the transmitted frames. According to the frame type, the parser creates either a time-domain waveform frame or an FFT frame. It also verifies the frame structure and integrity before forwarding the data to the rest of the application.

The data-model layer stores the decoded measurement information. The main data objects include the acquired samples, sampling frequency, sequence number, RMS voltage, maximum voltage, RMS current, THD, fundamental frequency, sag and swell status, and voltage-unbalance information.

The visualization layer receives the decoded data and renders either the waveform or the FFT spectrum. Finally, the event-management module processes and stores the detected event records for later consultation.

This modular organization simplifies maintenance and makes it possible to modify one part of the application without significantly affecting the remaining components.

2.12.2 Wireless Communication

The HC-05 module illustrated in **Figure 2.16** implements the Bluetooth Classic Serial Port Profile (SPP), which emulates a conventional UART communication channel over a wireless Bluetooth link. From the microcontroller point of view, the module behaves exactly like a standard serial interface, allowing the firmware to transmit and receive bytes without handling the Bluetooth protocol stack, HC-05 integrates its own Bluetooth controller (CSR BC417 chip) which manages the entire Bluetooth protocol stack.

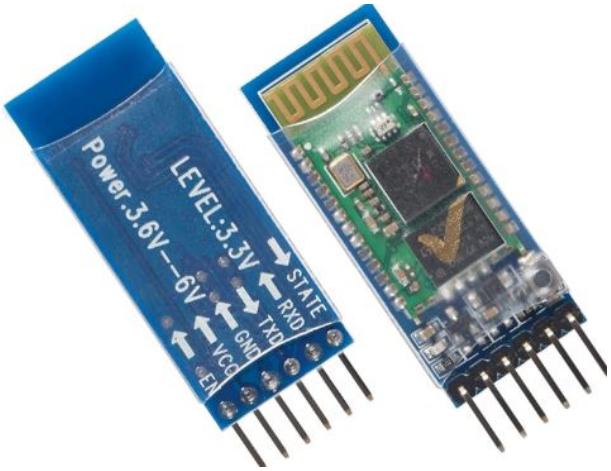


Figure 2.16: Low-cost Bluetooth 2.0 SPP (Serial Port Protocol) module.

This solution considerably simplifies the firmware implementation since all Bluetooth link management, pairing procedures, error detection, and radio communication are handled internally by the HC-05 module . Consequently, the STM32H743 only exchanges UART data frames while the module transparently transfers them to the mobile application.

The HC-05 Bluetooth module is factory-configured with a default UART baud rate of 9600 bps in data mode. Although this speed is sufficient for simple command exchange, it becomes a limiting factor when transmitting large acquisition frames containing oscilloscope samples and harmonic analysis results. Therefore, the UART baud rate was reconfigured to 115200 bps using the HC-05 AT command mode. This eightfold increase in communication speed significantly reduces frame transmission time and enables a higher refresh rate for the real-time visualization of power quality measurements on the mobile application.

Data Representation and Encoding

Several application-level data encoding formats can be transported through Bluetooth. The most common formats are:

Table 2.6: Comparison of common Bluetooth data encoding formats.

Format	Readability	File Size	Primary Use Case
ASCII	Human-readable	Medium	Basic text rendering
CSV	Human-readable	Small	Spreadsheets and databases
JSON	Human-readable	Large	APIs and web data exchange
Binary	Machine-readable	Very compact	Fast processing and large data transmission

Among these possibilities, the binary representation was selected because it minimizes the number of transmitted bytes, allowing higher refresh rates while reducing the UART bandwidth.

Although binary transmission significantly reduces the communication overhead, it does not provide any information about frame synchronization, packet integrity, message type, or payload length.

For this reason, a lightweight application protocol named SCP1 (Smart Communication Protocol version 1) was specifically designed for this project. SCP1 defines a complete frame structure including synchronization bytes, packet identification, payload size, sequence numbering, integrity verification using CRC-16, and support for multiple measurement packet types.

Communication Frame Format

The communication Frame Format used in this work is illustrated in **Figure 2.17**

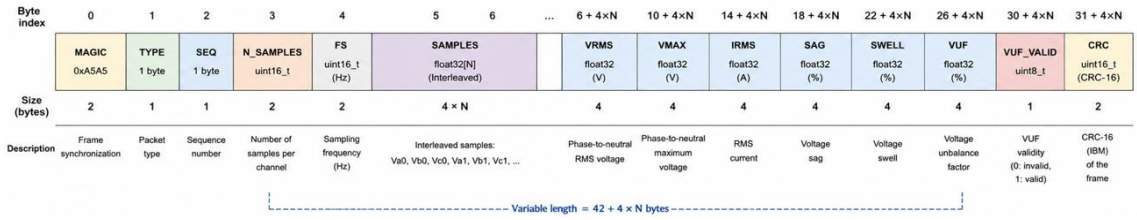


Figure 2.17: Low-cost Bluetooth 2.0 SPP (Serial Port Protocol) module.

Table 2.7: Structure of the real-time measurement data frame.

Field	Type	Size (bytes)	Description
MAGIC	uint16_t	2	Synchronization word (constant value `0xAA55`).
TYPE	uint8_t	1	Packet type identifier (`0x01` for Scope Frame, `0x02` FFT Frame).
SEQ	uint8_t	1	Incremental sequence number (0–255).
N_SAMPLES	uint16_t	2	Number of samples acquired per phase.
FS	uint16_t	2	Sampling frequency (Hz).
SAMPLES	float32	$4 \times N$	Interleaved voltage samples: $V_a[k], V_b[k], V_c[k]$, where $k = 0, \ldots, N-1$.
VRMS	float32	4	RMS phase-to-neutral voltage (V).
VMAX	float32	4	Peak voltage (V).
IRMS	float32	4	RMS current (A).
SAG	float32	4	Voltage sag magnitude (%).
SWELL	float32	4	Voltage swell magnitude (%).
VUF	float32	4	Voltage Unbalance Factor (VUF) (%).
VUF_VALID	uint8_t	1	VUF validity flag (0 = invalid, 1 = valid).
CRC	uint16_t	2	CRC-16 (IBM) computed over the entire frame except the CRC field.

N_SAMPLES = 1024 : Number of waveform samples transmitted for the selected phase.

Although the current implementation always transmits 1024 waveform samples per frame, the `N_SAMPLES` field is retained to explicitly specify the payload size. This facilitates frame decoding in the mobile application while improving the flexibility and maintainability of the communication protocol.

The embedded system acquires and processes the three-phase voltage signals internally to compute all electrical parameters. However, to reduce the Bluetooth communication bandwidth, only the waveform or the FFT of the selected phase is included in each transmission frame.

CRC Error Detection

To ensure reliable communication between the embedded system and the mobile application, a 16-bit CRC is computed over the entire data frame, excluding the CRC field itself, before transmission. Upon reception, the mobile application recalculates the CRC using the received data and compares it with the transmitted CRC value. If both values match, the frame is considered valid, the measurement data are processed, and the application displays the status "CRC: OK" to confirm successful integrity verification. Otherwise, the frame is rejected and a "CRC Error" message is generated, indicating that the received data may have been corrupted during transmission.

2.13 Software Design

This section presents the software design of the proposed mobile application. UML diagrams are used to describe the software architecture, the interactions between the different software components, and the deployment of the application on the target hardware. These diagrams provide a clear representation of the application's structure and behavior while facilitating the understanding of the overall software organization.

All UML diagrams presented in this chapter were generated using PlantUML. The diagrams were described using PlantUML's domain-specific language (DSL), allowing the UML models to be created from a textual specification rather than by manual graphical editing.

2.13.1 UML Class Diagram

The UML class diagram in **Figure 2.18** illustrates the static structure of the mobile application by presenting its main classes, their attributes, methods, and relationships. It provides an overview of the application's internal organization, including the Bluetooth communication manager, the SCP1 protocol parser, the data models, and the visualization components used for oscilloscope and FFT displays.

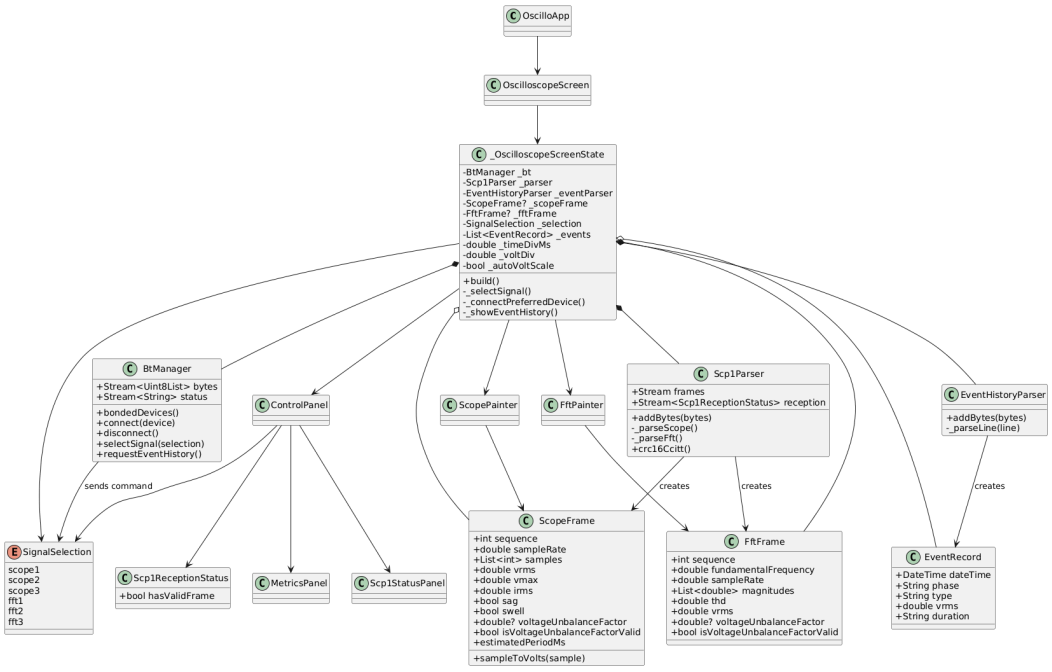


Figure 2.18: UML class diagram.

2.13.2 UML Sequence Diagram

The UML sequence diagram in **Figure 2.19** describes the dynamic interactions between the system components during a typical acquisition session. It illustrates the chronological exchange of messages between the user, the Flutter application, the Bluetooth communication layer, the STM32 microcontroller, and the data processing modules, from establishing the Bluetooth connection to displaying the processed measurements on the user interface.

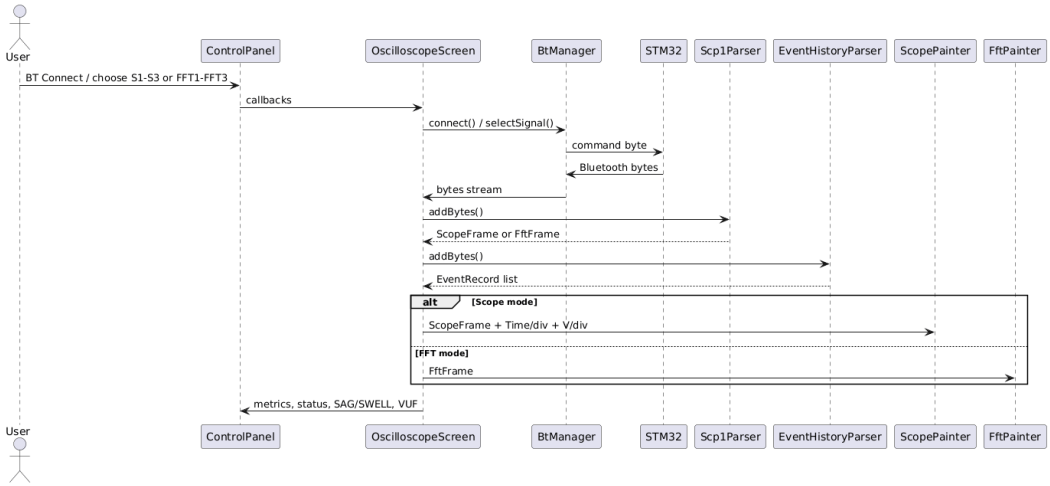


Figure 2.19: UML sequence diagram.

2.13.3 UML Deployment Diagram

The UML deployment diagram in **Figure 2.20** illustrates the physical deployment of the software components across the hardware platform. It shows how the embedded firmware is executed on the STM32H743 microcontroller, how the HC-05 Bluetooth module enables wireless communication, and how the Flutter application running on the Android smartphone receives, processes, and visualizes the transmitted measurement data.

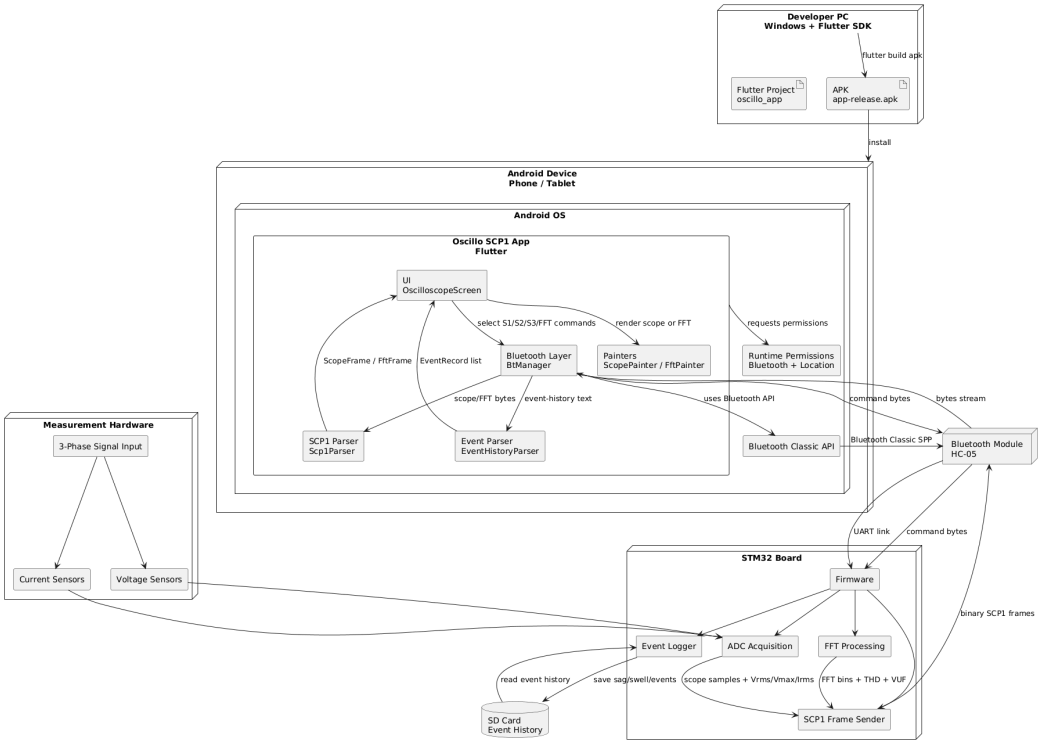


Figure 2.20: UML deployment diagram.

2.14 Implementation Challenges

During the development of the mobile application and its communication with the embedded system, several technical challenges were encountered. The main issues and their corresponding solutions are summarized below:

- **No data frames were received by the application.**
  - **Cause:** The UART baud rate configured on the STM32 did not match the baud rate configured for the HC-05 Bluetooth module.
  - **Solution:** Both devices were configured to operate at the same communication speed (115200 bps), allowing successful frame reception.
- **The application failed to detect the beginning and the end of received frames.**
  - **Cause**: The transmitted frames did not include a unique synchronization header, preventing the parser from identifying valid frame boundaries.
  - **Solution:** A fixed frame header (magic number) and a well-defined frame structure were introduced in the custom SCP1 protocol, enabling reliable frame synchronization.
- **Custom STM32 code disappeared after regenerating the project with STM32CubeMX.**
  - **Cause:** Some application code was written outside the USER CODE BEGIN / USER CODE END sections.
- **Slow waveform and FFT updates for the third phase.**
  - **Cause:** The third ADC was initially configured to use the Basic DMA (BDMA), whereas the other ADCs used the DMA controller. This heterogeneous DMA configuration introduced inefficient data transfers between the acquisition and processing stages, resulting in noticeably slower waveform and FFT updates for the third phase.
  - **Solution:** The third ADC was reconfigured in STM32CubeMX to use the DMA controller instead of BDMA. Using a common DMA architecture for all ADCs eliminated the transfer bottleneck and restored smooth real-time updates of the waveform and FFT for the third phase.
- **"ST-LINK is not in DFU mode" error during programming.**
  - **Cause:** STM32CubeProgrammer displayed the *"ST-LINK is not in DFU mode"* error because the ST-LINK USB driver installed on the host computer was outdated or improperly configured, preventing the debugger from being correctly recognized.
  - **Solution:** The issue was resolved by updating the **STMicroelectronics ST-LINK driver** through the **Windows Device Manager**. After installing the correct driver, STM32CubeProgrammer successfully detected the ST-LINK, allowing normal firmware programming and debugging operations.
- **System startup blocked when the SD card is missing.**

- **Cause:** During system initialization, the firmware executes `HAL_SD_Init()` to initialize the SD card interface. If the SD card is absent, improperly inserted, or the SDMMC interface is not correctly configured, the initialization fails and the firmware enters `Error_Handler()`, resulting in an infinite loop before reaching the main application.
  In this case, the mobile application also does not display any signals, since no data acquisition stream is started without successful SD card initialization.
- **Solution:** This behavior was intentionally retained as a fail-safe mechanism. Since the SD card is required for continuous measurement logging, preventing the system from starting ensures that no measurements are acquired without being recorded.
  Consequently, the absence of data on the mobile application implicitly informs the user that the SD card must be inserted or correctly connected before the system can operate normally.

2.15 PCB Design and Fabrication

The schematic of the proposed board was designed using **KiCad**, a free and open-source electronic design automation (EDA) software. The developed PCB serves as a **breakout board**, i.e., an interface board that integrates and interconnects multiple hardware modules while exposing their signals through dedicated connectors and pin headers for easy access and expansion. In this design, the breakout board combines the sensing modules, the STM32H7 development board, and a set of connectors and headers to facilitate power distribution and input/output interfacing.

The PCB was designed as a **two-layer board**. It includes a dedicated **220 V AC power section** capable of carrying currents of up to **5 A**, with trace widths selected accordingly to ensure reliable current handling. To enhance electrical safety and reduce electromagnetic interference, adequate **clearance and isolation distances** were maintained between the high-voltage power section and the low-voltage digital circuitry, following recommended PCB design practices as illustrated in **Figure 2.22**.
The schematic diagram of the proposed PCB is illustrated in **Figure 2.21** below.

Figure 2.21: Schematic of the proposed PCB.

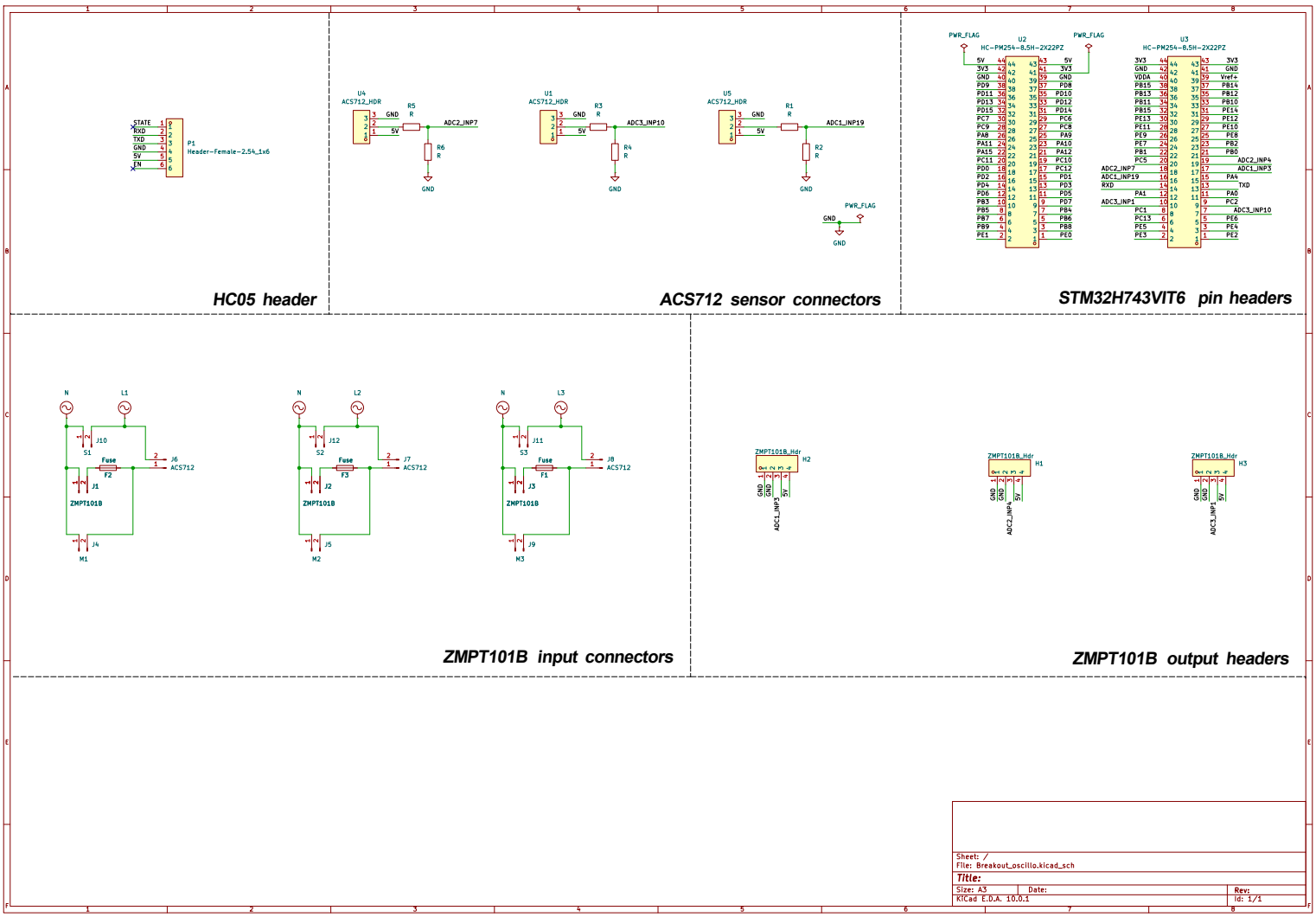


Figure 2.22 and **Figure 2.23** present the PCB layout and the corresponding three-dimensional (3D) model of the proposed board, respectively.

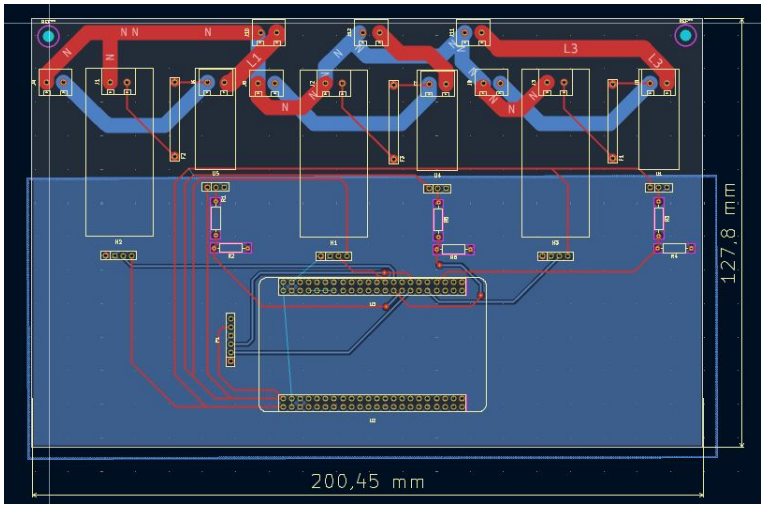


Figure 2.22: PCB for the proposed board.

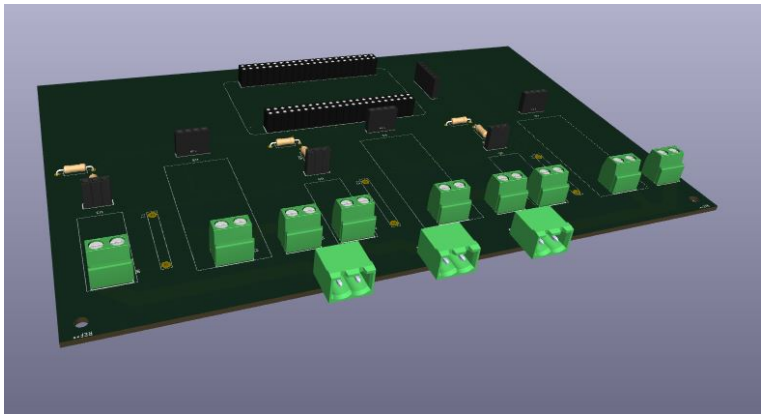


Figure 2.23: 3D visualization of the proposed PCB.

The PCB was fabricated in the school's electronics laboratory using an LPKF CNC prototyping system. Since this was the first experience with this manufacturing process, significant effort was devoted to learning both the machine operation and its associated software. The fabrication procedure required mastering several critical steps, including camera calibration, fiducial recognition, and the establishment of accurate machine reference points to ensure precise alignment between the two PCB layers.

During the fabrication process, a positioning error occurred between the drilling stage and the subsequent milling of the copper traces as illustrated in **Figure 2.24** due to an error in one of the three fiducial reference points, resulting in a misalignment of a few millimeters. This offset between the drilled holes and the designed track layout prevented proper correspondence in the PCB, ultimately rendering the PCB unusable and requiring the entire manufacturing process to be restarted. This issue highlighted the critical importance of precise registration and alignment throughout all fabrication steps.

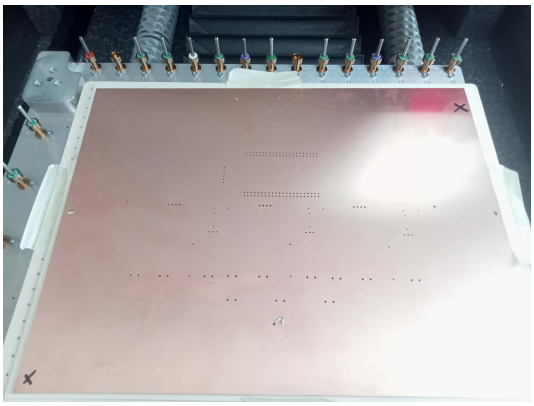


Figure 2.24: Error between the drilling stage and the subsequent milling of the copper traces

The manufacturing workflow began with the drilling operation performed on the LPKF CNC machine, as shown in **Figure 2.25a**. The drilled board in **Figure 2.25b** was then transferred to the chemical metallization process in **Figure 2.26b**, where the through-holes were plated to establish electrical conductivity between the two copper layers. This stage required approximately three hours and involved successive immersion of the PCB in five chemical baths as illustrated in **Figure 2.26a**, each with carefully controlled processing times. After metallization, the board was returned to the CNC machine for milling the copper traces on the first layer. Finally, the PCB was flipped and realigned using the fiducial marks before machining the copper traces on the second layer, completing the fabrication process.



(a) LPKF CNC machine used for PCB drilling and milling.



(b) PCB mounted on the LPKF CNC machine after the drilling process.

Figure 2.25: PCB fabrication using the LPKF CNC prototyping system.



(a) Chemical baths



(b) LPKF CNC machine used for chemical metallization process.

Figure 2.26: Chemical metallization process.

The final PCB

The final breakout PCB for the prototype is illustrated in **Figure 2.27**.

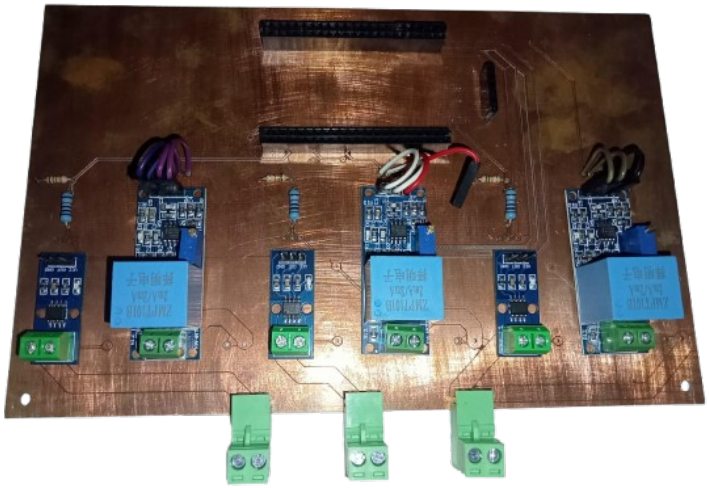


Figure 2.27: Final Breakout PCB for the Prototype

2.16 Conclusion

This chapter presented the engineering design of the proposed power quality analyzer by translating the theoretical concepts introduced in the previous chapter into a complete hardware and software architecture. The system specifications were established according to the relevant IEC standards, guiding the selection of the sensing circuits, embedded processing platform, communication interface, signal processing methodology, and software architecture. In addition, the PCB design and fabrication process, together with the practical implementation constraints, were discussed to ensure the feasibility and reliability of the proposed solution.
The engineering decisions presented in this chapter provide the foundation for the realization of the prototype and prepare the transition from system design to its practical implementation and performance evaluation.

Chapter 3

System Implementation, Experimental Testing, and Metrological Validation

3.1 Introduction

Following the system design and methodological choices presented previously, this chapter focuses on the practical implementation and experimental validation of the developed power quality analyzer.

It presents the final prototype, data acquisition configuration, debugging and validation methods, laboratory and real-network measurements, sensor calibration, voltage unbalance evaluation, and frequency-domain validation. The implementation status of THD and power measurements, together with the main experimental limitations, is also discussed.

3.2 Project Presentation

This project presents the development of a three-channel Power Quality Analyzer (PQA) based on the STM32H743 microcontroller. The system simultaneously acquires three synchronized analog signals using the three internal ADCs of the STM32H743. The sampled data are transferred to DMA buffers to ensure efficient real-time acquisition with minimal CPU intervention. The acquired signals can be monitored in real time, processed through Real Fast Fourier Transform (RFFT) algorithms for harmonic analysis, and stored on an SD card for long-term recording and event tracking. To maintain a responsive user interface, only the selected channel is transmitted via Bluetooth/UART to a mobile application for live visualization, while all synchronized raw data are continuously saved on the SD card.

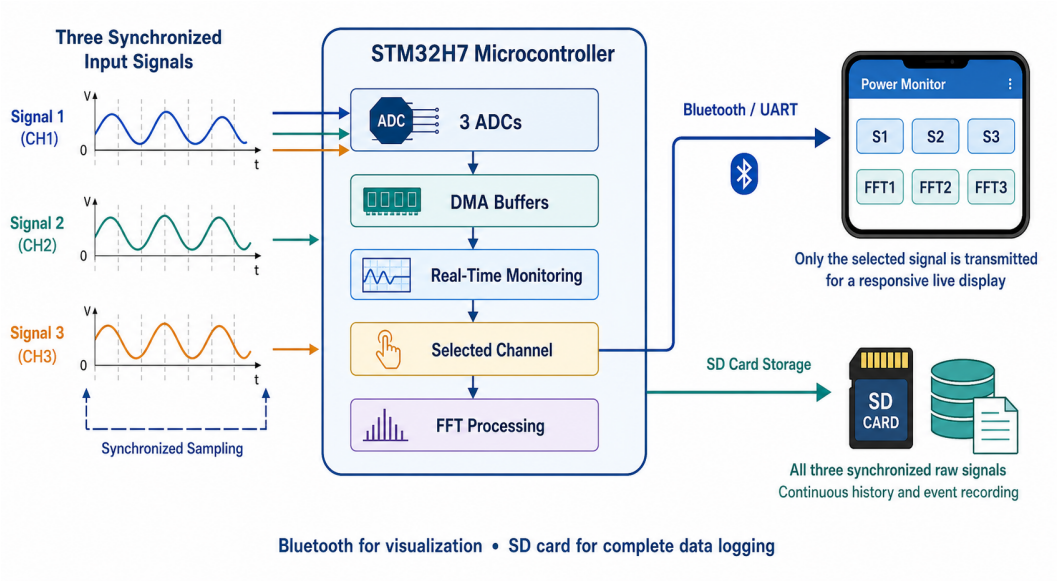


Figure 3.1: Overall architecture of the proposed three-channel power quality monitoring system.

3.3 Data Acquisition Configuration

This section presents the configuration of the main parameters involved in the data acquisition process, including timer settings, ADC and DMA configuration, and ADC sampling time optimization.

3.3.1 STM32 Timer configuration

$$\text{TIM CLOCK} = \frac{\text{APB TIM CLOCK}}{\text{PSC+1}}$$

$$\text{FREQUENCY} = \frac{\text{TIM CLOCK}}{\text{ARR+1}}$$

$$\text{DUTY (\%)} = \frac{\text{CCRx}}{\text{ARR+1}} \times 100$$

According to the MCU datasheet, the STM32H743 block diagram shows that TIM1 is connected to the APB2 bus, which is an internal communication bus linking the CPU to high-speed peripherals. It operates at up to 120 MHz for peripherals (UART, SPI, I2C) and up to 240 MHz for timers (TIM1, TIM8, TIM16, TIM17), depending on the APB prescaler configuration.

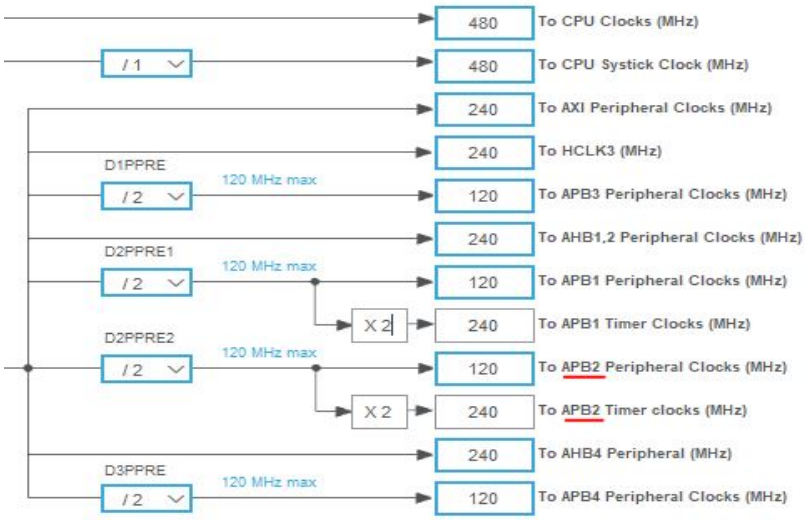


Figure 3.2: Advanced Peripheral Bus 2

The timer is configured in PWM mode on the STM32H743, with a 50% duty cycle defined by the CCRx register (i.e., CCRx = ARR/2). To ensure efficient and autonomous operation, DMA is used in memory-to-peripheral mode to automatically update the timer register without CPU intervention.

The sampling frequency is directly generated by the hardware timer. Each timer event triggers a conversion on the AD7606 via the CONVST signal, ensuring that the sampling frequency is equal to the timer frequency.

The selection of the sampling frequency is a critical step for accurate signal acquisition and analysis. As previously discussed in Chapter 2, entitled *Signal Processing*, the sampling frequency must satisfy the following condition:

$$f_s \geq 2f_{max}$$

In power quality applications, the fundamental frequency is:

$$f_0 = 50\,\text{Hz}$$

However, the signal also contains higher-order harmonics. Considering harmonics up to the 40th order:

$$f_{max} = 40 \times 50 = 2000\,\text{Hz}$$

Applying the Nyquist criterion:

$$f_s \geq 2 \times 2000 = 4000\,\text{Hz}$$

Thus, the minimum required sampling frequency is 4 kHz. However, this value represents only the theoretical lower bound. In practice, power quality measurement systems must strictly adhere to international standards such as **IEC 61000-4-7**, which defines measurement techniques for harmonics and interharmonics.

According to this standard, spectral analysis must be performed over a rigid and continuous **200 ms time window**, yielding a mandatory frequency resolution of exactly $\Delta f = 5$ Hz.

To process this window efficiently using standard Fast Fourier Transform (FFT) algorithms, the total number of points (N) within the 200 ms window must be a power of two ($N = 2^m$). For this reason, a sampling frequency of:

$$f_s = 10,24\,\text{kHz}$$

is selected. This choice provides significant advantages. First, it yields exactly:

$$N = f_s \times 200\,\text{ms} = 10240 \times 0.2 = 2048 \text{ samples per window}$$

Because 2048 is a perfect power of two (2^{11}), it allows for optimal execution of the Radix-based FFT algorithm on the microcontroller. Furthermore, this choice results in a high, stable number of samples per individual grid period:

$$N_{period} = \frac{f_s}{f_0} = \frac{10240}{50} = 204.8 \text{ samples per period}$$

This ensures that the 200 ms analysis window encompasses exactly 10 complete cycles of a 50 Hz fundamental frequency. This precise alignment prevents spectral leakage and enables accurate grouping of harmonic and interharmonic bins as mandated by the standard. This selected sampling frequency offers an ideal trade-off between computational cost and measurement precision, while remaining fully compatible with the capabilities of the AD7606 analog-to-digital converter and the STM32H743 microcontroller.

$$\text{TIM1 CLOCK} = \frac{\text{APB2 TIM CLOCK}}{\text{PSC+1}} = \frac{240\,\text{MHz}}{23+1} = 10\,\text{MHz}$$

$$\text{FREQUENCY} = \frac{\text{TIM1 CLOCK}}{\text{ARR+1}} = \frac{10\,\text{MHz}}{975+1} = 10,24\,\text{kHz}$$

$$\text{DUTY (\%)} = \frac{\text{CCR4}}{\text{ARR+1}} \times 100 = \frac{488}{975+1} \times 100 = 50\%$$

- CCR4: Capture Compare Register 4 associated with Timer 1 : `.TIM1-> CCR4 =488;`

Figure **3.3** shows the 10,24 kHz PWM signal obtained at the output of the STM32 Timer. The measured frequency matches the theoretical value calculated during the Timer configuration (PSC and ARR registers), which validates the correct setup of the peripheral. This test confirms the proper operation of the Timer in PWM mode.

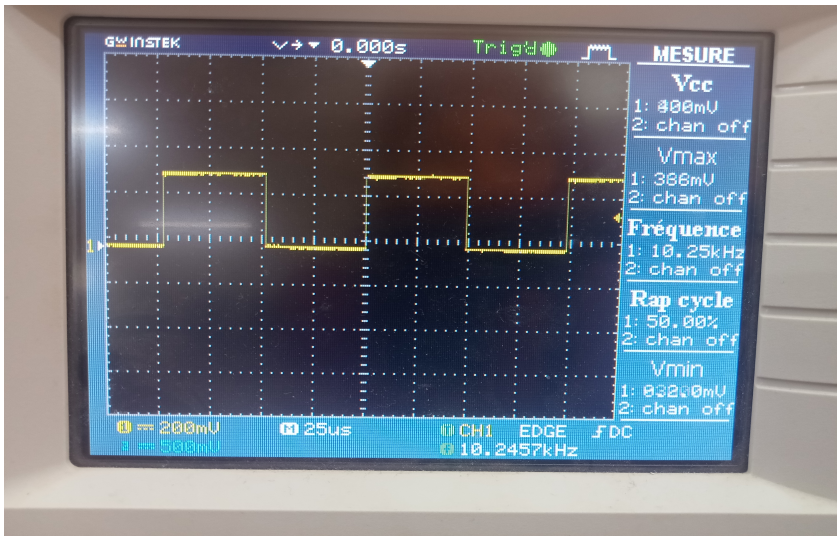


Figure 3.3: PWM Signal Generated by the STM32 Timer (Oscilloscope Visualization)

3.3.2 ADC3 Acquisition and DMA Configuration

During the experimental tests, abnormal behavior was observed on the third ADC channel, including delayed updates and incorrect waveform and FFT displays. The investigation showed that ADC3 was configured to use the BDMA controller, unlike ADC1 and ADC2, which use the standard DMA controller. This configuration created a memory-access incompatibility between the BDMA transfer path and the acquisition buffer location. After relocating the ADC3 DMA buffer to a memory region accessible by BDMA, the third channel operated correctly and its real-time and FFT results became stable.

3.3.3 ADC Sampling Time Optimization

The STM32H743 ADC uses a sample-and-hold mechanism to acquire the analog input signal. During the sampling phase, the selected ADC input is internally connected to a sampling capacitor. This capacitor must charge to a voltage sufficiently close to the actual input voltage before the analog-to-digital conversion begins. Consequently, the ADC sampling time directly influences the accuracy and stability of the acquired samples.

The sampling time is expressed in ADC clock cycles and can be configured independently for each ADC channel. For the STM32H743, the available sampling times include **1.5, 2.5, 8.5, 16.5, 32.5, 64.5, 387.5, and 810.5** ADC clock cycles.[28]

During the experimental validation of the developed system, significant fluctuations were initially observed in the ADC measurements displayed through ***Live Expressions*** and the mobile application as illustrated in **Figure 3.4**. Increasing the ADC sampling time to 64.5 ADC clock cycles resulted in noticeably more stable measurements as illustrated in **FIgure 3.5**. This improvement can be explained by the longer acquisition interval, which allows the ADC sampling capacitor more time to charge and settle before conversion.

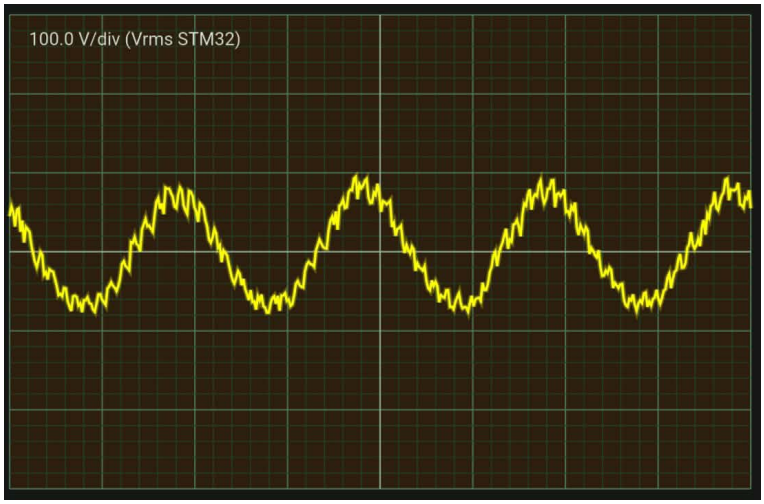


Figure 3.4: Signal before increasing the ADC sampling time



Figure 3.5: Signal before ADC sampling time optimization

Therefore, the sampling time represents a compromise between **conversion speed** and **measurement accuracy**. Since the developed power-quality analyzer operates at a sampling frequency that does not require the maximum conversion speed of the STM32H743 ADC, a longer sampling time can be selected to improve measurement stability without compromising the required acquisition rate.

3.4 Laboratory testing

Before testing the developed system with a real 220 V AC voltage signal, preliminary laboratory tests were performed using a low-voltage signal generated by the STM32H743 Digital-to-Analog Converter (DAC). A 50 Hz signal limited to the 3.3 V range was used to safely verify the acquisition chain and validate the data transfer to the mobile application without applying mains voltage to the prototype.

Once the acquisition and communication stages were successfully verified, the system was tested using the real AC voltage signal through the voltage-sensing stage. The overall firmware workflow used during these laboratory tests is illustrated in **Figure 3.6**, including signal generation and acquisition, signal processing, power-quality parameter computation, data transmission, and measurement storage.

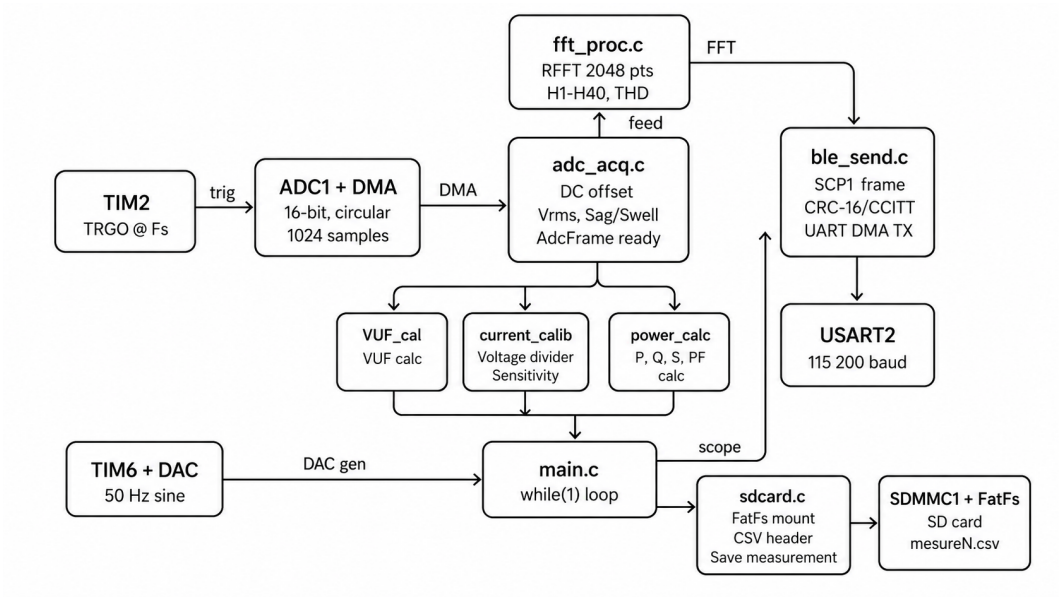


Figure 3.6: Validation test bench architecture for signal acquisition and processing.

3.5 Debugging and Validation Methods

During the development and integration of the embedded system and the mobile application, several debugging tools were used to isolate communication issues and verify the correctness of the transmitted data.

- **USB CDC (Virtual COM Port):** The USB CDC class was configured in STM32CubeMX to create a virtual COM port between the STM32H743 and the host computer. This interface was used to print UART debugging messages, monitor the program execution, and verify the data transmitted through the UART interface independently of the Bluetooth communication. It proved particularly useful for identifying firmware issues and validating the UART output before testing the Bluetooth link.

- **PuTTY Terminal:** PuTTY was used as a serial terminal to display the data received through the virtual COM port or UART interface. It enabled real-time observation of transmitted messages.

- **Serial Bluetooth Terminal Mobile Application:** Before integrating the custom mobile application, the Serial Bluetooth Terminal application was used to validate the Bluetooth communication independently. It allowed direct visualization of the raw data received from the HC-05 module, making it possible to determine whether communication problems originated from the STM32 firmware or from the custom mobile application.

- **STM32CubeIDE Live Expressions:** The Live Expressions feature of STM32CubeIDE was used to monitor important variables in real time during program execution, such as ADC values, RMS measurements, and other calculated parameters. This method was particularly useful for validating the acquisition and processing stages before transmitting the results to the mobile application. Variables intended for continuous monitoring were declared as global variables and, when they were modified asynchronously or needed to be observed reliably during debugging, as `volatile`, preventing the

compiler from optimizing away accesses that must remain visible to the program and debugger.

When the custom mobile application displayed no data, the same transmitted frames were verified using USB CDC, PuTTY, the Serial Bluetooth Terminal application and STM32CubeIDE Live Expressions. Comparing the outputs from these tools made it possible to isolate communication errors, distinguish firmware-related issues from application-level problems, and validate the integrity of the transmitted UART/Bluetooth data.

3.6 Real-Time Voltage Measurement

3.6.1 Voltage sensor ZMPT101B

After validating the acquisition and communication stages using the low-voltage DAC signal, the three ZMPT101B voltage sensors were calibrated before testing the system with the 220 V AC mains voltage. The calibration was performed by adjusting the potentiometer available on the ZMPT101B modules while monitoring its output with an oscilloscope. The potentiometer was adjusted to obtain a suitable output amplitude within the input range of the acquisition circuit. As shown in **Figure 3.7**, the measured signal presents a frequency of approximately 50 Hz and a maximum voltage of approximately 3.16 V. This calibration step ensured that the sensor output remained within a safe voltage range before being connected to the STM32 acquisition stage.

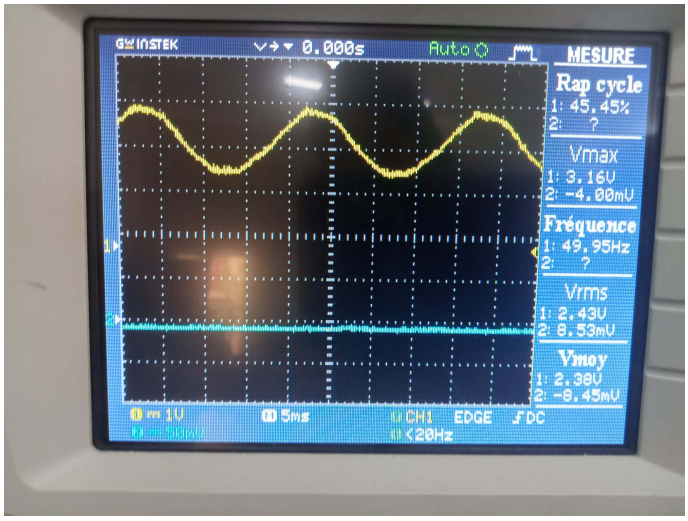


Figure 3.7: Calibration of the ZMPT101B output using the onboard potentiometer and oscilloscope

After the calibration of the voltage sensors and the validation of the acquisition chain, real-time voltage measurements were performed to evaluate the operation of the developed system under practical conditions. The acquired voltage waveform was transmitted to the mobile application, where it was displayed together with the main calculated electrical quantities.

The application provides the RMS voltage (V_{RMS}) and the maximum voltage (V_{max}), allowing the user to simultaneously observe the waveform and its associated numerical parameters. Figure 3.8 shows an example of the real-time voltage measurement displayed by the developed mobile application.

Figure 3.8: Real-time voltage waveform and calculated electrical parameters

In addition to the individual voltage measurements, the system includes a voltage unbalance evaluation based on the RMS magnitudes of the three phase voltages. This functionality was evaluated separately, as described in the following subsection.

3.6.2 Voltage Unbalance Measurement

In a three-phase system, voltage unbalance can be evaluated using different approaches. The Voltage Unbalance Factor (VUF) based on symmetrical components is commonly expressed as the ratio between the negative-sequence and positive-sequence voltage components:

$$VUF = \frac{|V_2|}{|V_1|} \times 100 \tag{3.1}$$

where V_1 and V_2 represent the positive- and negative-sequence voltage components, respectively as presented in **Chapter 02**. This method requires both the magnitude and phase information of the three phase voltages.

In the developed system, the phase information can be obtained from the frequency-domain processing of the three voltage signals. However, during the experimental tests, simultaneous measurements of the three phases were strongly affected by disturbances present in the laboratory environment. Therefore, reliable experimental validation of the phase displacement between the three channels could not be achieved.

Furthermore, applying the same single-phase source simultaneously to the three voltage inputs would not constitute a valid test of the symmetrical-component VUF method, since the three input signals would not reproduce the approximately 120° phase displacement of a real balanced three-phase system.

Consequently, the experimental validation was focused on voltage magnitude unbalance rather than phase-based VUF. The unbalance was evaluated from the RMS values of the three voltage channels. First, the average RMS voltage was calculated as:

$$V_{\text{avg}} = \frac{V_{1,\text{RMS}} + V_{2,\text{RMS}} + V_{3,\text{RMS}}}{3} \tag{3.2}$$

The deviation of each phase voltage from the average value was then determined, and the maximum deviation was selected:

$$\Delta V_{\max} = \max\left(|V_{1,\text{RMS}} - V_{\text{avg}}|, |V_{2,\text{RMS}} - V_{\text{avg}}|, |V_{3,\text{RMS}} - V_{\text{avg}}|\right) \tag{3.3}$$

Finally, the voltage magnitude unbalance percentage was calculated as:

$$U_V(\%) = 100 \times \frac{\Delta V_{\max}}{V_{\text{avg}}} \tag{3.4}$$

This approach evaluates the maximum deviation of the phase-voltage magnitudes from their average value. It therefore provides an indication of voltage magnitude unbalance without requiring the phase-angle information needed for the symmetrical-component VUF calculation.

It should be emphasized that the resulting value should not be interpreted as the negative-sequence VUF. The two methods characterize voltage unbalance using different

definitions. In this work, the RMS-deviation method was retained for the experimental validation because the available laboratory conditions did not allow reliable simultaneous three-phase phase-angle validation.

The application displayed an unbalance value of **0.52%** as illustrated in **Figure 3.8**. Although this parameter is labeled as VUF in the application interface, the experimentally evaluated value corresponds to the RMS-based voltage magnitude unbalance method described above.

3.7 Frequency-Domain Validation

3.7.1 FFT Validation Using the DAC-Generated 50 Hz Signal

Before applying the FFT algorithm to the real mains voltage, its frequency-domain operation was verified using a controlled 50 Hz signal generated by the STM32 DAC. As shown in **Figure 3.9**, the dominant spectral component is correctly detected at the 50 Hz bin, highlighted in yellow. This test provides a controlled verification of the implemented frequency-analysis chain.

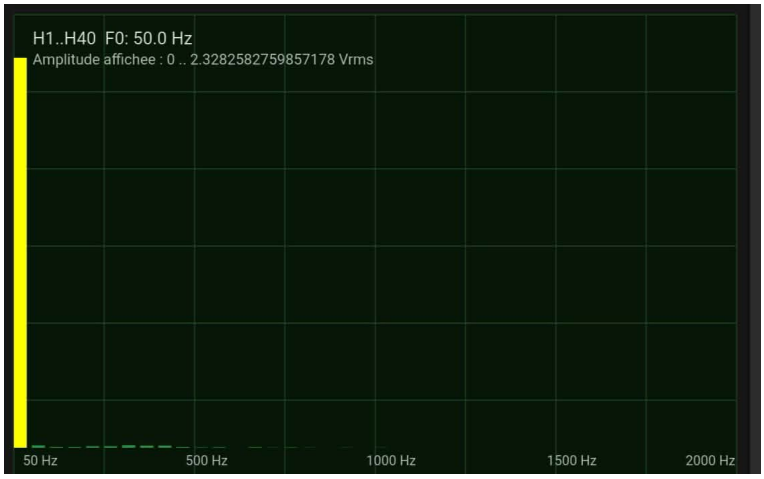


Figure 3.9: FFT analysis of the DAC-generated 50 Hz signal

3.7.2 FFT Analysis of the Real Network Voltage

Unlike the controlled DAC signal, the real mains signal was not perfectly aligned with the expected FFT bin under the acquisition conditions. As shown in **Figure 3.10**, the highest spectral magnitude was observed at the 55 Hz bin.

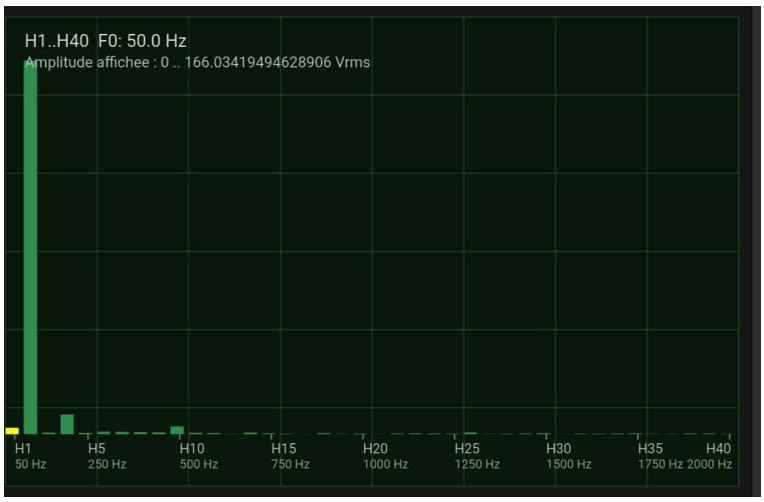


Figure 3.10: FFT analysis of the real network voltage

Considering the FFT frequency resolution of 5 Hz, the spectrum is evaluated only at discrete frequency bins separated by 5 Hz. Therefore, the dominant component observed at the 55 Hz bin indicates that the signal energy is mainly concentrated around this frequency bin, but does not necessarily mean that the actual mains frequency is exactly 55 Hz.

3.7.3 THD Implementation and Validation Status

The harmonic extraction and THD computation algorithms were implemented as part of the signal-processing chain, as described in **Section 2.11.3**. However, due to the limited experimental validation time available at the final stage of the project, the THD results could not be sufficiently verified against a reference instrument and were therefore not integrated into the final mobile application interface. Consequently, no experimentally validated THD value is reported in this section. Further validation using calibrated reference equipment is required before considering the THD measurement fully validated.

3.7.4 Power Measurement Implementation Status

The developed system was initially designed to include the measurement of active power, reactive power, and power factor. The theoretical principles and corresponding calculation methods were presented in the previous sections of this work.

However, reliable experimental validation of these quantities requires simultaneous acquisition of the voltage and current signals with appropriate synchronization and controlled load conditions. For the complete three-phase implementation, the three voltage and current channels must also be acquired and validated simultaneously.

During the experimental phase, priority was given to the validation of the voltage and current acquisition, RMS calculation, voltage unbalance evaluation, and frequency-domain analysis. Due to the limited time available for laboratory testing and the difficulties encountered during simultaneous multi-channel measurements, the active power, reactive power, and power factor measurements could not be fully implemented and experimentally validated.

Consequently, experimentally validated values for these parameters are not reported in the final mobile application. Their complete implementation and validation constitute an extension of the present work and would require controlled load tests and comparison with a calibrated reference instrument.

3.8 Conclusion

This chapter presented the practical implementation and experimental validation of the developed power quality analyzer. The data acquisition configuration was verified through the STM32 timer, ADC, and DMA stages, while the optimization of the ADC sampling time improved the stability of the acquired signals. Preliminary tests using a controlled 50 Hz DAC-generated signal also confirmed the correct operation of the acquisition, processing, and communication chain before measurements were performed on the real electrical network.

After calibration of the voltage sensors, the system successfully provided real-time waveform visualization and the calculation of the main voltage parameters. The voltage magnitude unbalance measurement produced an experimental value of 0.52%, while the FFT implementation correctly identified the 50 Hz component of the controlled test signal and provided the spectral representation of the real network voltage. These results confirmed the correct operation of the main acquisition and frequency-domain processing functions of the prototype.

However, the experimental validation of THD, active and reactive power, and power factor could not be completed under the available laboratory conditions and time constraints. These parameters therefore remain outside the fully validated experimental results presented in this chapter.

General Conclusion

This thesis focused on the design and development of an STM32-based embedded system for real-time electrical power quality analysis. The main objective was to implement the acquisition and digital processing of electrical signals directly on the embedded platform and to evaluate its ability to calculate and visualize the main power quality parameters.

The research hypothesis established at the beginning of this work stated that an STM32-based embedded system could perform real-time acquisition and processing of electrical signals to accurately estimate the main power quality parameters, including RMS voltage, frequency components using FFT, THD, and voltage unbalance. The experimental results obtained during this work support this hypothesis. The developed system was able to acquire electrical signals, process them in real time, calculate the required parameters, and transmit the resulting data through Bluetooth for visualization on a mobile application.

The implementation of the Fast Fourier Transform was validated using a controlled 50 Hz signal generated by the STM32 DAC. The fundamental component was correctly detected at the corresponding 50 Hz frequency bin, confirming the correct operation of the implemented frequency-domain processing. Measurements were also performed on the real electrical network after sensor calibration. In the three-voltage-input configuration, a voltage unbalance factor of approximately 0.52% was obtained. These experiments demonstrated the ability of the implemented system to perform real-time voltage measurements and power quality calculations using the STM32H743 microcontroller.

Particular attention was also given to harmonic analysis according to IEC 61000-4-7 and to the implementation of RMS, FFT, THD, and voltage unbalance calculations. The project therefore provided a practical implementation of several measurement and signal-processing methods used in power quality analysis while taking into consideration the recommendations of IEC 61000-4-30, IEC 61000-4-7, and IEEE 1159 throughout the study and design process.

The development of this project also provided valuable practical experience in configuring the AD7606 in SPI mode and establishing reliable communication with the STM32 microcontroller. Particular attention was given to the generation and timing of the SPI clock (SCLK), communication debugging procedures, and the influence of the SPI clock prescaler on data integrity and acquisition performance. These challenges significantly improved my understanding of high-speed digital interfaces, embedded system debugging, and mixed-signal data acquisition systems.

Limitations

Despite the obtained results, several limitations were encountered during the development of this work.

- One of the major challenges was the restricted access to international standards, particularly the **IEC** and **IEEE** standards, which are generally available only through paid subscriptions. In addition, although numerous recent research papers on power quality have been published, a significant proportion of them are also accessible only through subscription-based digital libraries. As a result, the study relied primarily on publicly available scientific articles, open-access publications, technical documentation, conference papers, and a limited number of educational resources, including specialized online lectures, to understand and interpret the relevant standards and recommended measurement procedures.

- Another challenge was related to the multidisciplinary nature of the project. This work lies at the intersection of electronics, electrical power systems, and industrial power networks. As an electronics engineering student, the academic curriculum provided only limited coverage of advanced topics related to electrical power systems, power quality, and industrial distribution networks. Consequently, additional time and effort were required to acquire the necessary background knowledge before addressing the design and implementation aspects of the project.

- A further limitation was related to the experimental environment and the sensors used during the tests. Magnetic fields present in the laboratory could disturb the digital part of the system and affect the stability of the measurements. In addition, the ZMPT101B voltage sensor and the ACS712 current sensor showed a certain level of instability during practical measurements. These limitations affected the repeatability and reliability of some experimental results. For a future implementation, more suitable and stable sensing solutions should be considered, such as the sensors suggested and discussed in **Section 2.8** and **Section 2.9**.

Future Perspectives

Several improvements can be considered as future extensions of the developed system. One of the main perspectives is to extend the analyzer toward a more complete power quality monitoring system by incorporating additional voltage- and current-related disturbances and completing the measurement functions required for a more comprehensive power quality assessment.

Another important perspective concerns communication and remote monitoring. Although the adopted Bluetooth solution satisfies the requirements of the developed prototype, it is not considered the final architecture envisioned for the project. From an engineering perspective, a Wi-Fi-based Internet of Things (IoT) architecture using an ESP32 module would constitute a more scalable solution for industrial deployment. Such an architecture would enable remote monitoring through a local network or the Internet, cloud data logging, web-based visualization dashboards, real-time notifications, and future integration with industrial IoT platforms.

Nevertheless, the primary objective of this work was not the development of an IoT monitoring system but the implementation of a power quality analyzer based on an embedded platform. Particular emphasis was placed on the implementation of digital signal

processing algorithms, harmonic analysis according to IEC 61000-4-7, and the development of measurement algorithms on the STM32H743 microcontroller, which represented a new embedded platform within this work.

Considering the limited duration of the project and the need to prioritize the core measurement functionalities, a simpler Bluetooth-based communication architecture was therefore selected. This decision reduced software complexity while allowing more time to be devoted to the implementation, verification, and validation of the measurement algorithms. The migration toward an ESP32-based IoT architecture therefore constitutes a natural extension of the present work.

Another future perspective is the preparation of the developed Power Quality Analyzer for official product certification through **IANOR**. IANOR, the Algerian Institute for Standardization, is the national organization responsible for standardization and conformity assessment in Algeria. Throughout this study and the design process, particular attention was given to complying, as much as possible, with the requirements of relevant international standards, including IEC 61000-4-30, IEC 61000-4-7, and IEEE 1159. Future work could therefore focus on performing the required conformity tests and preparing the necessary technical documentation for certification.

Such certification, together with the completion of the remaining measurement functions and the integration of remote monitoring capabilities, would represent an important step toward the industrialization and commercialization of the developed Power Quality Analyzer. The prototype developed during this project could therefore serve as a basis for a future commercial product intended for electrical installation monitoring and power quality analysis.

Bibliography

[1] Vijay G Neve, Pallavi V. Pullawar, Chetan H. Kidile. *Power quality issues & detection methodes for voltage sag and swell*, I J R B A T, Issue (Special-16), Vol. II, July 2020: 71–79.

[2] W. Mack Grady (The University of Texas at Austin, Austin, TX), Surya Santoso (Electrotek Concepts, Inc., Knoxville, TN). *Understanding Power System Harmonics*, Grady/Santoso, September 1, 2001.

[3] Irena Wasiak. *Handbook of Power Quality*. University of Bergamo, Italy, 2008.

[4] `https://www.se.com/ca/en/faqs/FA409853/`, accessed on 26/06/2026.

[5] Baylor University. *Symmetrical Components*, 2020.

[6] N. Shabbir, L. Kütt, M. Jarkovoi, M. N. Iqbal, A. Rassõlkin and K. Daniel. *An overview of measurement standards for power quality*, Agronomy Research 19(S1), 944–960, May 13, 2021.

[7] Frédéric de Coulon. *Théorie et traitement des signaux*. EPFL Press, 14 septembre 2013, 4th edition, 568 pages.

[8] `https://www.analog.com/en/resources/glossary/sampling-rate.html#:~:text=An%20ADC%20takes%20a%20continuous,)%20or%20Hertz%20(Hz`, accessed on 06/03/2026.

[9] *The Scientist and Engineer's Guide to Digital Signal Processing*, Chapter 12.

[10] Robert Matusiak. *Implementing Fast Fourier Transform Algorithms of Real-Valued Sequences With the TMS320 DSP Platform*, Texas Instruments, SPRA291, August 2001.

[11] Pierre Duhamel and Henk Hollmann. *Implementation of "split-radix" FFT algorithms for complex, real, and real-symmetric data*, IEEE, Issy-les-Moulineaux (France), 1985.

[12] Mario Garrido, Keshab K. Parhi and Jesus Grajal. *A Pipelined FFT Architecture for Real-Valued Signals*, IEEE Transactions on Circuits and Systems, December 2009.

[13] `https://www.youtube.com/watch?v=DsRKzajToXs`, accessed on 05/07/2026.

[14] Touat Lilia, Sifouane Fatma. *Compensation de l'énergie réactive au niveau de l'hôpital d'AZAZGA*, Master thesis. Supervisor: C. BIROUCHE, 2009/2010.

[15] Baylor University. *Engineering Recommendation P29, Planning limits for voltage unbalance in the United Kingdom.*, The Electricity Council (UK), London, 1989.

[16] Michael Ingram, Rasel Mahmud, and David Narang. *Background Information on the Power Quality Requirements in IEEE Std 1547-2018*, National Renewable Energy Laboratory, October 2021.

[17] Jorge Luis Díaz-Rodríguez[a], Luis David Pabón-Fernández[b] & Jorge Luis Contreras-Peña[c]. *Low-cost platform for the evaluation of single phase electromagnetic phenomena of power quality according to the IEEE 1159 standard*, DYNA 82 (194), September 24, 2015.

[18] https://www.elspec-ltd.com/knowing-iec-61000-4-30-class-a/?, accessed on 30/03/2026.

[19] International Electrotechnical Commission, *IEC 61000-4-7: Electromagnetic Compatibility (EMC) – Part 4-7: Testing and Measurement Techniques – General Guide on Harmonics and Interharmonics Measurements and Instrumentation*, IEC, Geneva, Switzerland, 2002, amended 2008.

[20] Angel Arranz-Gimon, Angel Zorita-Lamadrid, Daniel Morinigo-Sotelo, Vanesa Fernandez-Cavero, Oscar Duque-Perez. *Harmonic measurement and analysis system for characterization of adjustable speed drives*, CC BY-NC-ND license, September 2024.

[21] CHK Power Quality Pty Ltd. *Class A Measurements of Interharmonics*, CHK Power Quality Pty Ltd, October–November 2023.

[22] https://www.analog.com/en/resources/analog-dialogue/articles/power-quality-monitoring-part-1-the-importance-of\-compliant-power-quality-measurements.html, accessed on 06/07/2026.

[23] Sabrina MOKRANI, Damya OUMESSAOUD. *Conception et Réalisation d'un Oscilloscope Numérique Avec le microcontrôleur STM32*, Master thesis. Supervisor: Mrs HEMDANI, Mrs DAOUI, 2020.

[24] Carmine Noviello. *Mastering STM32*. Leanpub, 2018-08-17.

[25] https://technolabelectronics.com/?product=ac-voltage-sensor-module-zmpt101b-single-phase&srsltid=AfmBOooQdqEjwEQPc25wfE92mu4Tc26I8x4O4TI77fRwe3Qq_8KYzEKa, accessed on 26/06/2026.

[26] https://www.mathworks.com/matlabcentral/answers/356692-how-to-normalize-a-fft-to-plot-in-frequency-domain, accessed on 01/08/2026.

[27] https://arm-software.github.io/CMSIS_5/DSP/html/group__RealFFT.html, accessed on 01/08/2026.

[28] *Reference manual STM32H742, STM32H743/753 and STM32H750 Value line advanced Arm®-based 32-bit MCUs*, STMicroelectronics.

[29] Math HJ Bollen. *Understanding Power Quality Problems*. IEEE Press, 2000.

[30] Ahmed I. Zayed. *Advanceas in Shannon's Sampling Theory*. CRC Press, 1993.

[31] Salah Eddine BEKHOUCHE. *Réalisation d'un oscilloscope numérique portatif à affichage sur écran PC via le port USB*, Master thesis. Supervisor: M. Kahoul Nadir, 2013.

[32] *Manuel d'utilisation, Modèle: 2540C, Oscilloscopes numériques 2 voies, Oscilloscopes à signaux mixtes*.

[33] Shazma KHAN, Balvinder SINGH, Prachi MAKHIJA. *A Review on Power Quality Problems and its Improvement Techniques*, GWEC, IEEE, 2017.

[34] Angel Arranz-Gimon, Angel Zorita-Lamadrid, Daniel Morinigo-Sotelo, Oscar Duque-Perez. *Analysis of the use of the Hanning Window for the measurement of interharmonic distortion caused by close tones in IEC standard framework*, Electric Power Systems Research, Accepted 26 January 2022.

[35] *ZMPT101B Current-type Voltage Transformer datasheet*, Qingxian Zeming Langxi Electronic.

[36] `https://youtu.be/HKju4xDROxs?si=q_gNAp6pEmTppx7R`, accessed on 05/07/2026.

Annexe

Nom du projet : AmanPower
Équipe du projet:

- **Encadrant 01:** Dr Ghouti ABDELLAOUI
- **Encadrante 02:** DR Faiza MIMOUNI
- **Porteuse du projet:** Amina HAMRI

Présentation du projet

Ce projet s'inscrit dans le cadre de l'arrêté 1275/008 relatif à la création d'une entreprise économique.

Idée du projet

Le projet consiste à développer un Analyseur de Qualité de l'Énergie destiné aux utilisateurs industriels, agricoles et professionnels qui souhaitent surveiller la qualité de leur alimentation électrique et réduire l'impact des perturbations électriques sur leurs équipements et leurs activités.

Cette solution répond à un problème concret : les perturbations du réseau électrique peuvent entraîner des pertes énergétiques, des dysfonctionnements des équipements, des arrêts de production imprévus et une dégradation prématurée des systèmes électriques sensibles. Dans de nombreux cas, l'identification de l'origine de ces problèmes nécessite des équipements spécialisés et coûteux.

Le système proposé surveille en continu le réseau électrique et analyse les principaux paramètres de qualité de l'énergie afin de détecter les conditions anormales et les perturbations du réseau. L'analyse est réalisée conformément aux exigences IEC ciblées en matière de qualité de l'énergie, permettant à l'utilisateur de mieux comprendre les conditions électriques affectant l'installation.

L'analyseur enregistre les mesures des trois phases et stocke les données pour une analyse ultérieure. L'utilisateur peut accéder aux mesures et à l'historique des événements via une application mobile connectée par Bluetooth, sans nécessiter de connexion Internet. Cela permet de superviser directement l'installation sur site et d'identifier plus facilement les

anomalies récurrentes.

La valeur du projet réside dans l'association de la surveillance de la qualité de l'énergie, de la détection des perturbations, du stockage local des données et de la supervision mobile au sein d'un seul produit portable. La solution est conçue pour être abordable, facile à déployer, fabriquée localement afin de réduire la dépendance aux équipements importés, et personnalisable selon les besoins spécifiques des entreprises industrielles, des exploitations agricoles, des centres de données, des bureaux d'études, des laboratoires et des institutions publiques.

Objectifs du projet

Les principaux objectifs du projet sont :

- Assurer une surveillance fiable de la qualité de l'énergie afin de détecter les perturbations électriques et les conditions de fonctionnement anormales.
- Contribuer à réduire les pertes énergétiques et les arrêts des équipements en identifiant les causes des anomalies électriques.
- Proposer une alternative locale et abordable aux équipements importés d'analyse de la qualité de l'énergie.
- Permettre un accès facile aux mesures et à l'historique des événements grâce à une application mobile connectée par Bluetooth, sans nécessiter de connexion Internet.
- Fournir une solution portable et personnalisable adaptée aux besoins spécifiques des utilisateurs industriels, agricoles et professionnels.

Modèle économique du projet

Le modèle économique du projet est structuré selon les neuf blocs du canevas du modèle économique. Il présente la proposition de valeur de l'Analyseur de Qualité de l'Énergie, les segments de clientèle ciblés, les relations avec les clients, les canaux de distribution, les activités et ressources clés, les partenaires clés, la structure des coûts et les flux de revenus.

Proposition de valeur

La proposition de valeur repose sur un Analyseur de Qualité de l'Énergie fabriqué localement, conçu pour surveiller en continu le réseau électrique et détecter les perturbations de la qualité de l'énergie susceptibles d'affecter les équipements, l'efficacité énergétique et la continuité des activités.

Le système analyse les principaux paramètres électriques afin d'identifier les conditions de fonctionnement anormales et les perturbations du réseau. Les mesures et les événements détectés sont stockés localement, permettant aux utilisateurs de consulter l'historique de l'installation électrique et de mieux identifier les causes des anomalies récurrentes.

L'analyseur peut être connecté à une application mobile via Bluetooth, permettant aux utilisateurs d'accéder aux mesures et à l'historique des événements sans nécessiter de connexion Internet. Le produit est conçu pour être portable, facile à déployer sur site et accessible aux techniciens ne nécessitant pas d'outils hautement spécialisés d'analyse de la qualité de l'énergie.

Le projet propose également une alternative locale et abordable aux analyseurs de qualité de l'énergie importés. La solution peut être personnalisée selon les exigences du client et adaptée à différentes applications industrielles, agricoles, de laboratoire et professionnelles.

Segments de clientèle ciblés

Le projet cible deux principaux segments de clientèle :

- Le segment **B2B** comprend les entreprises industrielles souhaitant réduire les pertes énergétiques, identifier les causes des arrêts de production et des dysfonctionnements électriques, et améliorer la fiabilité de leurs installations. Il comprend également les centres de données privés nécessitant une alimentation électrique de haute qualité, les bureaux d'études spécialisés en efficacité énergétique et installations électriques, ainsi que les exploitations agricoles utilisant des pompes d'irrigation de forte puissance nécessitant une surveillance continue de la qualité de l'énergie.
- Le segment **B2G** comprend les hôpitaux et les institutions publiques exploitant des équipements électriques sensibles, les centres de données publics nécessitant une alimentation électrique fiable, ainsi que les universités et laboratoires réalisant des mesures, des essais et des analyses de la qualité de l'énergie.

Relations avec les clients

Les relations avec les clients reposent sur un accompagnement technique personnalisé avant et après la vente de l'Analyseur de Qualité de l'Énergie.

La communication avec les clients peut être assurée par messagerie, e-mail, appels téléphoniques et contact direct. Un suivi après-vente et une assistance technique sont assurés afin d'accompagner les clients dans l'utilisation de l'analyseur. Les avis des clients sont également recueillis afin d'améliorer continuellement le produit et de l'adapter aux besoins spécifiques des applications.

Canaux de distribution

Les principaux canaux de distribution comprennent le site web de l'entreprise, les salons et expositions industriels spécialisés, la prospection directe auprès des entreprises industrielles, les réseaux professionnels tels que LinkedIn, ainsi que les plateformes B2B dédiées aux équipements industriels.

Des partenariats avec des distributeurs et des intégrateurs de solutions électriques sont également envisagés afin de faciliter l'accès aux clients professionnels et d'élargir la portée commerciale du produit.

Activités clés

Les activités clés comprennent la recherche et développement, la fabrication et l'assemblage de l'Analyseur de Qualité de l'Énergie, le développement et la mise à jour du logiciel embarqué et de l'application mobile, les essais, la calibration et la validation des mesures selon les exigences IEC, la configuration du produit selon les besoins du client, l'emballage, la commercialisation, la distribution, le support technique et le service après-vente.

Ressources clés

Les ressources clés comprennent des ressources humaines et matérielles. Les ressources humaines sont principalement constituées d'un ingénieur en électronique, d'un ingénieur en informatique et d'un responsable commercial.

Les ressources matérielles comprennent des ordinateurs, un oscilloscope de référence, du matériel de mesure et de calibration, un banc de test, des équipements de prototypage électronique, des logiciels de conception électronique et de développement, ainsi qu'un local technique nécessaire au développement, aux essais et à l'assemblage du produit.

Partenaires clés

Les partenaires clés du projet comprennent les fournisseurs de composants électroniques, les distributeurs de matériel électrique et industriel, les fabricants de PCB et de boîtiers, les fournisseurs d'emballage, les entreprises de logistique et de livraison, les prestataires comptables, les banques et la NESDA.

Ces partenaires interviennent principalement dans l'approvisionnement en composants, la fabrication, la logistique, le financement, l'accompagnement du projet et la distribution du produit.

Structure des coûts

La structure des coûts comprend les composants électroniques, la fabrication du PCB et du boîtier, le câblage et les circuits auxiliaires, les modules de communication Bluetooth, le développement du logiciel embarqué et de l'application mobile, l'emballage, la logistique, les salaires, la location du local, les charges d'électricité et d'Internet, le marketing, la publicité, la prospection commerciale et la documentation technique.

Les coûts variables sont principalement liés à la production et à la livraison de chaque analyseur, tandis que les coûts fixes comprennent les salaires, la location du local, les charges, le développement logiciel, le marketing et les dépenses administratives.

Flux de revenus

Les flux de revenus reposent principalement sur la vente de l'Analyseur de Qualité de l'Énergie standard à un prix d'environ **140,000 DA par unité**.

Des revenus supplémentaires sont générés par les versions personnalisées de l'analyseur, à partir d'environ **180,000 DA par unité**, selon les fonctionnalités requises et les spécifications du client.

Le projet génère également des revenus grâce au conseil technique et aux interventions spécialisées, estimés entre **10,000 DA et 20,000 DA par intervention**.

Canevas du modèle économique du projet

Le tableau suivant résume les neuf blocs du modèle économique et relie la proposition de valeur, les clients, les activités, les ressources, les partenaires, les coûts et les revenus.

<table>
<tr>
<td rowspan="2">(7)
Les partenaires clés

• Fournisseurs de composant électroniques.
• Distributeurs de matériel électrique et industriel
• Sous-traitants pour la fabrication des PCB et des boîtiers
• Prestataire comptable.
• Entreprise de livraison
• NESDA
• Bank</td>
<td>(5)
Les activités clés
• R&D
• Tests, calibration et validation des mesures selon les normes IEC
• Support technique et accompagnement spécialisé.
• Emballage
• Commercialisation et distribution.</td>
<td rowspan="2">(1)
Proposition de valeur
- Appareille de détection des perturbations de la qualité de réseau 220V
- Analyse complète de la qualité de l'énergie conformément aux normes IEC.
- Application mobile accessible via Bluetooth sans internet.
- Réduction des coûts
- Produit local
- Appareil portable et facile à déployer sur site.
- Alertes en temps réel pour prévenir les dégâts matériels.
- Stockage local des données.
- Historique des événements réseau pour identifier les causes des anomalies.
- Analyseur personnalisés selon les besoins spécifiques du client
- Interface intuitive, accessible aux techniciens non spécialisés.</td>
<td rowspan="2">(3)
Relation avec clients

• Communication en ligne (messagerie, e-mail, appels).
• Visites sur site auprès des agriculteurs pour recueillir leurs retours d'expérience.
• Communication directe et personnalisée.
• Suivi après-vente.</td>
<td rowspan="2">(2)
Le segment de client
B2B :
- Les entreprises industrielles souhaitant réduire leurs coûts énergétiques.
- Les entreprises industrielles souhaitant identifier l'origine des pertes énergétiques, des arrêts de production et des dysfonctionnements électriques.
- Entreprises privées exploitant des data centers et nécessitant une alimentation électrique de haute qualité.
Exemple : ICOSNET
- Bureaux d'études spécialisés en efficacité énergétique et installations électriques.
- Agriculteurs souhaitant protéger leurs systèmes de pompage coûteux.
- Exploitations agricoles utilisant des pompes d'irrigation électriques de forte puissance nécessitant une surveillance continue de la qualité de l'énergie.

B2G :
- Hôpitaux disposant d'équipements médicaux</td>
</tr>
<tr>
<td>(6)
Les ressources
Equipe :
• Ingénieur en électronique
• Ingénieur en informatique
• Responsable commerciale
Ressources matérielles :
• Oscilloscope de référence
• Ordinateurs
• Matériel de mesure et de calibration
• Banque de test</td>
</tr>
<tr>
<td colspan="3"></td>
<td>(4)
Canaux de distribution
- Salons et foires industrielles spécialisées.
- Prospection directe auprès des entreprises industrielles.
- Partenariats avec des distributeurs et intégrateurs de solutions électriques.
- Plateformes B2B d'équipements industriels (TINSAL, OPTIPROD).</td>
<td></td>
</tr>
</table>

	• Locale technique • Logiciels de conception électronique et de développement • Équipements de prototypage électronique		- LinkedIn pour cibler les professionnels et décideurs industriels. - Site web professionnel avec présentation technique et demande de devis. - Plateformes en ligne (réseaux professionnels)	sensibles aux perturbations électriques. - Universités et laboratoires réalisant des mesures et analyses électriques - Institutions publiques exploitant des data centers critiques nécessitant une alimentation électrique fiable.

(8) La structure de couts :

La matière première et emballage :
- Microcontrôleur :10 000 DA
- Boîtier, carte électronique, câblage : 5 000– 30 000 DA
- Module Bluetooth : 1 300 DA
- Composants électroniques passifs et circuits auxiliaires : 20 000 DA
- Développement logiciel embarqué et application mobile : 50 000 DA/mois
- Cout d'emballage : 200 – 300 DA/unité

Local et charges :
- Location du local : 30 000 DA
- Électricité, Internet et autres charges : 20 000 DA

Les salaires :
- Ingénieur électronique : 80 000 DA/mois
- Ingénieur informatique : 60 000 DA/mois
- Responsable commerciale : 50 000 DA

Commercialisation et distribution :
- Marketing et publicité : 20 000 - 50 000 DA/mois
- Déplacement et prospection : 20 000DA
- Livraison et logistique : 1 000 – 2 000 DA/unité
- Documentation commerciale, brochures et démonstrations : 5 000 – 15 000 DA

(9) Le flux (sources) de revenu :
- Vente d'analyseur (forme standard) : 140 000 DA
- Vente d'analyseur (forme personnalisé) : à partir de 180 000 DA
- Conseil technique : 10 000 – 20 000 DA / intervention

	• Locale technique • Logiciels de conception électronique et de développement • Équipements de prototypage électronique		- LinkedIn pour cibler les professionnels et décideurs industriels. - Site web professionnel avec présentation technique et demande de devis. - Plateformes en ligne (réseaux professionnels)	sensibles aux perturbations électriques. - Universités et laboratoires réalisant des mesures et analyses électriques - Institutions publiques exploitant des data centers critiques nécessitant une alimentation électrique fiable.

(8) La structure de couts :

La matière première et emballage :
- Microcontrôleur :10 000 DA
- Boîtier, carte électronique, câblage : 5 000– 30 000 DA
- Module Bluetooth : 1 300 DA
- Composants électroniques passifs et circuits auxiliaires : 20 000 DA
- Développement logiciel embarqué et application mobile : 50 000 DA/mois
- Cout d'emballage : 200 – 300 DA/unité

Local et charges :
- Location du local : 30 000 DA
- Électricité, Internet et autres charges : 20 000 DA

Les salaires :
- Ingénieur électronique : 80 000 DA/mois
- Ingénieur informatique : 60 000 DA/mois
- Responsable commerciale : 50 000 DA

Commercialisation et distribution :
- Marketing et publicité : 20 000 - 50 000 DA/mois
- Déplacement et prospection : 20 000DA
- Livraison et logistique : 1 000 – 2 000 DA/unité
- Documentation commerciale, brochures et démonstrations : 5 000 – 15 000 DA

(9) Le flux (sources) de revenu :
- Vente d'analyseur (forme standard) : 140 000 DA
- Vente d'analyseur (forme personnalisé) : à partir de 180 000 DA
- Conseil technique : 10 000 – 20 000 DA / intervention

Le canevas du modèle économique présenté dans le **Tableau 3** met en évidence un modèle économique fondé sur la commercialisation d'un Analyseur de Qualité de l'Énergie fabriqué localement, complété par des versions personnalisées et des services de conseil technique.

La mise en œuvre du projet repose également sur un réseau de fournisseurs de composants électroniques, de fabricants de PCB et de boîtiers, de partenaires logistiques, d'organismes de soutien financier et de partenaires de distribution. La commercialisation s'appuie sur la prospection directe, les salons industriels, les plateformes professionnelles, les distributeurs et les canaux de communication en ligne adaptés aux segments B2B et B2G.

Analyse stratégique SWOT

L'analyse SWOT identifie les principaux facteurs internes et externes susceptibles d'influencer le développement et la commercialisation de l'Analyseur de Qualité de l'Énergie.

Facteurs	Facteurs contribuant à la réalisation des objectifs	Facteurs pouvant entraver la réalisation des objectifs
Facteurs internes	**Forces** 1. Produit fabriqué localement, réduisant la dépendance aux analyseurs de qualité de l'énergie importés. 2. Surveillance de la qualité de l'énergie et détection des perturbations selon les exigences IEC ciblées. 3. Supervision mobile via Bluetooth sans nécessiter de connexion Internet. 4. Stockage local des données et historique des événements facilitant l'analyse des anomalies électriques. 5. Solution portable et personnalisable adaptée aux différents besoins des clients. 6. Alternative plus abordable aux équipements professionnels importés.	**Faiblesses** 1. Nouveau produit encore peu connu sur le marché lors de la phase initiale de commercialisation. 2. Dépendance à des fournisseurs externes pour certains composants électroniques et la fabrication des PCB. 3. La calibration et la validation nécessitent des équipements spécialisés. 4. Ressources humaines et financières limitées pendant la phase de démarrage. 5. Nécessité d'un support technique continu et de mises à jour logicielles.
Facteurs externes	**Opportunités** 1. Besoin croissant de surveillance de la qualité de l'énergie dans les installations industrielles et professionnelles. 2. Marché potentiel comprenant les industries, les exploitations agricoles, les centres de données, les hôpitaux, les laboratoires et les bureaux d'études. 3. Intérêt croissant pour la réduction des pertes énergétiques et des arrêts de production. 4. Possibilité de remplacer des analyseurs importés coûteux par une solution fabriquée localement. 5. Possibilité de partenariats avec des distributeurs de matériel électrique et des intégrateurs de systèmes. 6. Accès à des programmes de financement et d'accompagnement des entreprises tels que la NESDA.	**Menaces** 1. Présence de fabricants internationaux établis d'analyseurs de qualité de l'énergie. 2. Variation des prix et de la disponibilité des composants électroniques importés. 3. Retards possibles dans l'approvisionnement en composants et les services de fabrication. 4. Exigences élevées des clients en matière de précision, de fiabilité et de conformité aux normes. 5. Évolution technologique rapide nécessitant une amélioration continue du produit.

Table 4: Analyse SWOT du projet d'Analyseur de Qualité de l'Énergie.

L'analyse présentée dans le **Tableau 4** met en évidence un projet qui se différencie techniquement par la surveillance continue de la qualité de l'énergie, la détection des perturbations, le stockage local des données, la supervision mobile et la possibilité d'adapter l'analyseur aux exigences spécifiques des clients.

Toutefois, le principal enjeu ne réside pas uniquement dans la solution technique. Une entrée réussie sur le marché nécessitera également une validation terrain élargie, une disponibilité fiable des composants électroniques, une forte crédibilité des mesures et un position-

nement commercial clair face aux analyseurs de qualité de l'énergie importés déjà présents.

Besoins du projet en ressources humaines

Au démarrage de l'activité, la structure humaine reste volontairement limitée afin de maîtriser les charges de fonctionnement tout en couvrant les principaux besoins techniques et commerciaux du projet.

L'équipe initiale se compose d'un **ingénieur en électronique**, responsable du développement matériel, des essais, de la calibration, de l'intégration du produit et du suivi technique ; d'un **ingénieur en informatique**, responsable du logiciel embarqué, de l'application mobile, du traitement des données et des mises à jour du système ; et d'un **responsable commercial**, responsable de la prospection clients, de la communication commerciale, des devis et du suivi client. :chatgpt-content-referenceindex="0"

Les activités spécialisées supplémentaires, telles que la fabrication des PCB, la production des boîtiers, la comptabilité et la logistique, peuvent être confiées à des prestataires externes afin de limiter les charges fixes pendant les premières phases du projet. :chatgpt-content-referenceindex="1"

Étude financière du projet

L'étude financière regroupe l'investissement initial, les approvisionnements de production, les charges de personnel, les services externes, les coûts de fonctionnement et les revenus prévisionnels.

Les valeurs présentées dans les sections suivantes sont basées sur les estimations préliminaires établies dans le canevas du modèle économique. Les coûts liés aux composants, à la fabrication, aux équipements et aux services pourront être ajustés ultérieurement selon les devis des fournisseurs et le volume de production. :chatgpt-content-referenceindex="2"

Estimation du montant total de l'investissement

Tableau 5 l'investissement initial couvre les ressources nécessaires au développement, à l'assemblage, aux essais, à la calibration et à la validation de l'Analyseur de Qualité de l'Énergie, ainsi qu'à l'organisation du local technique.

Cet investissement comprend principalement des ordinateurs, un oscilloscope de référence, du matériel de mesure et de calibration, un banc de test, des équipements de prototypage électronique, des logiciels de développement et le local technique nécessaire au développement et à la validation du produit.

Les composants électroniques, les PCB, les boîtiers, le câblage, les modules de communication, l'emballage et les autres éléments directement associés à la production des unités commercialisées sont comptabilisés séparément dans les coûts de production et d'approvisionnement.

Désignation	Qté	P.U. (DA)	Montant (DA)
Ordinateur de développement (16 Go RAM, SSD 512 Go)	2	95,000	190,000
Oscilloscope numérique de référence (2 voies, 100 MHz)	1	67,400	67,400
Multimètre numérique True RMS	1	12,000	12,000
Alimentation de laboratoire (30 V / 5 A)	1	17,500	17,500
Station de soudage et de reprise	1	18,450	18,450
Kit d'outillage électronique professionnel	1	52,600	52,600
Accessoires de mesure et de calibration	1 lot	25,000	25,000
Équipements du banc de test électrique	1 lot	60,000	60,000
Équipements de prototypage électronique	1 lot	20,000	20,000
Équipements de protection ESD (tapis, bracelet antistatique et accessoires)	1 lot	4,000	4,000
Logiciels de conception électronique et de développement	1 lot	0	0
Bureau de travail	2	30,000	60,000
Chaise de bureau	2	9,000	18,000
Armoire de rangement pour composants électroniques	1	19,500	19,500
Aménagement et accessoires du local technique	1 lot	25,000	25,000
		Total	**589,450 DA**
NB : Les montants indiqués sont estimés selon les prix actuels du marché en Algérie. Les prix peuvent varier selon le fournisseur, la marque, la disponibilité et les spécifications des équipements.			

Table 5: Estimation du montant total de l'investissement initial.

Estimation des approvisionnements en matières premières

Cette estimation concerne les composants électroniques, les matériaux de fabrication et les consommables nécessaires à la production de l'Analyseur de Qualité de l'Énergie au cours des trois premières années. Le volume de production prévisionnel est fixé à 35 unités la première année, 55 unités la deuxième année et 80 unités la troisième année.

La version commercialisée repose sur une architecture plus robuste que le prototype expérimental, notamment en matière d'acquisition des signaux, de mesure électrique, de protection, de communication, d'intégration du PCB et de conception du boîtier.

Hypothèse de production

	Année 1	Année 2	Année 3
Nombre de systèmes produits	35	55	80

Table 6: Hypothèse de production sur trois années.

Tableau 6 présente les prévisions de production retenues pour les trois premières années du projet.

Approvisionnements du système standard

Matières premières		Année 1	Année 2	Année 3
Microcontrôleur STM32	**Qté**	35	55	80
	P.U. (DA)	10 000	10 000	10 000
	Valeur d'achat	**350 000**	**550 000**	**800 000**
Circuit de mesure et de conditionnement de tension	**Qté**	35	55	80
	P.U. (DA)	3 000	3 000	3 000
	Valeur d'achat	**105 000**	**165 000**	**240 000**
Circuit de mesure et de conditionnement de courant	**Qté**	35	55	80
	P.U. (DA)	3 000	3 000	3 000
	Valeur d'achat	**105 000**	**165 000**	**240 000**
Module de communication Bluetooth	**Qté**	35	55	80
	P.U. (DA)	1 300	1 300	1 300
	Valeur d'achat	**45 500**	**71 500**	**104 000**
PCB électronique dédié	**Qté**	35	55	80
	P.U. (DA)	6 000	6 000	6 000
	Valeur d'achat	**210 000**	**330 000**	**480 000**
Circuit d'alimentation et de régulation de tension	**Qté**	35	55	80
	P.U. (DA)	3 500	3 500	3 500
	Valeur d'achat	**122 500**	**192 500**	**280 000**
Composants passifs et circuits auxiliaires	**Qté**	35	55	80
	P.U. (DA)	4 000	4 000	4 000
	Valeur d'achat	**140 000**	**220 000**	**320 000**
Boîtier de protection	**Qté**	35	55	80
	P.U. (DA)	10 000	10 000	10 000
	Valeur d'achat	**350 000**	**550 000**	**800 000**
Connecteurs et borniers	**Qté**	35	55	80
	P.U. (DA)	1 500	1 500	1 500

Matières premières		Année 1	Année 2	Année 3
	Valeur d'achat	**52 500**	**82 500**	**120 000**
Câblage interne	**Qté**	35	55	80
	P.U. (DA)	2 000	2 000	2 000
	Valeur d'achat	**70 000**	**110 000**	**160 000**
Matériel de montage et de fixation	**Qté**	35	55	80
	P.U. (DA)	500	500	500
	Valeur d'achat	**17 500**	**27 500**	**40 000**
Emballage et conditionnement	**Qté**	35	55	80
	P.U. (DA)	300	300	300
	Valeur d'achat	**10 500**	**16 500**	**24 000**
Total		**1 806 000 DA**	**2 838 000 DA**	**4 128 000 DA**

Table 7: Estimation des approvisionnements en matières premières pour l'Analyseur de Qualité de l'Énergie standard.

L'évolution du budget d'approvisionnement en matières premières est directement liée à l'augmentation planifiée du volume de production et des ventes. Les prix unitaires d'achat ont volontairement été maintenus constants sur la période de trois ans afin de simplifier les prévisions financières.

Toutefois, les estimations du **Tableau 7** devront être révisées au moment du lancement commercial selon les devis réels des fournisseurs, la disponibilité des composants, les variations du taux de change et les conditions d'achat pour des quantités plus importantes.

Le coût estimé des matières premières nécessaires à la fabrication d'un Analyseur de Qualité de l'Énergie standard est de **51 600 DA par unité**.

Options supplémentaires

L'Analyseur de Qualité de l'Énergie standard peut être complété par des fonctions optionnelles selon les exigences spécifiques du client. Deux configurations supplémentaires sont considérées : une option de protection automatique de la pompe et une option de supervision à distance par IoT.

Pour l'estimation financière, il est supposé qu'environ 20% des systèmes vendus chaque année intégreront chacune des options supplémentaires, correspondant à 7 unités la première année, 11 unités la deuxième année, et 16 unités la troisième année.

a. Option de protection automatique de la pompe

Cette option est principalement destinée aux installations agricoles utilisant des pompes électriques d'irrigation. Lorsque l'analyseur détecte une condition électrique susceptible d'endommager la pompe, telle qu'une variation importante de tension, une perte de phase ou un déséquilibre de tension, il peut générer une commande pour arrêter la pompe.

L'analyseur ne coupe pas directement l'alimentation de la pompe. À la place, une sortie de commande isolée pilote un relais externe ou un contacteur adapté à la puissance électrique de l'installation.

Composants supplémentaires		**Année 1**	**Année 2**	**Année 3**
Module de commande à relais isolé	**Qté**	7	11	16
	P.U. (DA)	1 200	1 200	1 200
	Valeur d'achat	**8 400**	**13 200**	**19 200**
Interface de commande isolée, protections et borniers	**Qté**	7	11	16
	P.U. (DA)	1 000	1 000	1 000
	Valeur d'achat	**7 000**	**11 000**	**16 000**
Coût supplémentaire total		**15 400 DA**	**24 200 DA**	**35 200 DA**

Table 8: Estimation du coût de l'option de protection automatique de la pompe.

Tableau 8 présente le coût matériel supplémentaire estimé de l'option de protection automatique de la pompe qui est donc de **2 200 DA par analyseur équipé**.

b. Option de supervision à distance par IoT

Cette option ajoute une connectivité Wi-Fi à l'Analyseur de Qualité de l'Énergie grâce à un module ESP32. Elle permet aux mesures électriques et aux événements détectés d'être transmis vers une plateforme de supervision à distance.

L'utilisateur peut ainsi superviser l'installation à distance, consulter l'historique des événements et recevoir des alertes sans être physiquement présent à proximité de l'analyseur. La communication Bluetooth reste disponible pour la supervision locale sans connexion Internet.

Composants supplémentaires		**Année 1**	**Année 2**	**Année 3**
Module Wi-Fi ESP32	**Qté**	7	11	16
	P.U. (DA)	1 700	1 700	1 700
	Valeur d'achat	**11 900**	**18 700**	**27 200**
Interface d'alimentation, de protection et de connexion	**Qté**	7	11	16
	P.U. (DA)	800	800	800
	Valeur d'achat	**5 600**	**8 800**	**12 800**
Coût supplémentaire total		**17 500 DA**	**27 500 DA**	**40 000 DA**

Table 9: Estimation du coût de l'option de supervision à distance par IoT.

Tableau 9 présente le coût matériel supplémentaire estimé de l'option de supervision à distance par IoT qui est donc de **2 500 DA par analyseur équipé**.

Estimation des coûts de la main-d'œuvre

Au démarrage de l'activité, l'équipe se compose d'un ingénieur en électronique, d'un ingénieur en informatique et d'un responsable commercial. Cette structure couvre les principales activités techniques, logicielles et commerciales du projet.

Intitulé du poste	**Nombre de salariés**	**Année 1**	**Année 2**	**Année 3**
Ingénieur en électronique	1	960 000 DA	1 008 000 DA	1 058 400 DA
Ingénieur en informatique	1	720 000 DA	756 000 DA	793 800 DA
Responsable commercial	1	600 000 DA	630 000 DA	661 500 DA
Total des charges de personnel		**2 280 000 DA**	**2 394 000 DA**	**2 513 700 DA**

Table 10: Estimation des coûts de la main-d'œuvre sur trois années.

Le Tableau 10 présente les charges de personnel estimées nécessaires pour assurer le développement du produit, la maintenance logicielle, le support technique, la prospection clients et le suivi commercial.

La structure organisationnelle proposée reste relativement légère durant les trois premières années. La fabrication spécialisée, la logistique, la comptabilité et d'autres activités occasionnelles peuvent être externalisées lorsque cela est nécessaire afin de limiter les charges permanentes de personnel.

Estimation des services externes

Durant les premières années d'activité, le projet vise à limiter les services externes à ceux nécessaires au fonctionnement, à la commercialisation et à la continuité de l'activité. Les dépenses augmentent progressivement selon la croissance prévue de la production et des ventes.

Désignation	Année 1	Année 2	Année 3
Location du local technique	360 000 DA	378 000 DA	396 900 DA
Électricité, Internet et autres charges	240 000 DA	252 000 DA	264 000 DA
Marketing et publicité	240 000 DA	360 000 DA	480 000 DA
Déplacements et prospection commerciale	20 000 DA	30 000 DA	40 000 DA
Livraison et logistique	52 500 DA	82 500 DA	120 000 DA
Documentation commerciale, brochures et démonstrations	10 000 DA	12 500 DA	15 000 DA
Prestations comptables	60 000 DA	72 000 DA	84 000 DA
Maintenance et petites réparations	24 000 DA	30 000 DA	36 000 DA
Total	**1 006 500 DA**	**1 217 000 DA**	**1 435 900 DA**

Table 11: Estimation des services externes sur trois années.

Tableau 11 montre que les dépenses de services externes sont principalement liées à la location du local, aux charges, aux activités de marketing, à la prospection commerciale et à la logistique.

Les dépenses de marketing et de logistique augmentent progressivement avec l'activité commerciale et le volume de production. La fabrication des PCB, la fabrication des boîtiers et les autres éléments directement associés à chaque analyseur ne sont pas inclus dans ce tableau car ils sont déjà pris en compte dans les coûts des matières premières et de production.

Estimation des coûts d'amortissement des investissements

L'investissement matériel initial est amorti selon la méthode linéaire sur une période de cinq ans. Les équipements sont regroupés en catégories homogènes afin de déterminer une dotation annuelle aux amortissements stable.

Aucun investissement matériel supplémentaire important n'est prévu durant les trois premières années dans cette prévision financière.

Désignation	Montant investi (DA)	Durée d'amortissement (années)	Dotation annuelle (DA)
Équipements techniques, de mesure et de test	276 950	5	55 390
Matériel informatique	190 000	5	38 000
Mobilier et équipements du local technique	122 500	5	24 500
Total	**589 450**	**–**	**117 890 DA**

Table 12: Estimation des coûts d'amortissement des investissements.

La dotation annuelle aux amortissements est donc estimée à **117 890 DA** comme présenté dans le **Tableau 12**. Ce montant reste constant sur la période considérée car l'équipement initial est amorti selon la méthode linéaire sur cinq ans

Cette approche permet de répartir le coût de l'investissement initial sur sa durée d'utilisation prévue et de distinguer l'effet de l'investissement initial en équipements de l'évolution des charges d'exploitation et de production.

Estimation des revenus du projet

Estimation du volume des ventes annuelles

Les prévisions de ventes annuelles sont réparties entre l'Analyseur de Qualité de l'Énergie standard et deux configurations améliorées : la version avec protection automatique de la pompe et la version avec supervision à distance par IoT.

Les prévisions supposent que 60% de la production annuelle est vendue sous forme de version standard, tandis que 20% est équipée de l'option de protection automatique de la pompe et 20% de l'option de supervision à distance par IoT. Les prix unitaires de vente sont maintenus constants sur la période de trois ans afin d'établir une prévision financière stable et lisible.

Désignation	Année 1	Année 2	Année 3
Système standard	21	33	48
Prix de vente unitaire (DA)	140 000	140 000	140 000
Ventes (DA)	**2 940 000**	**4 620 000**	**6 720 000**
Système avec protection automatique de la pompe	7	11	16
Prix de vente unitaire (DA)	180 000	180 000	180 000
Ventes (DA)	**1 260 000**	**1 980 000**	**2 880 000**
Système avec supervision à distance par IoT	7	11	16
Prix de vente unitaire (DA)	180 000	180 000	180 000
Ventes (DA)	**1 260 000**	**1 980 000**	**2 880 000**
Interventions de conseil technique	10	15	20
Prix unitaire (DA)	15 000	15 000	15 000
Revenus (DA)	**150 000**	**225 000**	**300 000**
Chiffre d'affaires total	**5 610 000 DA**	**8 805 000 DA**	**12 780 000 DA**

Table 13: Estimation des ventes annuelles et des revenus.

Tableau 13 montre que la croissance du chiffre d'affaires est principalement portée par l'augmentation planifiée du nombre d'analyseurs vendus. Le système standard reste l'offre commerciale principale, tandis que les versions avec protection de la pompe et IoT proposent des configurations à plus forte valeur ajoutée adaptées aux besoins spécifiques des clients.

Le conseil technique constitue un flux de revenus supplémentaire sans modifier le rôle central de la vente des analyseurs dans le modèle économique du projet.

Comptes de résultat annuels

Le compte de résultat annuel met en relation le chiffre d'affaires prévisionnel avec les achats de matières premières consommés, les charges externes, les coûts de personnel, les amortissements et la fiscalité estimée afin d'évaluer la performance financière du projet.

Désignation	Année 1	Année 2	Année 3
Chiffre d'affaires (1)	5 610 000 DA	8 805 000 DA	12 780 000 DA
Achats consommés (2)	1 838 900 DA	2 889 700 DA	4 203 200 DA
Charges externes (3)	1 006 500 DA	1 217 000 DA	1 435 900 DA
Valeur ajoutée = (1) – (2) – (3) (4)	**2 764 600 DA**	**4 698 300 DA**	**7 140 900 DA**
Charges de personnel (5)	2 280 000 DA	2 394 000 DA	2 513 700 DA
Excédent brut d'exploitation = (4) – (5) (6)	**484 600 DA**	**2 304 300 DA**	**4 627 200 DA**
Amortissements (7)	117 890 DA	117 890 DA	117 890 DA
Résultat d'exploitation = (6) – (7) (8)	**366 710 DA**	**2 186 410 DA**	**4 509 310 DA**
Impôt estimatif sur le résultat (19%) (9)	69 675 DA	415 418 DA	856 769 DA
Résultat net = (8) – (9)	**297 035 DA**	**1 770 992 DA**	**3 652 541 DA**
Évolution du chiffre d'affaires	–	**+56.95%**	**+45.14%**

Table 14: Comptes de résultat annuels prévisionnels.

Tableau 14 indique un résultat prévisionnel positif dès la première année. La première année correspond à la phase de lancement commercial au cours de laquelle les charges fixes de fonctionnement et de personnel représentent une part importante du chiffre d'affaires.

À partir de la deuxième année, l'augmentation du volume des ventes entraîne une amélioration significative de la performance d'exploitation. Cette tendance se poursuit au cours de la troisième année avec le développement des activités de production et de commercialisation.

Pour cette prévision financière préliminaire, un taux d'imposition de 19% est utilisé comme hypothèse d'estimation. La fiscalité applicable devra être confirmée avec le comptable selon le statut juridique et l'activité de l'entreprise.

Résultat de l'étude

Cette étude montre que le projet d'Analyseur de Qualité de l'Énergie présente un potentiel commercial dans le domaine de la surveillance de la qualité de l'énergie électrique, notamment pour les installations industrielles, les systèmes agricoles, les centres de données, les laboratoires, les bureaux d'études et les autres installations nécessitant un fonctionnement électrique fiable.

L'étude financière a permis d'identifier et d'estimer les principales ressources nécessaires au lancement du projet, notamment l'investissement initial en équipements, les matières premières, les ressources humaines, les services externes et les charges de fonctionnement. Le modèle économique repose principalement sur la vente de l'analyseur standard, complétée par des configurations proposant la protection automatique de la pompe et la supervision à distance par IoT, ainsi que des services de conseil technique spécialisés.

Les prévisions financières indiquent un résultat net prévisionnel positif de **297 035 DA** durant la première année. Cette période correspond principalement à la phase d'introduction sur le marché, au cours de laquelle les charges de personnel et de fonctionnement restent importantes par rapport au volume initial des ventes.

À partir de la deuxième année, l'augmentation prévue des ventes améliore le résultat net à environ **1 770 992 DA**. Au cours de la troisième année, le développement continu de l'activité commerciale porte le résultat net estimé à environ **3 652 541 DA**.

L'évolution du chiffre d'affaires prévisionnel, de **5 610 000 DA** au cours de la première année à **12 780 000 DA** au cours de la troisième année, illustre l'effet potentiel de l'augmentation de la capacité de production et du développement de configurations de produit à plus forte valeur ajoutée.

Avec un positionnement commercial adapté, une maîtrise des coûts de production, un approvisionnement fiable en composants et une validation terrain progressive, le projet peut proposer une alternative fabriquée localement aux Analyseurs de Qualité de l'Énergie importés tout en répondant aux besoins de surveillance et de protection des utilisateurs professionnels.

L'amélioration continue du produit, la fiabilité des mesures, le support technique et le développement progressif de la clientèle resteront des facteurs importants pour la pérennité de l'activité à long terme.